



Tubular Structure Design Using Laser Cutting Technology

Square Hollow Sections

Sofia Chaves Batista

Thesis to obtain the Master of Science Degree in

Civil Engineering

Supervisors: Professor Luís Manuel Calado de Oliveira Martins

Professor Jorge Miguel Silveira Filipe Mascarenhas Proença

Examination Committee

Chairperson: Professor Orlando José Barreiros D'Almeida Pereira

Supervisor: Professor Luís Manuel Calado de Oliveira Martins

Member of the Committee: Professor Alper Kanyilmaz

July 2021

Declaration

I declare that this document is an original work of my own authorship and that it fulfils all the requirements of the Code of Conduct and Good Practices of the Universidade de Lisboa.

Declaração

Declaro que o presente documento é um trabalho original da minha autoria e que cumpre todos os requisitos do Código de Conduta e Boas Práticas da Universidade de Lisboa.

Acknowledgments

First and foremost, I would like to express my sincere appreciation and gratitude to my supervisor, Professor Luís Calado, for encouraging and guiding me through this project. Without his immense knowledge, accuracy and patience, the goal of this thesis would not have been reached. A special thank you to Professor Jorge Proença for taking his time to review this thesis, as well as the suggestions provided.

To my family, for always pushing me forward in the journey that has been my student years and, with great effort, making sure I would get everything I needed. I will forever be thankful for all your kind-hearted words of advice and support.

To my amazing childhood friend, Valeriya Khrebtova, for always listening and giving the best advice on any problem I had.

At last, I would like to thank my amazing friends, Andreia Freitas, Duarte Gray e Rita Palma, that have accompanied me through the years, walking alongside me on this path, supporting me whenever I needed. Thank you for the friendship and beautiful memories I will cherish for years to come.

Abstract

The present dissertation comes as an extension of the European research project LASTEICON which aimed at the simplification of steel connections using laser cutting technology. The primary objective was the improvement of the mechanical behaviour of the joints with a simpler detailing and less steel quantity, while providing more quality, precision, and an environmentally friendly solution. This dissertation focuses on the use of steel tubular made trusses, with CHS and SHS cross-sections, where the connections were designed by creating an opening in the chords, using LCT, and extending its braces.

Considering the previously done experimental tests performed in IST laboratory, the approach adopted consisted of calibrating three numerical models, attesting for the accuracy of these models in representing the real structural behaviour of the trusses.

To establish a range of applicability and verify the benefits of using laser cut technology for this type of detail, in addition to a parametric analysis made for one of the trusses calibrated, a case study of the performance of these joints in a numerical model of a bigger structure was conducted. The results showed a substantial improvement in the global behaviour of the structure when compared to conventional manufacturing techniques, both in terms of resistance and stiffness.

Keywords:

- Laser cutting technology
- Tubular steel structures
- Steel hollow section joints
- Welded joints
- Finite elements analysis

Resumo

A presente dissertação ocorre no seguimento do projecto de investigação Europeu LASTEICON, que tem como objectivo a simplificação de ligações em aço, recorrendo à tecnologia de corte a laser. A principal finalidade deste projecto é a melhoria do comportamento mecânico de ligações metálicas, recorrendo a uma simplificação da geometria, com menor quantidade de aço, proporcionando ao mesmo tempo mais qualidade, precisão e uma solução sustentável. Esta dissertação incide na utilização de treliças tubulares em aço, com as secções transversais CHS e SHS, com as ligações concebidas criando uma abertura nas cordas, utilizando o corte a laser, e prolongando as diagonais.

Considerando os ensaios experimentais anteriormente realizados no laboratório do IST, a abordagem adoptada consistiu na calibração de três modelos numéricos, comprovando a exactidão destes modelos na representação do comportamento estrutural real das treliças.

Para estabelecer uma gama de aplicabilidade e verificar os benefícios da utilização da tecnologia de corte a laser para este tipo de pormenor, além de uma análise paramétrica feita para uma das treliças calibradas, foi realizado um caso de estudo relativo ao desempenho destas ligações num modelo numérico de uma estrutura em maior escala. Os resultados revelaram a melhoria substancial do comportamento global da estrutura quando comparada com outras técnicas convencionais de fabrico, tanto em termos de resistência como de rigidez.

Palavras-chave:

- Tecnologia de corte a laser
- Estruturas tubulares de aço
- Ligações tubulares de aço
- Ligações soldadas
- Análise de elementos finitos

Symbols

Roman letters: Lowercase

b_0	out-of-plane width of the chord	[mm]
b_1	out-of-plane width of the brace in compression	[mm]
b_2	out-of-plane width of the brace in tension	[mm]
d_0	diameter of the chord	[mm]
e	eccentricity between braces axis	[mm]
f_{y0}	yield strength of a chord member	[MPa]
f_u	ultimate strength	[MPa]
g	gap between brace axis	[mm]
h	height of the case study truss	[m]
h_0	depth of the chord in the plane of the lattice girder	[mm]
k_n	factor defined in the Table 7.10 of EC3-1-8	[-]
l_{infl}	influence length of the distribution load for the case study truss	[m]
p	distributed load for the case study truss	[KN/m]
t_0	wall thickness of the chord	[mm]

Roman letters: Uppercase

A	area of the chord	[m ²]
E	modulus of elasticity	[KN/m ²]
I	second moment of area	[m ⁴]
L	length of the case study truss	[m]
L_e	effective member length	[m]
M_{Rd}	design value of the resistance moment for the case study truss	[KNm]
N_{Rd}	design value of the resistance to axial forces in the case study truss chords	[KN]

N_s	ultimate load limit	[KN]
N_u	service load limit	[KN]
P	applied load in the case study truss nodes	[KN]
P_{cr}	critical buckling load	[KN]

Greek letters: Lowercase

γ_{M5}	partial safety factor for joints	[-]
γ	ratio of the chord width or diameter to twice its wall thickness	[-]
ε	total stain until failure	[-]
θ_i	angle between brace member i and the chord	[°]
λ_i	slenderness of member i	[-]
ν	Poisson ratio	[-]
ρ	density	[ton/mm ²]

Greek letters: Uppercase

Δ	chord surface deformation	[mm]
----------	---------------------------	------

Glossary

CAD	Computer Aided Design
CAE	Computer Aided Engineering
CHS	Circular Hollow Sections
EC3-1-1	Eurocode EN 1993-1-1
EC3-1-8	Eurocode EN 1993-1-8
EC3-1-5	Eurocode EN 1993-1-5
EU	European Union

FEA	Finite Elements Analysis
FEM	Finite Elements Method
HAZ	Heat Affected Zone
HEB	European Wide Flange Beams
IPE	European I Beams
IST	Instituto Superior Técnico
LASTEICON	Laser Technology for Innovative Joints in Steel Construction
LCT	Laser Cut Technology
LERM	Structures and Strength of Materials Laboratory
LVDT	Linear Variable Differential Transformers
RFCS	Research Fund for Coal and Steel
RHS	Rectangular Hollow Sections
SHS	Square Hollow Sections

Contents

Acknowledgments	i
Abstract.....	iii
Resumo	v
Symbols.....	vii
Roman letters: Lowercase.....	vii
Roman letters: Uppercase.....	vii
Greek letters: Lowercase.....	viii
Greek letters: Uppercase.....	viii
Glossary.....	viii
Contents	xi
List of Figures	xiii
List of Tables	xvii
1 Introduction.....	1
1.1 Concept and motivation for the research	1
1.2 Objectives of the research.....	1
1.3 Thesis framework	2
2 Literature review	3
2.1 LCT	3
2.2 Structural hollow sections.....	4
2.3 Truss girders.....	4
2.4 Hollow sections joint typologies.....	6
2.5 Failure modes and design regulations	7
2.5.1 Failure modes.....	7
2.5.2 Design regulations.....	9
i) Global analysis	9
ii) Strength criteria.....	11
iii) Deformation limit criteria	11
2.6 Experimental tests	12
2.7 Numerical modelling.....	14
2.7.1 Models for truss girders	14
2.7.2 Finite elements	15
2.7.3 Mesh.....	16
2.7.4 Welds.....	16
2.7.5 Material.....	16
3 Experimental and numerical studies	19
3.1 Introduction.....	19
3.2 Experimental studies	22

3.3	Numerical studies	23
3.4	Results from the analysis	28
3.5	Comparison between experimental and numerical models	32
4	Parametric studies	33
4.1	Parameters in study.....	33
4.2	Results from the analysis	36
4.2.1	Parameter: <i>to</i>	36
4.2.2	Parameter: <i>bo</i>	38
4.2.3	Parameter: <i>b1</i>	41
4.2.4	Parameter: <i>b2</i>	45
4.2.5	Parameter: <i>fy0</i>	48
4.2.6	Parameter: <i>g</i>	52
4.3	Analysis of the results.....	56
5	Case study.....	61
5.1	Design of the truss.....	61
5.2	Numerical studies	62
5.3	Results from the analysis	65
5.4	Analysis of the results.....	67
6	Conclusions and Future Developments	71
6.1	Conclusions	71
6.2	Future Developments	72
	Bibliography	73
	APPENDIX.....	77

List of Figures

Figure 2.1: Structural hollow section joints.....	4
Figure 2.2: Types of trusses - (a) Warren truss; (b) Pratt truss.	5
Figure 2.3: Example of truss connections – (a) Direct connection with contact overlap [20]; (b) Gusset connection [20]; (c) Flattened end connection [20]; (d) Catrus connection [21].	6
Figure 2.4: Types of joints in hollow section lattice girders - (a) Uniplanar joints; (b) Multiplanar joints [22].	7
Figure 2.5: Failure modes for joints between CHS brace and chord members [22].	8
Figure 2.6: Failure modes for joints between RHS brace and chord members [22].	9
Figure 2.7: Eccentricity of joints [22].....	10
Figure 2.8: Formula for design axial resistance between square or circular hollow section [22].	11
Figure 2.9: Chord surface deformation, Δ [28].....	12
Figure 2.10: Deformation limit criteria applied in the load-displacement curve of a joint [28].	12
Figure 2.11: Layout of the 3D experimental tubular truss [16].....	13
Figure 2.12: Midspan load-displacement curves [16].	13
Figure 2.13: Experimental test on a Warren truss.	14
Figure 2.14: Types of numerical modelling of trusses [6] - (a) beam model; (b) truss space model; (c) combined beam and truss space model; (d) isolated joint model.	15
Figure 2.15: Angles for quadrilateral elements [34].	16
Figure 2.16: Modelling of material behaviour proposed in the Eurocode [38].	17
Figure 3.1: Examples of joint details - (a) CHS with D2 joint; (b) SHS with D1 joint; (c) CHS with R joint.	20
Figure 3.2: Extrusion of the braces - (a) SHS with D1 joint; (b) CHS with D1v joint.	20
Figure 3.3: Models studied: (a) W_S_D1; (b) PS_S_D2; (c) W_S_D1.	21
Figure 3.4: For the truss W_R_D1: (a) support structure; (b) out-of-plane prevention system;(c) out-of-plane prevention system in the load application section; (d) connection between the truss and the support structure; (e) LDVT positioning.	23
Figure 3.5: Displacement application point and lateral constrains.....	24
Figure 3.6: Kinematic coupling constrain.	24
Figure 3.7: Most stressed joint: (a) W_R_D1; (b) PS_R_D2; (c) WS_R_D1.....	25
Figure 3.8: Spring model characteristics.	25
Figure 3.9: Weld model on a Warren joint and weld’s characteristics.	26
Figure 3.10: Local element sizing control and number of elements for the model: (a) W_S_D1; (b) WS_S_D1; (c) PS_S_D2	27
Figure 3.11: Load-displacement curves for W_S_D1 truss.	28
Figure 3.12: Critical joint deformation mode for W_S_D1 truss: (a) experimental test; (b) numerical simulation.....	28
Figure 3.13: Truss W_S_D1 deformed configuration and Von Mises stress distribution: (a) experimental test; (b) numerical simulation.....	29
Figure 3.14: Load-displacement curves for WS_S_D1 truss.....	29
Figure 3.15: Critical joint deformation mode for WS_S_D1 truss: (a) experimental test; (b) numerical simulation.....	30
Figure 3.16: Truss WS_S_D1 deformed configuration and Von Mises stress distribution: (a) experimental test; (b) numerical simulation.....	30
Figure 3.17: Load-displacement curves for PS_R_D2 truss.....	31
Figure 3.18: Detail of the deformation mode for PS_R_D2 truss: (a) experimental test; (b) numerical simulation.....	31

Figure 3.19: Truss PS_S_D2 deformed configuration and Von Mises stress distribution: (a) experimental test; (b) numerical simulation.....	32
Figure 4.1: Parameters for K and N gap joints [22].	33
Figure 4.2: Warren truss studied.....	35
Figure 4.3: Load-displacement curve for: (a) t_0 parameter study; (b) comparison between D1 and R for the t_0 parameter study.	36
Figure 4.4: Critical joint deformation for $t_0 = 6.3$ mm.	37
Figure 4.5: Critical joint deformation for $t_0 = 5$ mm.	37
Figure 4.6: Critical joint deformation for $t_0 = 8$ mm.	37
Figure 4.7: Load-displacement curve for $t_0 = 5$ mm: (a) b_0 parameter study; (b) comparison between D1 and R for the b_0 parameter study.	38
Figure 4.8: Load-displacement curve for $t_0 = 6.3$ mm: (a) b_0 parameter study; (b) comparison between D1 and R for the b_0 parameter study.	38
Figure 4.9: Load-displacement curve for $t_0 = 8$ mm: (a) b_0 parameter study; (b) comparison between D1 and R for the b_0 parameter study.	38
Figure 4.10: Critical joint deformation for $b_0 = 140$ mm and $t_0 = 6.3$ mm.....	39
Figure 4.11: Critical joint deformation for $b_0 = 160$ mm and $t_0 = 6.3$ mm.....	39
Figure 4.12: Critical joint deformation for $b_0 = 200$ mm and $t_0 = 6.3$ mm.....	39
Figure 4.13: Truss deformation and critical joint deformation for $b_0 = 250$ mm and $t_0 = 6.3$ mm.....	40
Figure 4.14: Critical joint deformation for $b_0 = 140$ mm and $t_0 = 5$ mm.....	40
Figure 4.15: Critical joint deformation for $b_0 = 160$ mm and $t_0 = 5$ mm.....	40
Figure 4.16: Critical joint deformation for $b_0 = 200$ mm and $t_0 = 5$ mm.....	40
Figure 4.17: Truss deformation and critical joint deformation for $b_0 = 160$ mm and $t_0 = 8$ mm.....	41
Figure 4.18: Critical joint deformation for $b_0 = 200$ mm and $t_0 = 8$ mm.....	41
Figure 4.19: Load-displacement curve for $t_0 = 5$ mm: (a) b_1 parameter study; (b) comparison between D1 and R for the b_1 parameter study.	41
Figure 4.20: Load-displacement curve for $t_0 = 6.3$ mm: (a) b_1 parameter study; (b) comparison between D1 and R for b_1 parameter study.	42
Figure 4.21: Load-displacement curve for $t_0 = 8$ mm: (a) b_1 parameter study; (b) comparison between D1 and R for b_1 parameter study.....	42
Figure 4.22: Critical joint deformation for $b_1 = 60$ mm and $t_0 = 6.3$ mm.....	43
Figure 4.23: Critical joint deformation for $b_1 = 80$ mm and $t_0 = 6.3$ mm.....	43
Figure 4.24: Critical joint deformation for $b_1 = 100$ mm and $t_0 = 6.3$ mm.....	43
Figure 4.25: Critical joint deformation for $b_1 = 80$ mm and $t_0 = 5$ mm.....	43
Figure 4.26: Critical joint deformation for $b_1 = 100$ mm and $t_0 = 5$ mm.....	44
Figure 4.27: Truss deformation for $b_1 = 80$ mm and $t_0 = 8$ mm.....	44
Figure 4.28: Critical joint deformation for $b_1 = 100$ mm and $t_0 = 8$ mm.....	44
Figure 4.29: Load-displacement curve for $t_0 = 5$ mm: (a) b_2 parameter study; (b) comparison between D1 and R for the b_2 parameter study.	45
Figure 4.30: Load-displacement curve for $t_0 = 6.3$ mm: (a) b_2 parameter study; (b) comparison between D1 and R for the b_2 parameter study.	45
Figure 4.31: Load-displacement curve for $t_0 = 8$ mm: (a) b_2 parameter study; (b) comparison between D1 and R for the b_2 parameter study.	45
Figure 4.32: Critical joint deformation for $b_2 = 70$ mm and $t_0 = 6.3$ mm.....	46
Figure 4.33: Critical joint deformation for $b_2 = 90$ mm and $t_0 = 6.3$ mm.....	46
Figure 4.34: Critical joint deformation for $b_2 = 70$ mm and $t_0 = 5$ mm.....	46
Figure 4.35: Critical joint deformation for $b_2 = 90$ mm and $t_0 = 5$ mm.....	47
Figure 4.36: Critical joint deformation for $b_2 = 70$ mm and $t_0 = 8$ mm.....	47

Figure 4.37: Truss deformation and critical joint deformation for $b_2 = 90$ mm and $t_0 = 8$ mm.....	47
Figure 4.38: Load-displacement curve for $t_0 = 5$ mm: (a) f_{y0} parameter study; (b) comparison between D1 and R for the f_{y0} parameter study.	48
Figure 4.39: Load-displacement curve for $t_0 = 6.3$ mm: (a) f_{y0} parameter study; (b) comparison between D1 and R for the f_{y0} parameter study.....	48
Figure 4.40: Load-displacement curve for $t_0 = 8$ mm: (a) f_{y0} parameter study; (b) comparison between D1 and R for the f_{y0} parameter study.	48
Figure 4.41: Critical joint deformation for $f_{y0} = 235$ mm and $t_0 = 6.3$ mm.....	49
Figure 4.42: Critical joint deformation for $f_{y0} = 275$ mm and $t_0 = 6.3$ mm.....	49
Figure 4.43: Critical joint deformation for $f_{y0} = 420$ mm and $t_0 = 6.3$ mm.....	49
Figure 4.44: Critical joint deformation for $f_{y0} = 460$ mm and $t_0 = 6.3$ mm.....	50
Figure 4.45: Critical joint deformation for $f_{y0} = 235$ mm and $t_0 = 5$ mm.....	50
Figure 4.46: Critical joint deformation for $f_{y0} = 275$ mm and $t_0 = 5$ mm.....	50
Figure 4.47: Critical joint deformation for $f_{y0} = 420$ mm and $t_0 = 5$ mm.....	50
Figure 4.48: Critical joint deformation for $f_{y0} = 460$ mm and $t_0 = 5$ mm.....	50
Figure 4.49: Critical joint deformation for $f_{y0} = 235$ mm and $t_0 = 8$ mm.....	51
Figure 4.50: Critical joint deformation for $f_{y0} = 275$ mm and $t_0 = 8$ mm.....	51
Figure 4.51: Critical joint deformation for $f_{y0} = 420$ mm and $t_0 = 8$ mm.....	51
Figure 4.52: Critical joint deformation for $f_{y0} = 460$ mm and $t_0 = 8$ mm.....	51
Figure 4.53: Load-displacement curve for $t_0 = 5$ mm: (a) g parameter study; (b) comparison between D1 and R for the g parameter study.....	52
Figure 4.54: Load-displacement curve for $t_0 = 6.3$ mm: (a) g parameter study; (b) comparison between D1 and R for the g parameter study.	52
Figure 4.55: Load-displacement curve for $t_0 = 8$ mm: (a) g parameter study; (b) comparison between D1 and R for g parameter study.	52
Figure 4.56: Critical joint deformation for $g = 40$ mm and $t_0 = 6.3$ mm.	53
Figure 4.57: Critical joint deformation for $g = 80$ mm and $t_0 = 6.3$ mm.	53
Figure 4.58: Critical joint deformation for $g = 120$ mm and $t_0 = 6.3$ mm.	53
Figure 4.59: Critical joint deformation for $g = 40$ mm and $t_0 = 5$ mm.	54
Figure 4.60: Critical joint deformation for $g = 80$ mm and $t_0 = 5$ mm.	54
Figure 4.61: Critical joint deformation for $g = 40$ mm and $t_0 = 8$ mm.	54
Figure 4.62: Critical joint deformation for $g = 80$ mm and $t_0 = 8$ mm.	54
Figure 4.63: Truss deformation for $g = 80$ mm, $t_0 = 6.3$ mm and $b_0 = 250$ mm.....	55
Figure 4.64: Critical joint deformation for $g = 80$ mm, $t_0 = 6.3$ mm and detail D2.....	55
Figure 4.65: Truss deformation for $g = 80$ mm, $t_0 = 6.3$ mm, $b_0 = 250$ mm and detail D2.	55
Figure 4.66: Truss deformation for $g = 80$ mm, $t_0 = 8$ mm, $b_0 = 250$ mm and detail D2.	55
Figure 4.67: Load-displacement curve reflecting the chord's width influence.....	57
Figure 4.68: Influence of the joint detail in its deformation and resistance.....	58
Figure 4.69: Nodes used for the deformation limit criteria.	58
Figure 4.70: Load-displacement curve for the critical node with a: (a) D1 joint detail; (b) D2 joint detail; (c) R joint detail.	59
Figure 5.1: Designed truss to be studied.....	61
Figure 5.2: Von Mises stress distributions, in MPa, for the designed truss from SAP 2000.	62
Figure 5.3: Layout of the models studied: (a) R_R_0; (b) R_D1_0; (c) D1_R_0; (d) D1_D1_0; (e) D1_R_20.	64
Figure 5.4: Boundary conditions and applied displacements.	64
Figure 5.5: Local element sizing control and number of elements for the structure.	65
Figure 5.6: Deformed configuration and Von Mises stress distribution for D1_D1_0.....	65

Figure 5.7: Joint deformation and Von Mises stress distribution for D1_D1_0..... 65
Figure 5.8: Deformed configuration and Von Mises stress distribution for R_R_0. 66
Figure 5.9: Joint deformation and Von Mises stress distribution for R_R_0. 66
Figure 5.10: Deformed configuration and Von Mises stress distribution for D1_R_0. 66
Figure 5.11: Joint deformation and Von Mises stress distribution for D1_R_0. 66
Figure 5.12: Deformed configuration and Von Mises stress distribution for R_D1_0. 66
Figure 5.13: Joint deformation and Von Mises stress distribution for R_D1_0. 67
Figure 5.14: Deformed configuration and Von Mises stress distribution for D1_R_20. 67
Figure 5.15: Joint deformation and Von Mises stress distribution for D1_R_20. 67
Figure 5.16: Comparison between model R_R_0 and the models R_D1_0, D1_R_0 and D1_D1_0. 68
Figure 5.17: Comparison between models R_R_0 and D1_R_0. 68
Figure 5.18: Comparison between models R_R_0 and D1_R_20. 69

List of Tables

Table 2.1: Comparison between cutting methods [4].	3
Table 2.2: Allowance for bending moments [22].	10
Table 3.1: Trusses studied - 16 Subtrusses and 9 Civil trusses.	19
Table 3.2: Material properties of the FEM models for ABAQUS.	23
Table 3.3: Initial out-of-plane displacements.	26
Table 4.1: Parameters in study.	34
Table 4.2: Initial out-of-plane displacement for the parametric studies.	35
Table 4.3: Steel properties for ABAQUS.	36
Table 4.4: Parameter b_0 - peak load increase, in percentage, from a regular detail to a D1 detail.	39
Table 4.5: Parameter b_1 - peak load increase, in percentage, from a regular detail to a D1 detail.	42
Table 4.6: Parameter b_2 - peak load increase, in percentage, from a regular detail to a D1 detail.	46
Table 4.7: Parameter f_{y0} - peak load increase, in percentage, from a regular detail to a D1 detail.	49
Table 4.8: Parameter g - peak load increase, in percentage, from a regular detail to a LCT detail.	53
Table 4.9: Slenderness ratio for parameter b_0 .	56
Table 4.10: Slenderness ratio for parameter b_1 .	56
Table 4.11: Slenderness ratio for parameter b_2 .	56
Table 4.12: Critical node resistance for model 6.3_180_90_80_355_80, and increased resistance, in percentage, from a regular detail to a LCT detail.	59
Table 5.1: Cross-section dimensions for the truss elements.	61
Table 5.2: Steel properties	62

1 Introduction

1.1 Concept and motivation for the research

According to the World Steel Association, after China, the EU is the second-largest producer of steel in the world, accounting for 8.5% of the global production [1]. With the production of 157 million tonnes of steel a year [1], the steel industry has a significant impact on the EU economy by endorsing employment and on the environment for increasing innovation and growth. Nonetheless, environmental and climate change regulation is a challenge for the industry. Notably, the most recent action plan, the European Green Deal, presented in December 2019, set a target of zero net emissions of greenhouse gases by 2050 [2].

Following the need to make the EU's economy sustainable and competitive, the Commission mobilized the Research Fund for Coal and Steel (RFCS), which financially supports research and innovation projects in the areas of coal and steel, in search of progressive technology and advanced production processes [3].

Intending to help achieve the targets set, the LASTEICON project was approved and funded. Using laser cut technology (LCT), its primary goal is to simplify steel joints by reducing the amount of welding and stiffener plates, particularly between CHS columns and I beams. To exploit the solution's extendibility, IST is responsible for the studies made regarding the applications in truss girders [4].

1.2 Objectives of the research

The primary objective of LASTEICON is to design new joint configurations that improve mechanical behaviour both for frame and truss structures, with less quantity of steel and simple detailing, proving to be an excellent alternative to the traditional type of connections. Additionally, these characteristics allow a more environmentally friendly solution with higher quality and precision, actively encouraging the use of hollow cross-sections. The use of LCT also reduces the risk associated with the fabrication process due to its computer-programmed automation [4]. The previous investigation made for truss girders in IST [5,6,7] proved the benefits of this new type of connections. Using tubular made trusses, with CHS and SHS cross-sections, numerical models and experimental tests were done to evaluate their structural performance, concluding that the LASTEICON designs enhance truss girders global behaviour [6].

Following the research done in the amplitude of the LASTEICON project, that allowed exploiting the benefits of using laser cut technology, the work carried out in this thesis aims to use ABAQUS, an advanced non-linear structural analysis software, to not only calibrate the previous numerical models but also do a parametric analysis to establish a range of applicability for this type of details and, ultimately, analyse the performance of laser cut details in a larger scale truss.

1.3 Thesis framework

This dissertation is structured in six chapters.

The present chapter gives a brief introduction to the topic covered in this work, describing the objectives, methodologies, and a succinct description of the structure of the document.

The second chapter, entitled “Literature review”, presents the different topics addressed in this work, namely the presentation of laser cutting technology, followed by information on truss girders with hollow sections and possible joint typologies. Lastly, it refers the design regulations and failure modes of the referred connections as well as suggestions for numerical modelling. A brief description is also given of experimental studies carried out in the context of the problem in question.

Chapter three, “Experimental and numerical studies”, elaborates on the geometry of the LCT joints to be studied and the dimensions and geometry of the trusses where they are to be inserted. A brief description is given of the experimental tests previously carried out in the IST laboratory and of the numerical modelling procedures employed. The results of the experimental tests and of the numerical analysis are then presented, along with the associated conclusions.

The fourth chapter, “Parametric studies”, constitutes a parametric study in a previous calibrated truss. After a description of the models and parameters adopted, the results obtained are displayed and analysed.

In the fifth chapter, “Case study”, a study of the performance of the innovative LCT connections in a numerically modelled structure with a more realistic geometry was conducted. After the introduction of the design of the structure, the results of the numerical analysis and conclusions are provided.

Finally, the sixth chapter presents the main conclusions of the work developed and some perspectives for future studies.

2 Literature review

2.1 LCT

As of today, the metal cutting techniques available in the market can be divided in:

- mechanical, covering methods such as saw cutting, drilling and water jet cutting;
- thermal, where laser cut, plasma and oxy-fuel (or flame) cutting methods are inserted;
- chemical.

Laser cutting is a thermal process that employs a concentrated laser beam in a small area of material until its melting point, with the possible aid of an assisting gas. Due to the non-contact procedure, the damage done to the material decreases [8].

Compared to traditional cutting techniques, the use of CAD programming in LCT leads to an increase in the cut's quality and precision while maintaining a safe work environment [9]. As a result of more automation, it is possible to achieve cost-effective manufacturing of parts and easy design changes, making it up to thirty times faster than conventional methods [10].

Among the numerous advantages, it is worth highlighting, in the context of this thesis, that adopting LCT allows an easy design of innovative connections, maintaining joint aesthetic, as well as enhancing global structural integrity [10].

All the qualities mentioned previously contribute to reducing the overall expenses in material and time spent on welding in the manufacturing life cycle, despite the higher initial investment cost of laser cutting machines. As for the environmental impact, since laser cutting operations produce much less amount of slag, noise, and pollution, its benefits suppress other cutting procedures [10].

Additionally, according to Harničárová *et al.* [8], compared to other technologies, such as oxygen cutting and plasma cutting, LCT has a much smaller heat-affected zone (HAZ). This feature prevents micro-cracks and material distortion, improving the behaviour under seismic loading of the connection. Studies made by D.Andrés *et al.* [11] attested to the conclusions mentioned above and concluded that laser and plasma cutting achieve higher tensile strength and yield compared to flame cutting.

Table 2.1 sums up a comparison of the benefits of LCT with other cutting technologies [4].

Table 2.1: Comparison between cutting methods [4].

	Laser CO2	Water jet	Plasma	Flame
Precision (mm)	0.05	0.2	0.5	0.75
Noise, pollution and danger	Very low	Unusually high	Medium	Low
Machine cleaning due to process	Low	High	Medium	Medium
Initial capital investment (1000 US \$)	300	300+	120+	200-500

2.2 Structural hollow sections

With the increased use of steel in construction, hollow sections became more widely recognized for their structural properties. In addition to an already significant resistance to tension, compression, bending, and torsion, filling them with concrete increases their strength and fire endurance [12].

Their axial symmetric geometry leads to a consistent behaviour in both directions, presenting a better strength-to-weight ratio that, apart from reducing the use of material, allows greater spans. Furthermore, due to the need for less fire and corrosion protection (as a result of fewer sharp edges) and reduced transportation costs, the use of this type of section becomes economically competitive [13].

Regardless of the many benefits presented, a vast amount of welds and local stiffeners makes their joint details complex and expensive, leading to a lack of aesthetic appearance, perceptible in Figure 2.1, slow design, and manufacturing process [10]. The studies carried out within this work intend to overcome this problem, focusing on circular hollow sections (CHS) and square hollow sections (SHS).



Figure 2.1: Structural hollow section joints.

2.3 Truss girders

Trusses are a widely embraced option for their cost-effective nature and applicability to larger spans due to their lightweight but still high resistance to loads. These structures are defined for their geometry, consisting of chords and braces (which wield primarily axial forces), connected with bolted or welded joints [14, 15]. On account of their structural properties and architecturally appealing shapes, it is common to see trusses applied to structures such as bridges, stadiums, offshore platforms and cranes [16].

A set of conditions must be considered to design a truss, such as static and fatigue strength, stability, maximum admissible deflection, fabrication, and maintenance while maintaining an economical and sustainable solution. To optimize its design, it is required to consider three categories: geometry, topology, and cross-sectional optimization [17].

Cross-sectional optimization focuses on finding the best shape to support a particular load, whether through the cross-section's mass or stiffness. As for geometry optimization, it deals with the position,

strength, and, to some degree, the truss's topology. For the last category, the topology optimization addresses the number and connectivity of the elements [18].

The two types of truss girders considered within this thesis are Warren and Pratt, portrayed in Figure 2.2 (a) and (b), respectively.

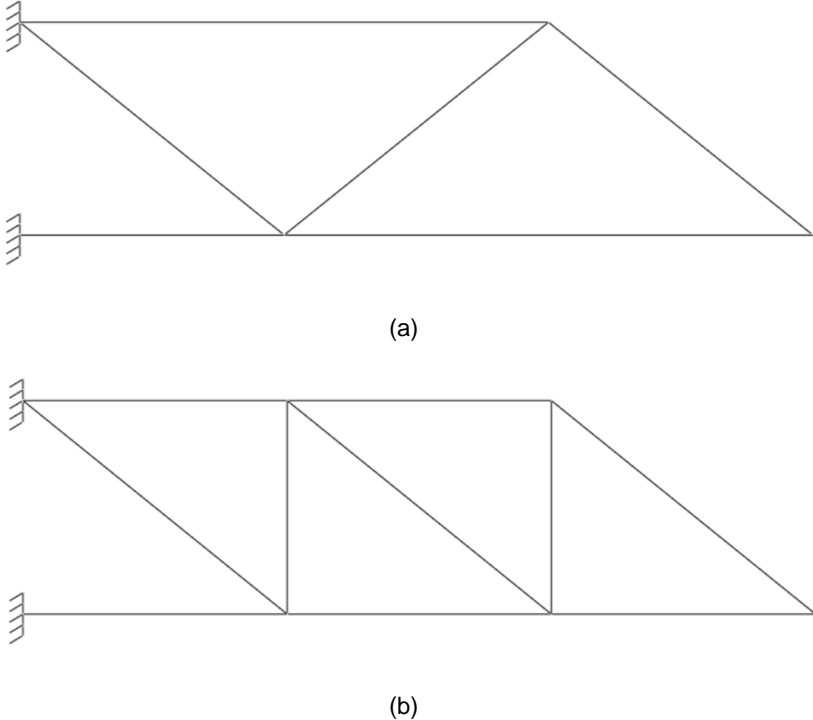


Figure 2.2: Types of trusses - (a) Warren truss; (b) Pratt truss.

Among the failure modes associated with truss girders, such as joint, support or member failure, if a slender member gets under compression, it can fail due to bending. This failure mode is called Euler buckling [18]. The critical buckling load is the maximum axial force that can be applied before the element buckles and is governed by the following equation:

$$P_{cr} = \frac{\pi^2 EI}{L_e^2} \quad [KN] \tag{2.1}$$

where E is the modulus of elasticity [KN/m²], I is the second moment of area [m⁴] and L_e is the effective member's length [m].

The slenderness, λ , and section shape influence the value of the critical buckling load. Thus, to increase the structure's overall buckling behaviour, a higher diameter (or with) to wall thickness of the sections is needed [19].

Another way to improve the performance is to look at the members' boundary conditions by having more rigid joints. The new LASTEICON joints intend to focus on this point and present more rigid and resistant joints, allowing a stability increase.

2.4 Hollow sections joint typologies

When designing a hollow section steel structure, it's essential to consider the joint behaviour, selecting the appropriate geometry that can achieve the desired load-bearing capacity and stiffness while still being an economical solution.

Among the different uniplanar hollow section node connections, the most standard and economical is a direct type, where the members are welded directly together. Even though gusseted connections withstand a substantial load transmitted through the node, the transfer of loads is indirect, and they are not as aesthetically pleasing [20]. As for small to moderate spans and statically loaded trusses, flattened connections can simplify fabrication and reduce cost [12]. Researchers at Dundee University also developed a new space truss system called Catrus, characterized by a continuous top and bottom chord and directed bolted members [21]. Figure 2.3 has depicted the referred tubular section connections for trusses.

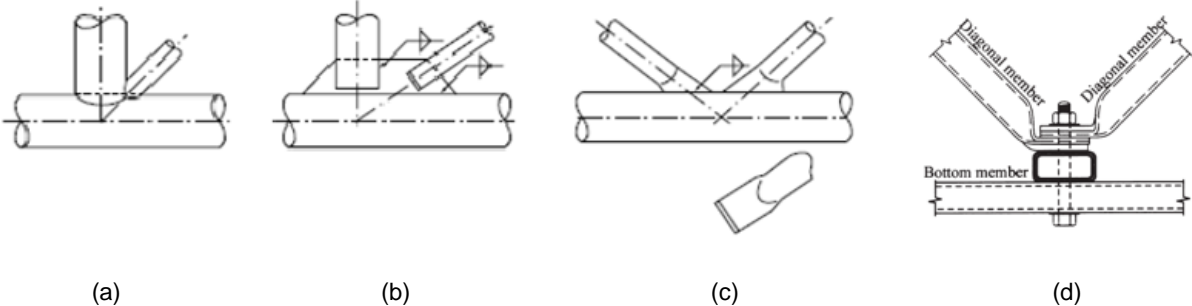
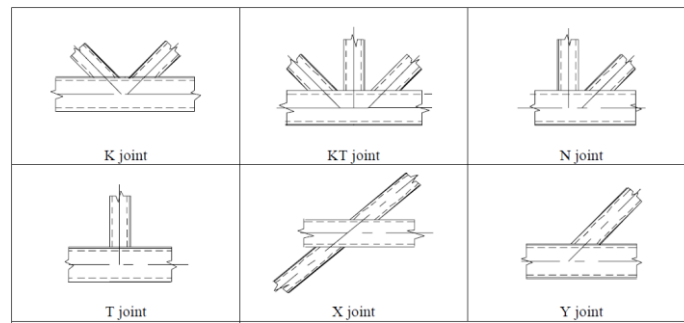
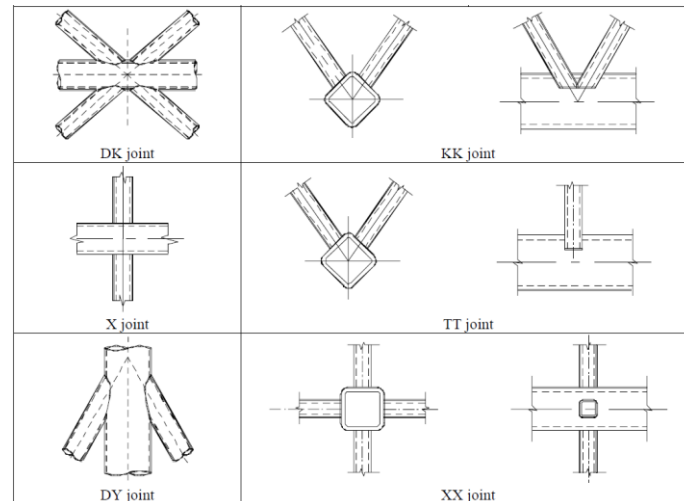


Figure 2.3: Example of truss connections – (a) Direct connection with contact overlap [20]; (b) Gusset connection [20]; (c) Flattened end connection [20]; (d) Catrus connection [21].

EC3-1-8 [22] details a variety of welded joints, portrayed in Figure 2.4, classified by their type of geometry, and introducing uniplanar joints and multiplanar ones.



(a)



(b)

Figure 2.4: Types of joints in hollow section lattice girders - (a) Uniplanar joints; (b) Multiplanar joints [22].

2.5 Failure modes and design regulations

2.5.1 Failure modes

To calculate the design joint resistances of connections, it is required to follow the load path to know the possible locals of failure. With the stiffness distribution, as well as the material behaviour, it is possible to determine the failure mode for each of those locations. The static design resistance of the joint will be the lowest value of the possible failure modes [19]. Figures 2.5 and 2.6 have illustrated the following failure modes for CHS and RHS joints [22].

- Mode a: Plastic failure of the chord face or chord cross-section;
- Mode b: Failure of the chord side wall or web by yielding, crushing or instability (cripling or buckling of the chord side wall or web) under the compression brace member;
- Mode c: Chord shear failure;

- Mode d: Punching shear failure of a hollow section chord wall (crack initiation leading to rupture of the chord member);
- Mode e: Brace failure with reduced effective width (cracking in the welds or the brace members);
- Mode f: Local buckling failure of a brace member or a hollow section chord member at the join location.

Mode	Axial loading	Bending moment
a		
b		
c		
d		
e		
f		

Figure 2.5: Failure modes for joints between CHS brace and chord members [22].

Mode	Axial loading	Bending moment
a		
b		
c		
d		
e		
f		

Figure 2.6: Failure modes for joints between RHS brace and chord members [22].

2.5.2 Design regulations

i) Global analysis

Predominantly, truss girders calculation models imply pinned connections, allowing the grid members to only be influenced by axial forces [23]. Moreover, the semi-empirical formulae provided in the EN 1993-1-8 [22] are only applied on the assumption that the lattice girder members are connected by pinned joints. In reality, joints are usually under complex loading conditions on account of bending moments that can occur from:

- Rotational stiffness of the nodes;
- Transverse load between truss nodes;
- Eccentricity in member connections.

Since rotational stiffness of the joints can cause secondary moments, they may be neglected for a certain joint geometry condition, referred on Eurocode 3.

Regarding the transverse loads, the resulting moments, whether in-plane or out-of-plane, should be considered in the design of the members to which they are applied.

As for moments resulting from eccentricities, in the design of tension members and connections, they may be neglected if the following limits are complied [22]:

$$-0,55 d_0 \leq e \leq 0,25 d_0 \quad (2.1)$$

$$-0,55 h_0 \leq e \leq 0,25 h_0 \quad (2.2)$$

where e is the eccentricity, defined in Figure 2.7, d_0 is the diameter of the chord and h_0 is the depth of the chord in the plane of the lattice girder.

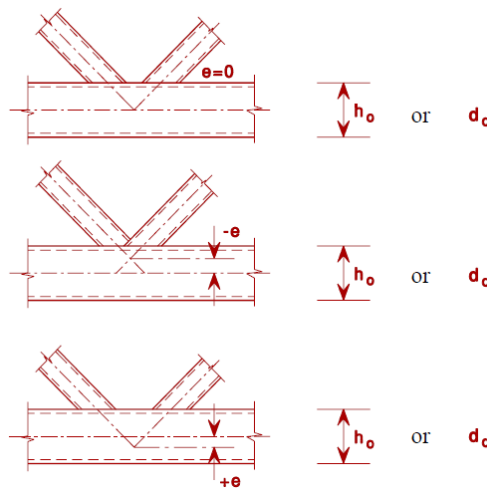


Figure 2.7: Eccentricity of joints [22].

Eurocode 3 [22] summarizes the cases where the moments should be taken into account in Table 2.2.

Table 2.2: Allowance for bending moments [22].

Type of component	Source of the bending moment		
	Secondary effects	Transverse loading	Eccentricity
Compression chord	Not if 5.1.5(3) is satisfied	Yes	Yes
Tension chord			No
Brace member			No
Joint			Not if 5.1.5(5) is satisfied

ii) Strength criteria

To be able to use the set of formulas present in Eurocode 3, to calculate the design axial resistance of welded joints, a set of conditions have to be fulfilled [22]:

- The cross-section of the members in compression should satisfy the Class 1 and Class 2 requirements for the condition of pure bending;
- The members meeting at a joint should keep their cross-section shape;
- The angle between adjacent brace members or between a chord and a brace should be, at the very least, 30°;
- If a joint is to have a gap, it has to be at least the sum of the thickness of the brace members in question ($t_1 + t_2$);
- In overlapped types of joints, to guarantee a proper transfer of shear force between brace members, the overlap should be at least 25%. When an overlapping brace member possesses a different thickness and/or a different strength grade, the member with the lowest $t_i f_{yi}$ value should overlap the other. If they have different widths, the narrower brace should overlap the wider one.

Figure 2.8 exemplifies one of the formulas available in EN 1993-1-8, in particular, for welded joints between a square or a circular hollow section.

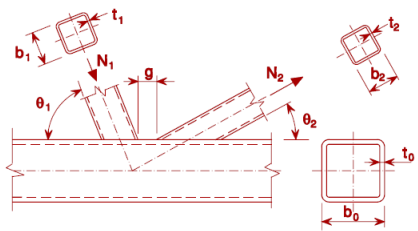
K and N gap joints	Chord face failure $\beta \leq 1,0$
	$N_{i,Rd} = \frac{8,9 \gamma^{0,5} k_n f_{y0} t_0^2 \left(\frac{b_1 + b_2}{2b_0} \right)}{\sin \theta_i} / \gamma_{M5}$

Figure 2.8: Formula for design axial resistance between square or circular hollow section [22].

iii) Deformation limit criteria

The joint strength, in hollow section joint research, is normally defined using the first maximum load in their respective load-deformation diagram. Lu *et al.* [24] and Yura *et al.* [25] proposed $0.03 d_0$ or b_0 as the deformation limit for the ultimate load capacity. For serviceability, a limit of $0.01 d_0$ or b_0 has shown to give acceptable deformations [19]. These values have been widely validated and adopted by other researchers [26, 27] and are represented in Figure 2.9.

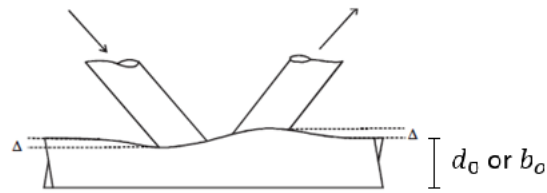


Figure 2.9: Chord surface deformation, Δ [28].

For joints that don't display defined load peaks in the load-deformation curve, the ultimate load can be obtained taking into account that [28]:

- If $\frac{N_u}{N_s} < 1.5$ then the ultimate limit controls the resistance;
- If $\frac{N_u}{N_s} \geq 1.5$ then the service limit controls the resistance.

This method is illustrated in Figure 2.10, where N_u is the ultimate load limit and N_s is the service load limit.

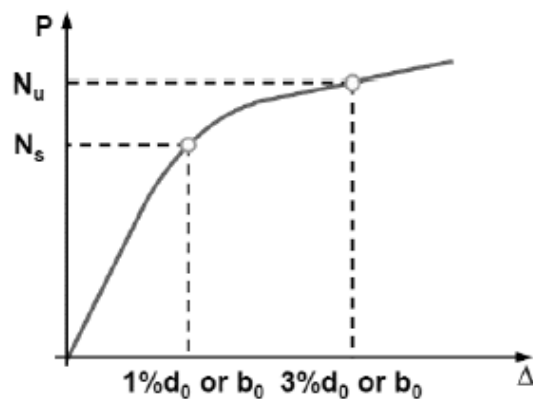


Figure 2.10: Deformation limit criteria applied in the load-displacement curve of a joint [28].

2.6 Experimental tests

The majority of the research made regarding truss joints focus on the behaviour of a particular joint instead of the overall performance of the truss [16]. Intending to probe the effect of two different reinforcing methods in strengthening the truss schematized in Figure 2.11, Yang *et al.* [16] carried out an experimental study on the static behaviour of a Warren truss with CHS members.

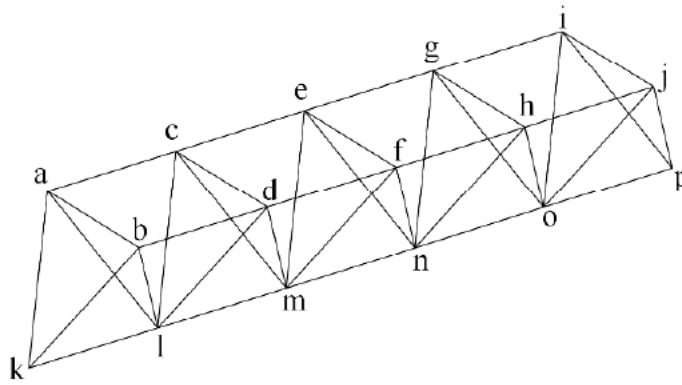


Figure 2.11: Layout of the 3D experimental tubular truss [16].

The specimens tested were:

- T-HN: A truss where the hidden part of the overlapped brace is not welded to the chord;
- T-HW: A truss where the hidden part of the overlapped brace is welded to the chord;
- TS-AS: A truss based on T-HN but strengthened by adding a half outer sleeve on each joint;
- TS-FC: A truss based on T-HN but strengthened by filling concrete into the top and bottom chord members.

The resulting midspan load-displacement curves of the bottom chord are displayed in Figure 2.12.

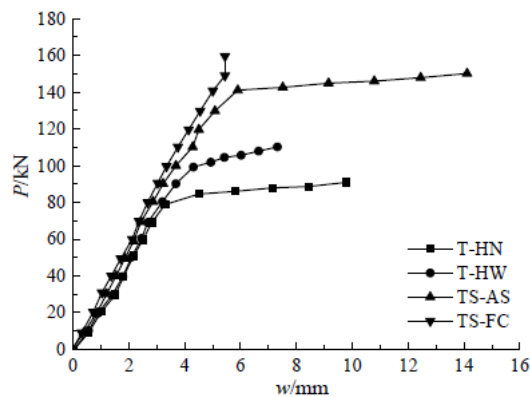


Figure 2.12: Midspan load-displacement curves [16].

The results indicate that reinforcing the top and bottom chords with concrete provides the highest increase of stiffness and resistance. Focusing on the steel only specimens, it is shown that the rigidity of a joint increases with the full welding of the joints and even more if it is reinforced with an outer sleeve. These results confirm that, by increasing the stiffness of the nodes, the global behaviour of the structure can be improved.

Previous experimental studies made in IST [40] covered CHS and SHS trusses with the new LASTEICON joints. Figure 2.13 is an example of one of the experimental tests carried out in the IST laboratory, LERM.



Figure 2.13: Experimental test on a Warren truss.

The results obtained will serve as a basis for the comparison and refinement of the numerical models in order to validate the parametric study carried out within the scope of this thesis.

2.7 Numerical modelling

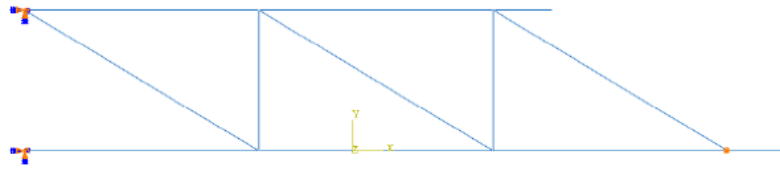
2.7.1 Models for truss girders

The Finite Elements Analysis (FEA) is a numerical technique, which for its diversity and flexibility as an analysis tool, is increasingly being adopted to solve complex engineering and scientific problems [29]. A powerful and widely used FEA tool, and the one being employed in this thesis, is ABAQUS.

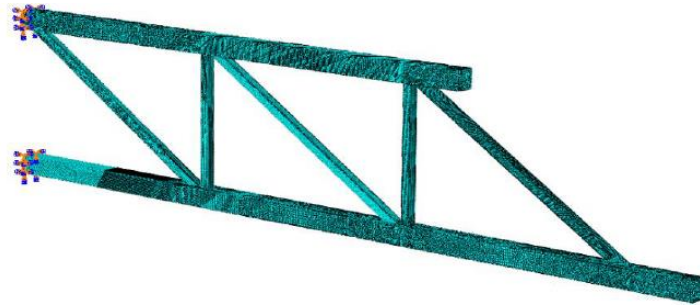
Depending on the accuracy required and calculation duration, Radić *et al.* [23] differentiate the following structural behaviour models:

- Beam model: simple and widely applicable, it allows conducting a linear and non-linear analysis. However, this type of modelling does not consider local effects in the joints;
- Truss space model: truss members are modelled with 3D shell elements. It is a highly accurate but complex model that includes global and local behaviour. Given the high computation demand is mostly used for research;
- Combined beam and truss space model: modelling approach where the joints are modelled by 3D shell elements and the other elements as beam elements. Doing so allows to decrease the complexity while keeping both global and local behaviour;
- Isolated joint model: model that only covers the local behaviour of a specific joint. Although the computational demand is low, the joints may not be influenced by the actual boundary conditions existing in the global model.

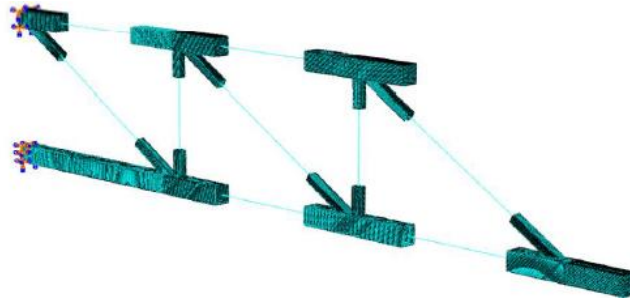
Figure 2.14 portrays the types of truss girder behaviour modelling described above.



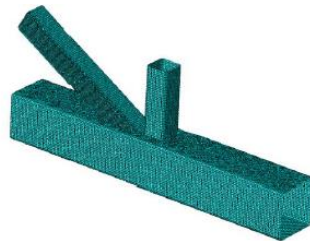
(a)



(b)



(c)



(d)

Figure 2.14: Types of numerical modelling of trusses [6] - (a) beam model; (b) truss space model; (c) combined beam and truss space model; (d) isolated joint model.

2.7.2 Finite elements

One way to model tubular members is to use shell elements. The adoption of quadrilateral shell elements over triangular elements is noted in many studies [30, 31, 32, 33] since they may suffer from shear locking and are limited to situations where the geometry of the element does not allow the use of

quadrilateral elements. As depicted in Figure 2.15, the internal angles for quadrilateral elements should be between 45° and 135° [34].

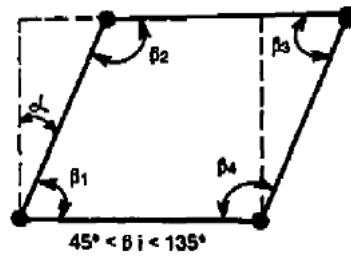


Figure 2.15: Angles for quadrilateral elements [34].

2.7.3 Mesh

In order to refine the mesh, it is possible to assign a different element type or divide the region into smaller sections to increase the number of elements.

It should be taken into account that refining a mesh always increases the computation time. Thus, it is important to do beforehand convergence studies to achieve the best ratio between the accuracy of the solution and computation time. Abambres and Arruda [34] suggest continuing the remeshing process until less than 5% difference in two consecutive analyses is achieved.

2.7.4 Welds

Some studies have been made without considering weld modelling [30], and Johansson and Löfberg [39] stated that if the weld has an adequate size and the same properties as the other truss members, then a failure in the weld can be neglected. Furthermore, Lie *et al.* [31] affirmed that only when the gap between braces is significantly wide does the increase in stiffness, due to the welds, is relevant to the joint's resistance and behaviour.

2.7.5 Material

One of the most common ways to express steel's plastic behaviour is by a bilinear diagram. As stated by Abambres and Arruda [34], perfectly plastic plateaus should be avoided when regarding the material stress-strain curve, for these could lead to numerical instability problems. Therefore, the literature on the subject [16, 35, 36, 37] suggests values between 1% and 5% of Young's Modulus to represent the linear strain-hardening.

Preliminary studies in the context of the LASTEICON project [5, 6, 7] adopted the value suggested in the Eurocode [38] for the linear strain-hardening, as illustrated in Figure 2.16.

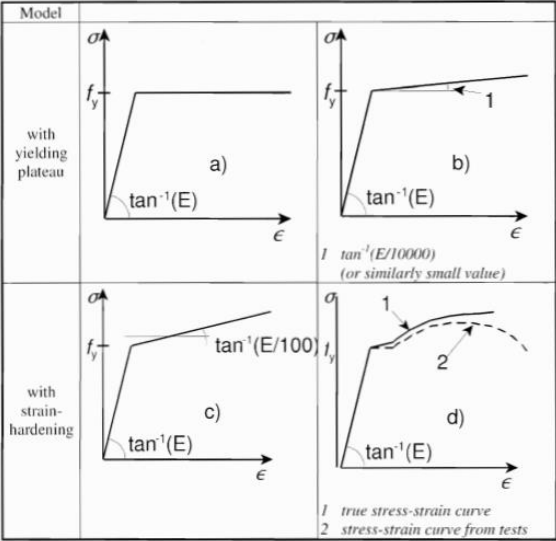


Figure 2.16: Modelling of material behaviour proposed in the Eurocode [38].

3 Experimental and numerical studies

3.1 Introduction

The two types of trusses, Subtrusses and Civil Trusses, tested in IST's laboratory and then modelled, are schematized in Table 3.1.

Subtrusses characterize by smaller chord and braces widths than Civil Trusses. Using the experimental tests to calibrate the FEM models, the research previously done as part of the LASTEICON project [41] concludes that if the braces have lower slenderness, then the behaviour of the critical node and the type of detail used does not influence the behaviour of the structure as much. Thus, as the Subtrusses do not represent the impacts that the new connections may have on the structure, it was opted to study the Civil trusses.

Table 3.1: Trusses studied - 16 Subtrusses and 9 Civil trusses.

Truss	Chord thickness [mm]	Cross-section	Truss type	Joint detail
Subtrusses	4	CHS / SHS	Pratt	R
				D1v
				D1d
	6.3	SHS	Warren	D2
				R
				D1
Civil Trusses	6.3	CHS	Pratt	D2
				Warren
				Warren with slope
	6.3	SHS	Pratt	D2
				Pratt with slope
				D2
			Warren	D1
				D2
				Warren with slope

The joint details designed are:

- D1: with the extension of one brace into the chord;
- D2: with the extension of half section of the two braces into the chord.

For Pratt trusses, two possibilities were considered for detail D1:

- D1v: where the prolonged brace was the vertical one;
- D1d: where the prolonged brace was the diagonal one.

As for Warren trusses, preliminary numerical studies [5] indicated that prolonging the brace with the smallest cross-section brings the most advantages. Some examples of this type of joints are displayed in Figure 3.1.

In both situations, a hole in the chord was made to allow the brace extension to cross the chord, as well as two slits in the chord's opposite face to insert two brace extrusions that allow the welding of the two members without any additional holes.

To evaluate their performance, numerical studies were made with regular joints (R) where the braces are simply welded to the chords face. Since this type of connection is the most common method to assemble hollow sections, its comparison with the innovative LASTEICON joints will allow perceiving the benefits of the LCT connection. This type of joint was always used in the connection between the trusses and the support structure.

Examples of the connections mentioned above are illustrated in Figure 3.1, and the braces extrusions can be viewed in Figure 3.2.

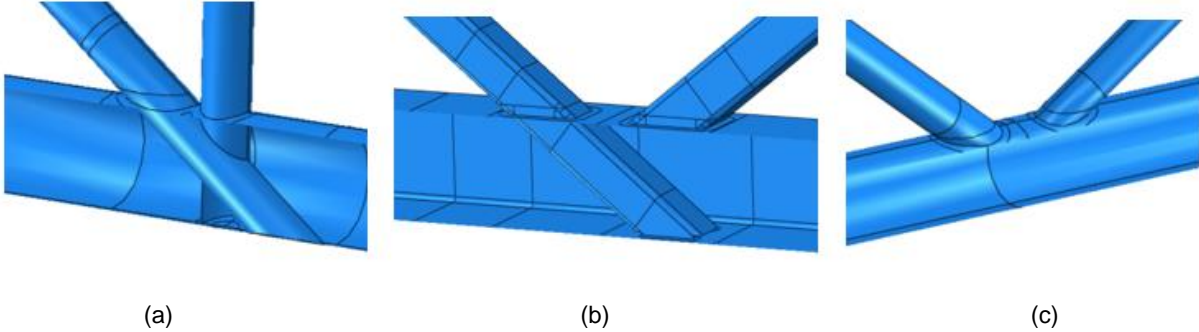


Figure 3.1: Examples of joint details - (a) CHS with D2 joint; (b) SHS with D1 joint; (c) CHS with R joint.

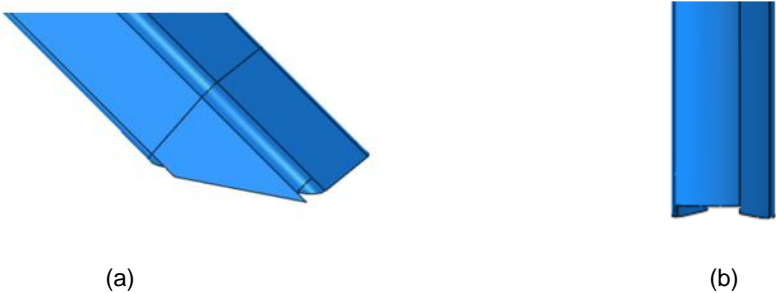


Figure 3.2: Extrusion of the braces - (a) SHS with D1 joint; (b) CHS with D1v joint.

To facilitate the identification of the trusses a classification was made, according to their differentiating characteristics:

- The first letter represents the type of truss: P for Pratt, PS if the Pratt truss as a slope, W for Warren and WS if the Warren truss as a slope;
- The second letter refers to the profile section: S for SHS and C for CHS;
- The last letter indicates the joint detail: R, D1v, D1d, D1 and D2.

The present thesis focuses on further developing the calibration of three numerically modelled Civil Trusses, previously studied, and illustrated in Figure 3.3. With the dimensions in mm, Figure 3.3 also indicates the type of joints applied to the connections between the members.

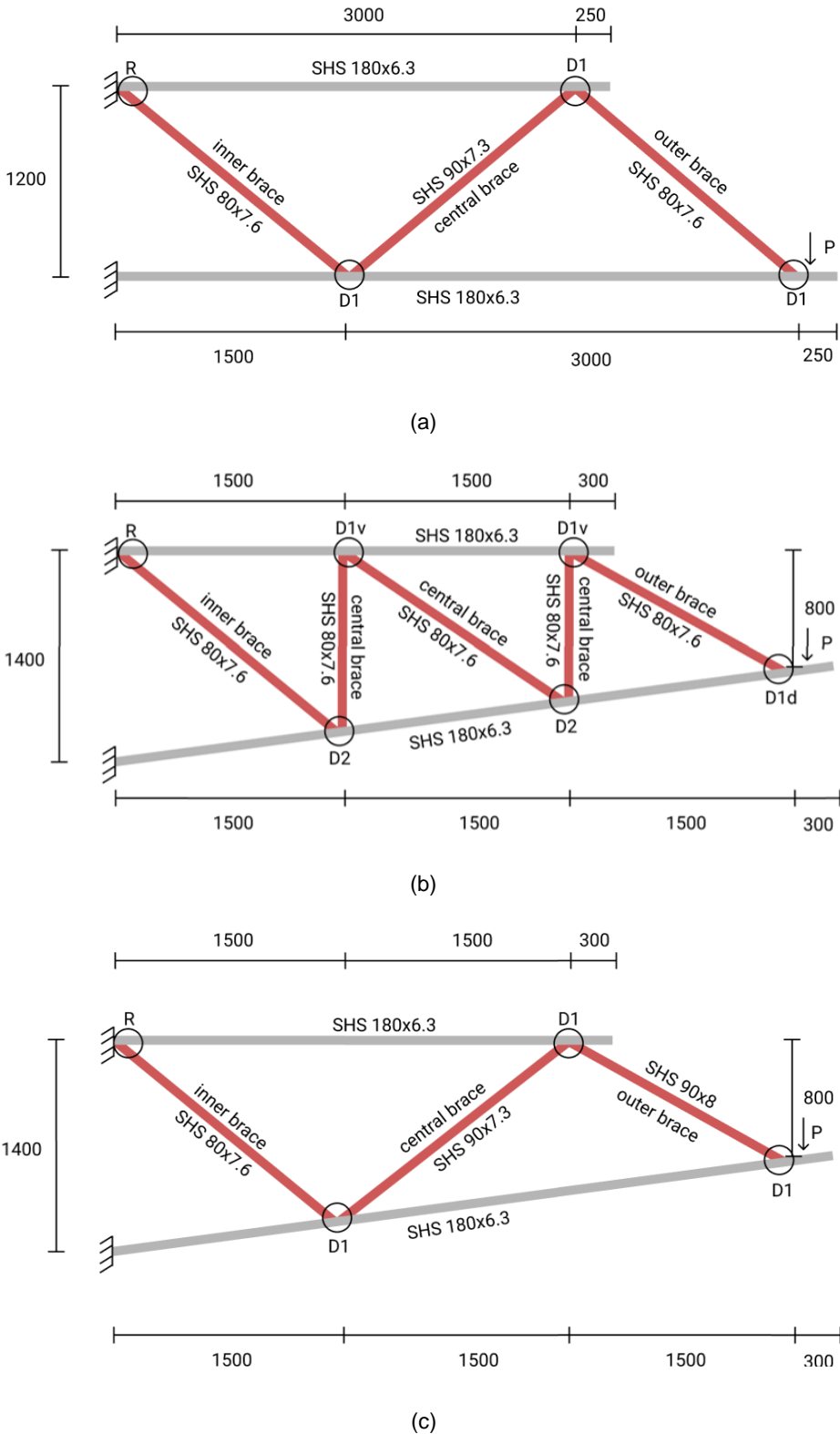


Figure 3.3: Models studied: (a) W_S_D1; (b) PS_S_D2; (c) W_S_D1.

3.2 Experimental studies

To be able to test the trusses in LERM, Structures and Strength of Materials Laboratory, a support structure was built [40]. The experimental setup can be viewed in Figure 3.4 (a). The support structure consists of:

- HEB300 and HEB400 columns;
- HEB300 and IPE600 upper beams;
- Out-of-plane prevention system, displayed in Figure 3.4 (b) and (c);
- Custom H columns;
- Reaction wall in reinforced concrete;
- Pre-stressed Dywidag rods that connect the structure to the reaction wall.

To better distribute the stresses and avoid prying forces, additional plates were welded on the truss's connection to the support structure. Figure 3.4 (c) depicts the load application section where another plate was welded to avoid local deformation.

Regarding the measuring equipment, twelve Linear Variable Differential Transformers (LVDT), present in Figure 3.4 (e), and two Strain Gauges, for each brace connecting in the critical node, were placed to [40]:

- Control the deformation of the support structure;
- Control the vertical and lateral displacement of the plates to identify the rigid rotation of the plates and truss.



(a)



(b)

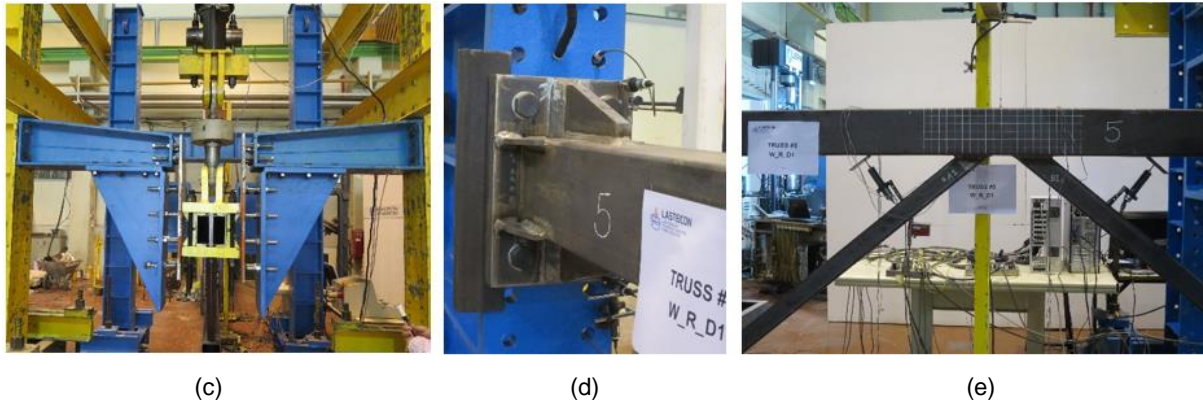


Figure 3.4: For the truss W_R_D1: (a) support structure; (b) out-of-plane prevention system; (c) out-of-plane prevention system in the load application section; (d) connection between the truss and the support structure; (e) LDVT positioning.

3.3 Numerical studies

As the previous IST researchers [5, 6, 7] involved in the LASTEICON project, ABAQUS CAE was the software used to create all numerical models. Before starting to define a model, a system of units must be chosen, and thus the set of units [N, mm] was used.

Material

A bilinear constitutive law was used to represent the non-linearity of the material in ABAQUS, with 0.01E for the strain-hardening, as suggested by Eurocode 3, Part 1-5.

In accordance with the tensile tests performed in a S355JR [42] to determinate the steel characteristics, in particular for SHS profiles, the values applied to the FEM models are depicted in Table 3.2. For the three FEM models in question the Poisson ratio and the density take the values of 0.3 and 7.85E-9 [ton/mm²], respectively. It is worth noting that the inner brace corresponds to the one closest to the fixed support and the outer diagonal to the one closest to the load application point.

Table 3.2: Material properties of the FEM models for ABAQUS.

Models	W_S_D1	WS_S_D1	PS_S_D2
<i>t</i> [mm]	Chords	6.3	
	Outer Brace	7.6	7.6
	Inner Brace		7.6
	Central Brace	7.3	7.6
<i>f_y</i> [MPa]	366		378
<i>f_u</i> [MPa]		519	
<i>E</i> [GPa]	210		220

When analysing Table 3.2, it is perceptible the different values for the modulus of elasticity, E. When performing the experimental tests for the model PS_S_D2 the results indicated a more rigid structure when compared to the other trusses, presumably due to pre-stressing, which prompted the adoption of

a higher modulus of elasticity. It is worth noting that the values for yield strength, f_y , and ultimate strength, f_u , are within the ranges of values obtained in the tensile tests carried out.

Accounting for the nonlinearity of the material, the type of analysis procedure used was Riks, which captures geometric nonlinearity, prior to buckling, as well as unstable post-buckling responses [33].

Boundary Conditions and applied displacement

A fixed support, represented in Figure 3.5, was used to model the connection between the truss and the support structure. The first approach to simulate this connection consisted of designing the connection plates, but it was later established that the results were consistent with using only the fixed boundary condition but at 250 mm from the extremity.

Following the testing method implemented for the experimental tests, an imposed displacement of 400 mm was introduced in the numerical models and is illustrated in Figure 3.5.

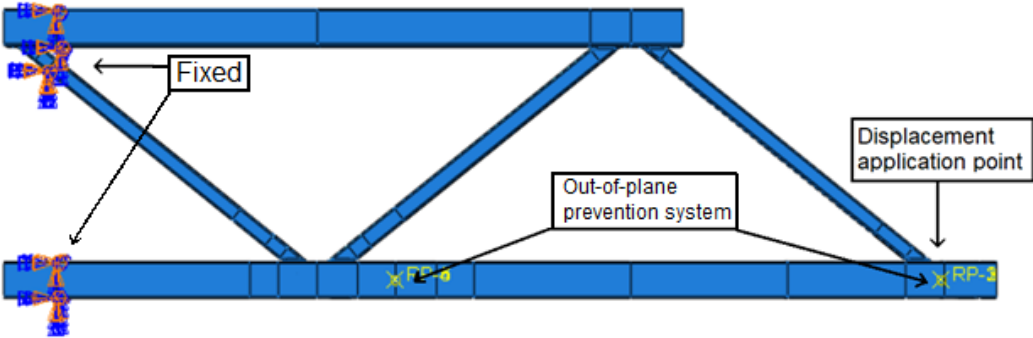


Figure 3.5: Displacement application point and lateral constraints.

The applied displacement is represented by a reference point, connected to the corresponding cross-section, with a kinematic coupling constraint, shown in Figure 3.6. In ABAQUS, this type of constraining restricts the motion of a set of nodes to the rigid body motion of the reference point [33].

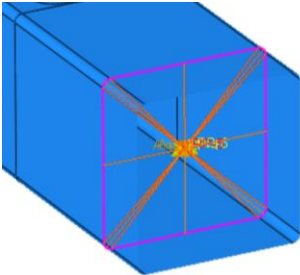


Figure 3.6: Kinematic coupling constrain.

Failure criteria

In order to guarantee the type of joint affects the strength and stiffness of the truss, the design assured the failure mechanism is located at the most stressed joint, as represented in Figure 3.7.

Considering the values proposed in the Literature review, the truss was designed so that the failure would occur when the deformation on the most stressed node reached 3% of the diameter of the chord. The alphabetically numbered nodes, in Figure 3.7, correspond to the out-of-plane prevention system.

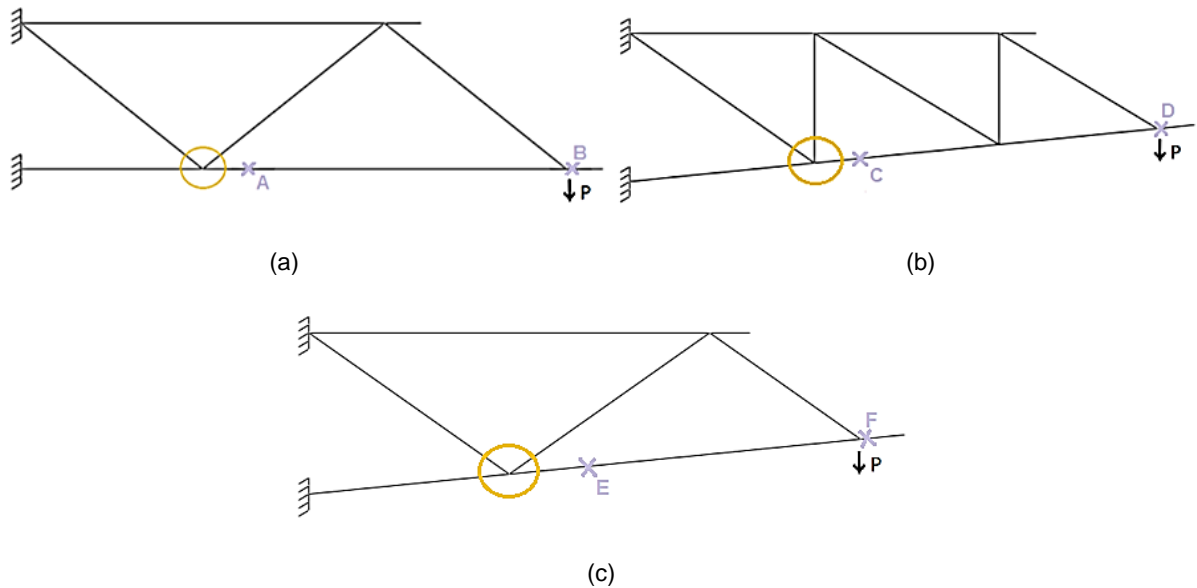


Figure 3.7: Most stressed joint: (a) W_R_D1; (b) PS_R_D2; (c) WS_R_D1.

Out-of-plane displacement prevention system

To simulate the out-of-plan prevention system created in the experimental tests, springs were added to the numerical models, in a reference point at the same location. The springs allowed the simulation of the gap between de truss and the prevention system, measured during the experimental study. The non-linear stiffness distribution of the springs used is represented in Figure 3.8, as well as the nodes where they were applied, perceptible in Figure 3.7.

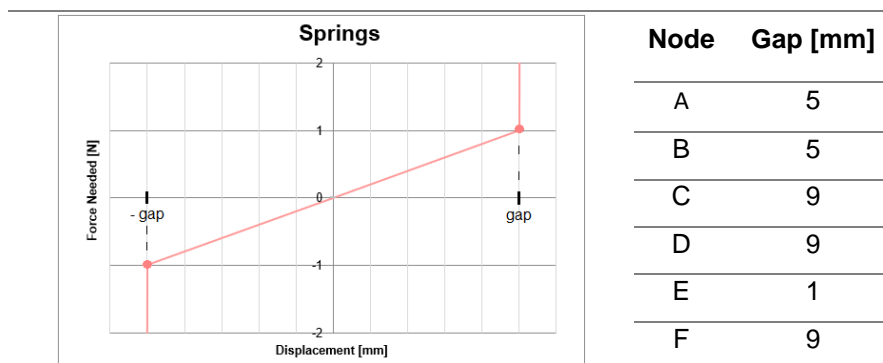


Figure 3.8: Spring model characteristics.

Initial out-of-plane displacement

After the installation of the trusses in the support structure, it was observed that these were not straight, as a result of an inclination or rotation. Thus, out-of-plane displacements were introduced in the models on specific reference points. Their values can be observed in Table 3.3. These out-of-plane displacements influence the failure mode of the truss since the compressed chord is more likely to

buckle under the secondary bending moments. It is noteworthy that the values displayed in Table 3.3 are applied gradually and incrementally, working towards the final solution. In these points the out-of-plane displacements will only reach the distance imposed by the modelled out-of-plane prevention system.

Table 3.3: Initial out-of-plane displacements.

Node	Horizontal [mm]	Vertical [mm]
A	0	0
B	0	0
C	200	0
D	300	500
E	200	0
F	200	0

Welds

The welding between the braces and the chords, exemplified in Figure 3.9, was simulated by partitioning the section around the connection of the elements and increasing its stiffness. Additionally, it shows the values used for all the numerical models, according to the technical catalogue of the welding material used.

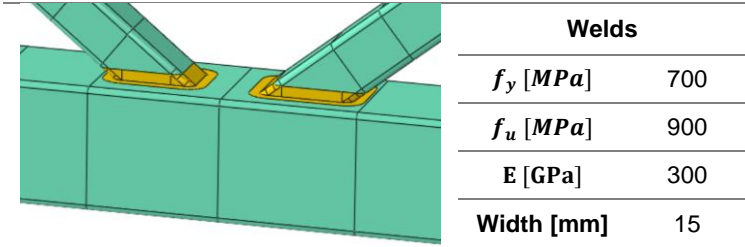
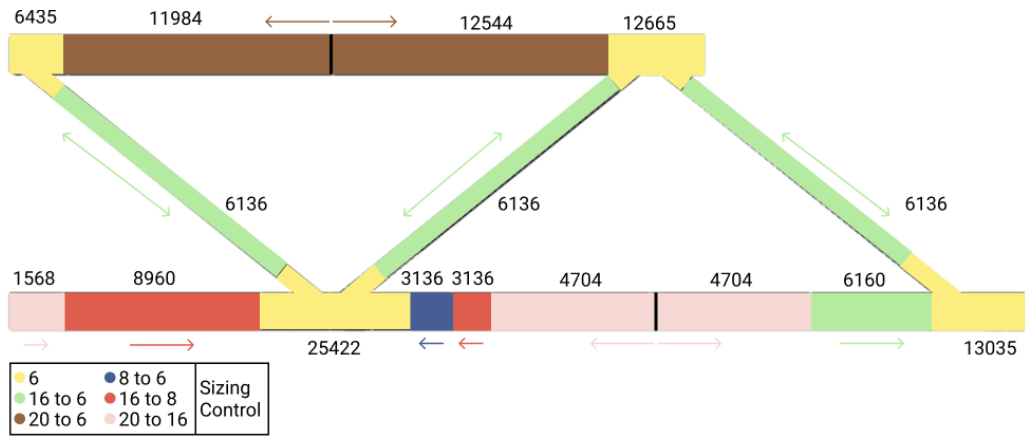


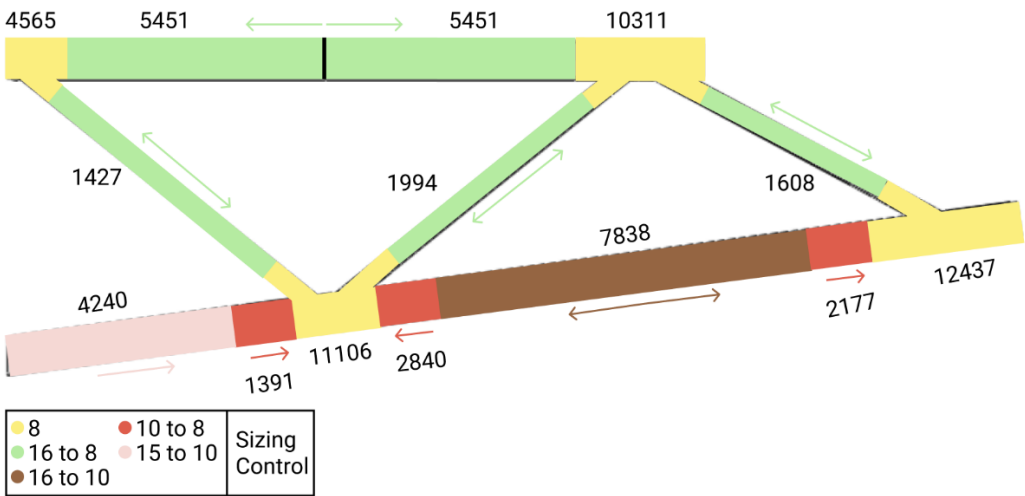
Figure 3.9: Weld model on a Warren joint and weld's characteristics.

Model Type / Mesh and type of element

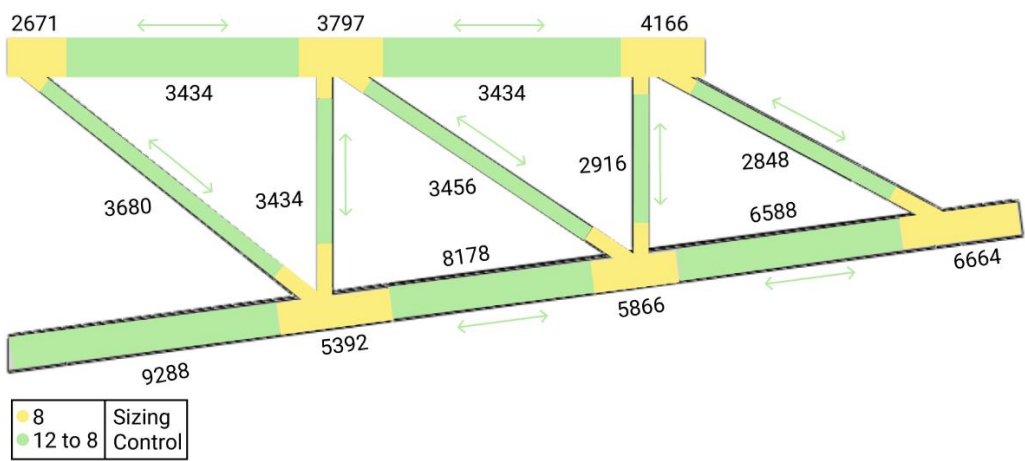
All the trusses mentioned were modelled with shell elements, decreasing stability problems during the analysis as well as achieving faster postprocessing. The elements are represented by their middle surface and the thickness of each element is later introduced when a section is assigned to an element [33]. A mesh convergence study was performed using an h-refinement where the number of elements is increased to achieve a finer mesh instead of changing the type of element. It was then opted to use S4R elements and refine the mesh in the areas with higher stresses gradients, namely in the joints. This way, a good ratio between computational time and solution precision is obtained, leading to approximately 6 hours of computational time. Figure 3.10 displays the number of elements and the sizing control applied to the models studied as well as the direction of its reduction in size and consequent increase in the number of elements. The geometry of the structure being assessed was considered in deciding the values in question.



(a)



(b)



(c)

Figure 3.10: Local element sizing control and number of elements for the model: (a) W_S_D1; (b) WS_S_D1; (c) PS_S_D2

History output

The output requested from the analysis are the Von Mises stress distribution of the entire model and the vertical displacement and force at the load application point.

3.4 Results from the analysis

The following subchapter presents the results of the deformed configuration, for both experimental and numerical tests, as well as their respective load-displacement curves. The referred displacement is the one measured at the point where the load is applied.

Truss W_S_D1

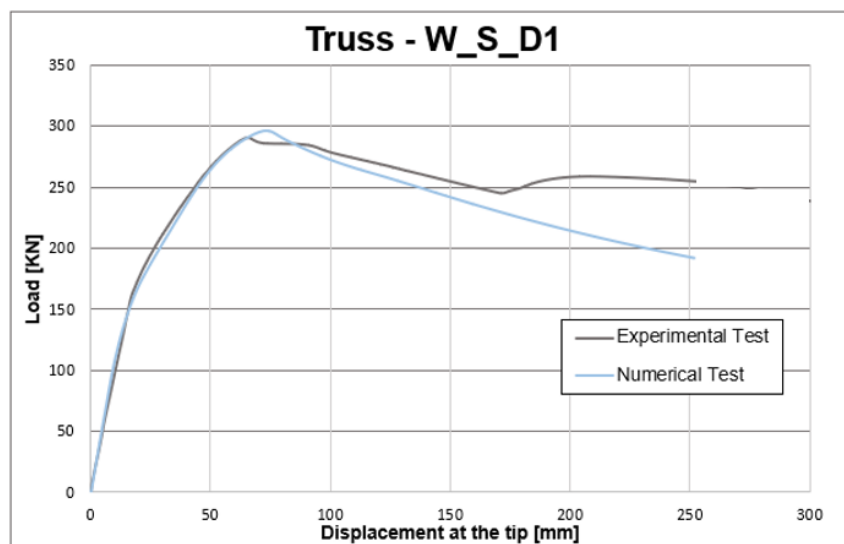
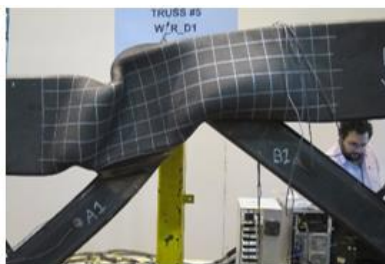
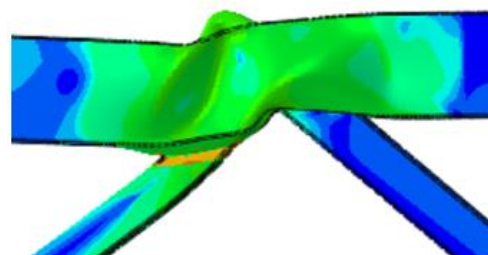


Figure 3.11: Load-displacement curves for W_S_D1 truss.

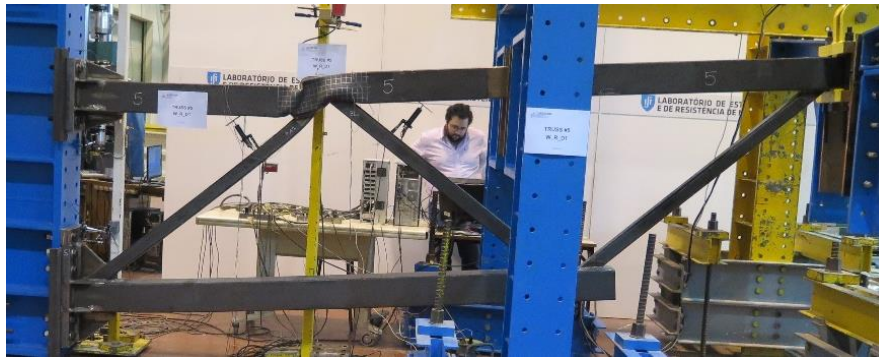


(a)

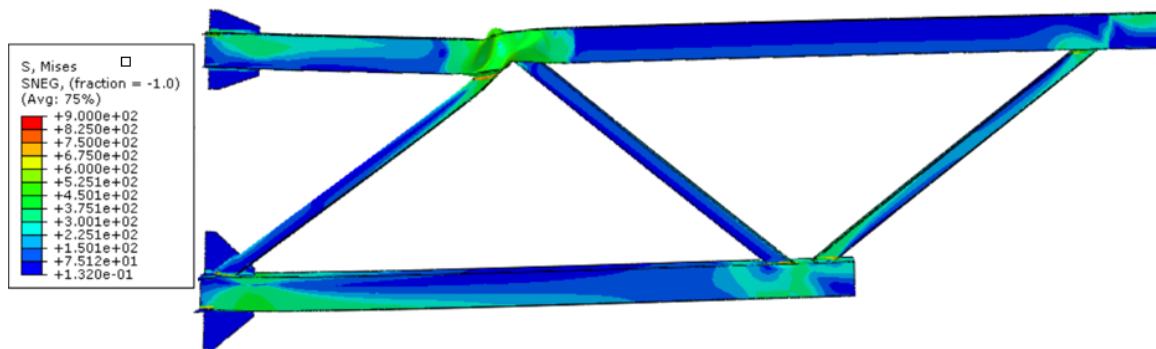


(b)

Figure 3.12: Critical joint deformation mode for W_S_D1 truss: (a) experimental test; (b) numerical simulation.



(a)



(b)

Figure 3.13: Truss W_S_D1 deformed configuration and Von Mises stress distribution: (a) experimental test; (b) numerical simulation.

Truss WS_S_D1

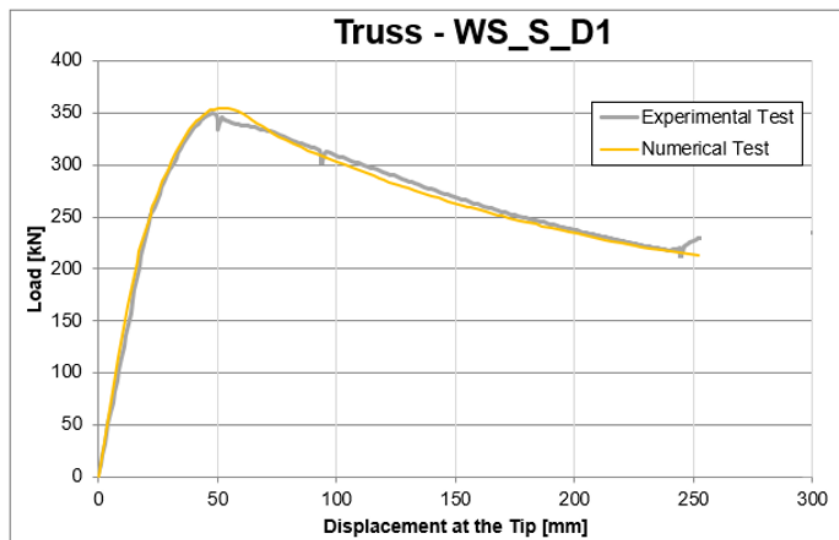


Figure 3.14: Load-displacement curves for WS_S_D1 truss.

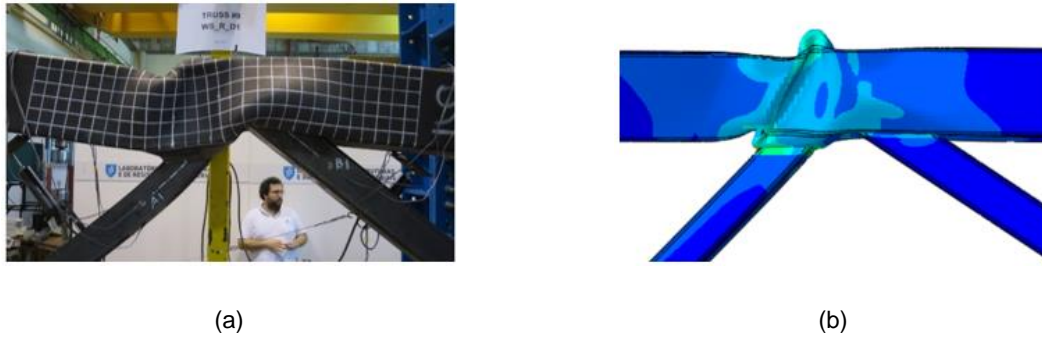
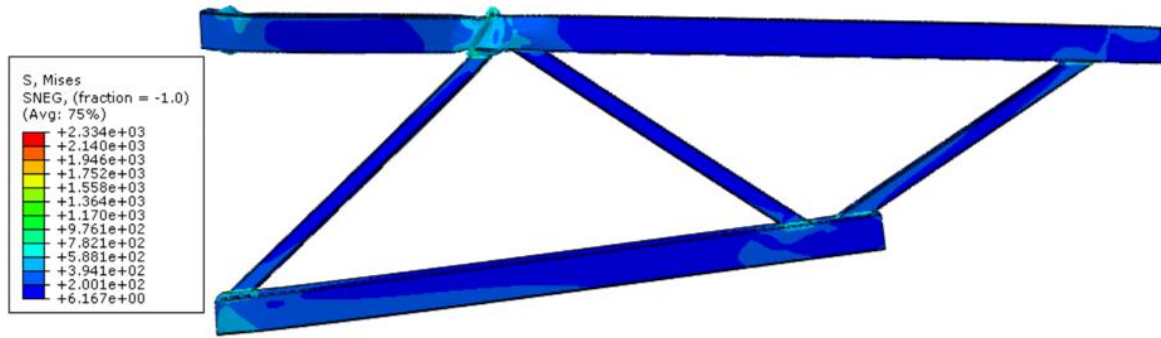


Figure 3.15: Critical joint deformation mode for WS_S_D1 truss: (a) experimental test; (b) numerical simulation.



(a)



(b)

Figure 3.16: Truss WS_S_D1 deformed configuration and Von Mises stress distribution: (a) experimental test; (b) numerical simulation.

Truss PS_S_D2

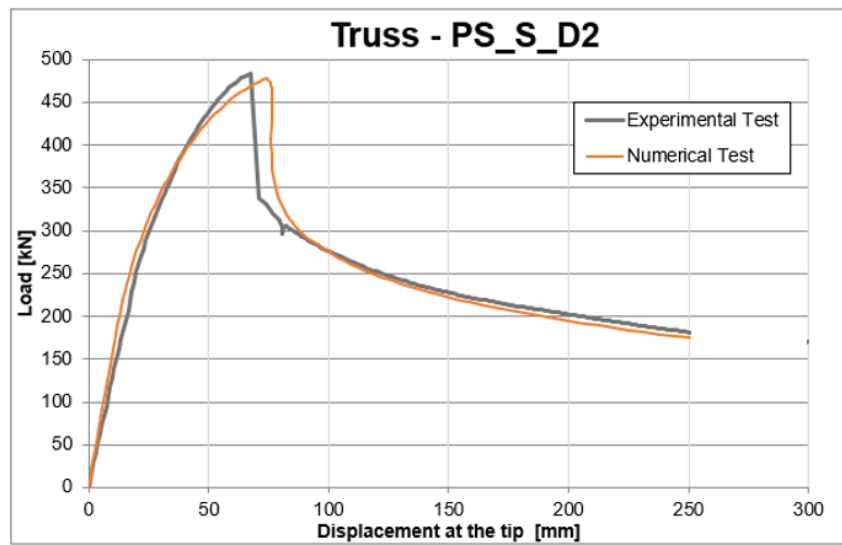
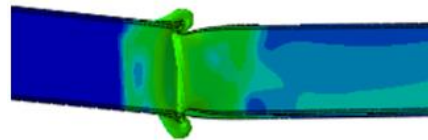


Figure 3.17: Load-displacement curves for PS_R_D2 truss.

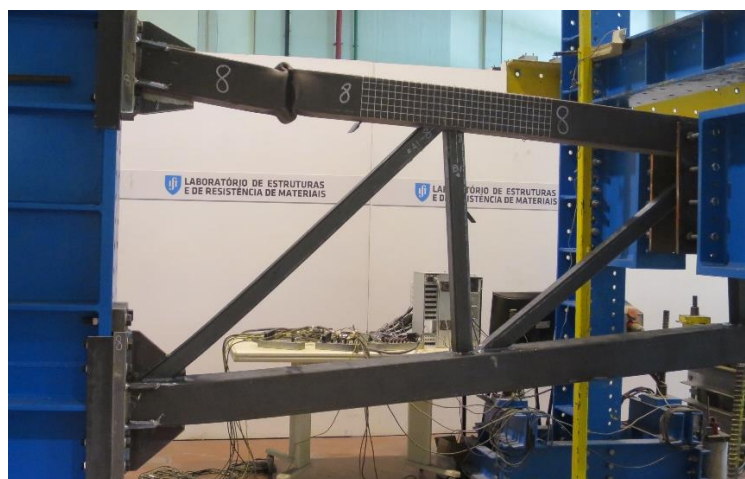


(a)



(b)

Figure 3.18: Detail of the deformation mode for PS_R_D2 truss: (a) experimental test; (b) numerical simulation.



(a)

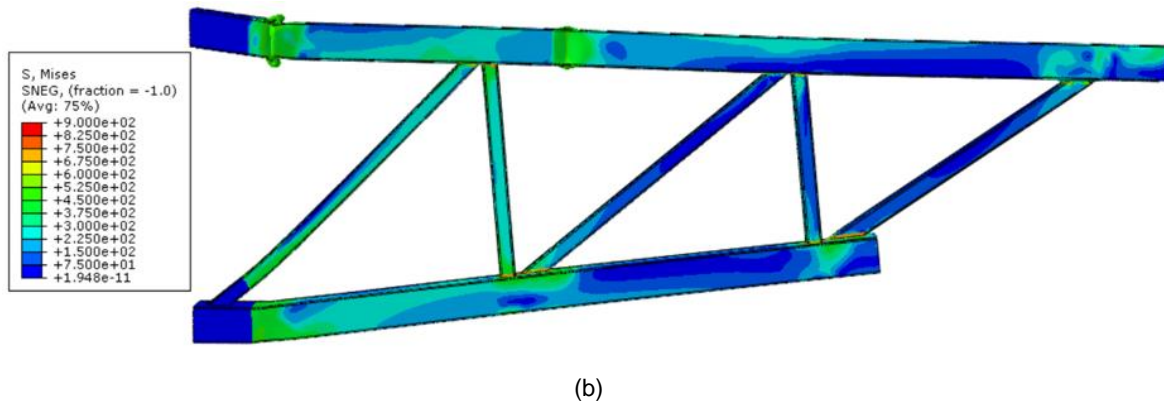


Figure 3.19: Truss PS_S_D2 deformed configuration and Von Mises stress distribution: (a) experimental test; (b) numerical simulation.

3.5 Comparison between experimental and numerical models

Comparing the results obtained and presented in the last subchapter regarding the trusses local and global behaviour, the similarity between the failure mode in the FEM models and the experimental tests is noticeable. Therefore, the numerical models predict with accuracy the behaviour of the critical node and the truss.

Looking in detail at Figures 3.11, 3.14 and 3.17, it is also observed that the numerical models give a reliable representation of the structure's stiffness and resistance.

For W_R_D1, the lack of contact in the numerical model resulted in it not capturing the increase in stiffness, after the peak load, of the experimental model. This feature was not introduced when modelling the trusses due to a high increase in computational time.

4 Parametric studies

4.1 Parameters in study

After the calibration of the three numerically modelled trusses mentioned in the previous chapter, a parametric study was carried out for the truss W_S_D1, consisting of SHS members and a D1 joint detail.

To choose the parameters to be analysed, the following equation, present in Eurocode 3 [22] to design the axial resistance of welded joints between SHS, was considered:

$$N_{i,Rd} = \frac{8,9\gamma^{0,5}k_n f_{y0} t_0^2}{\sin \theta_i} \left(\frac{b_1 + b_2}{2b_0} \right) / \gamma_{M5} \quad (4.1)$$

where:

- b_0 is the overall out-of-plane width of the chord;
- b_1 is the overall out-of-plane width of the brace in compression;
- b_2 is the overall out-of-plane width of the brace in tension;
- f_{y0} is the yield strength of a chord member;
- k_n is a factor defined in the Table 7.10 [22];
- t_0 is the wall thickness of the chord;
- θ_i is the included angle between brace member i and the chord ($i = 1, 2$ or 3);
- γ_{M5} is a partial safety factor for joints and is equal to 1 according to the National Annex;
- γ is the ratio of the chord width or diameter to twice its wall thickness.

Figure 4.1 [22] illustrates the parameters present in Equation 4.1 and Table 4.1 displays the models studied in the context of this thesis. It should be noted that the gap (g) between the brace members was chosen to be studied, instead of the angles between the chord and the braces, due to their mutual dependency.

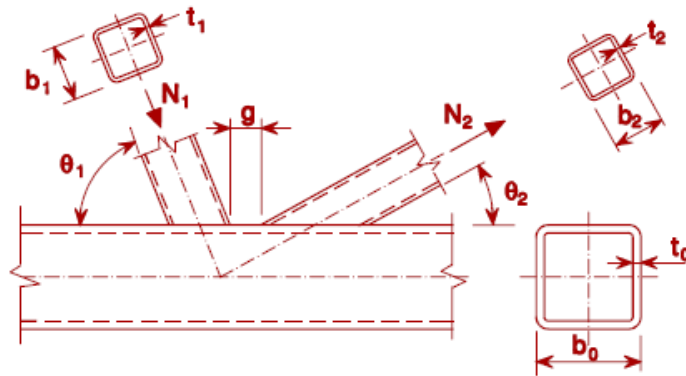


Figure 4.1: Parameters for K and N gap joints [22].

Table 4.1: Parameters in study.

Model	Parameters							
	g [mm]	θ_1 [°]	θ_2 [°]	f_{y0} [MPa]	t_0 [mm]	b_0 [mm]	b_1 [mm]	b_2 [mm]
D1_6.3_180_90_80_355_0	92.42	141.34	141.34	355	6.3	180	90	80
D1_5_180_90_80_355_0	92.42	141.34	141.34	355	5	180	90	80
D1_8_180_90_80_355_0	92.42	141.34	141.34	355	8	180	90	80
D1_6.3_140_90_80_355_0	92.42	141.34	141.34	355	6.3	140	90	80
D1_6.3_160_90_80_355_0	92.42	141.34	141.34	355	6.3	160	90	80
D1_6.3_200_90_80_355_0	92.42	141.34	141.34	355	6.3	200	90	80
D1_6.3_250_90_80_355_0	92.42	141.34	141.34	355	6.3	250	90	80
D1_5_140_90_80_355_0	92.42	141.34	141.34	355	5	140	90	80
D1_5_160_90_80_355_0	92.42	141.34	141.34	355	5	160	90	80
D1_5_200_90_80_355_0	92.42	141.34	141.34	355	5	200	90	80
D1_8_160_90_80_355_0	92.42	141.34	141.34	355	8	160	90	80
D1_8_200_90_80_355_0	92.42	141.34	141.34	355	8	200	90	80
D1_6.3_180_60_80_355_0	92.42	141.34	141.34	355	6.3	180	60	80
D1_6.3_180_80_80_355_0	92.42	141.34	141.34	355	6.3	180	80	80
D1_6.3_180_100_80_355_0	92.42	141.34	141.34	355	6.3	180	100	80
D1_5_180_80_80_355_0	92.42	141.34	141.34	355	5	180	80	80
D1_5_180_100_80_355_0	92.42	141.34	141.34	355	5	180	100	80
D1_8_180_80_80_355_0	92.42	141.34	141.34	355	8	180	80	80
D1_8_180_100_80_355_0	92.42	141.34	141.34	355	8	180	100	80
D1_6.3_180_90_70_355_0	92.42	141.34	141.34	355	6.3	180	90	70
D1_6.3_180_90_90_355_0	92.42	141.34	141.34	355	6.3	180	90	90
D1_5_180_90_70_355_0	92.42	141.34	141.34	355	5	180	90	70
D1_5_180_90_90_355_0	92.42	141.34	141.34	355	5	180	90	90
D1_8_180_90_70_355_0	92.42	141.34	141.34	355	8	180	90	70
D1_8_180_90_90_355_0	92.42	141.34	141.34	355	8	180	90	90
D1_6.3_180_90_80_235_0	92.42	141.34	141.34	235	6.3	180	90	80
D1_6.3_180_90_80_275_0	92.42	141.34	141.34	275	6.3	180	90	80
D1_6.3_180_90_80_420_0	92.42	141.34	141.34	420	6.3	180	90	80
D1_6.3_180_90_80_460_0	92.42	141.34	141.34	460	6.3	180	90	80
D1_5_180_90_80_235_0	92.42	141.34	141.34	235	5	180	90	80
D1_5_180_90_80_275_0	92.42	141.34	141.34	275	5	180	90	80
D1_5_180_90_80_420_0	92.42	141.34	141.34	420	5	180	90	80
D1_5_180_90_80_460_0	92.42	141.34	141.34	460	5	180	90	80
D1_8_180_90_80_235_0	92.42	141.34	141.34	235	8	180	90	80
D1_8_180_90_80_275_0	92.42	141.34	141.34	275	8	180	90	80
D1_8_180_90_80_420_0	92.42	141.34	141.34	420	8	180	90	80
D1_8_180_90_80_460_0	92.42	141.34	141.34	460	8	180	90	80
D1_6.3_180_90_80_355_40	130.54	39.04	39.04	355	6.3	180	90	80
D1_6.3_180_90_80_355_80	168.66	39.42	39.42	355	6.3	180	90	80
D1_6.3_180_90_80_355_120	206.76	39.81	39.81	355	6.3	180	90	80
D1_5_180_90_80_355_40	132.15	39.04	39.04	355	5	180	90	80
D1_5_180_90_80_355_80	170.24	39.42	39.42	355	5	180	90	80
D1_8_180_90_80_355_40	128.45	39.04	39.04	355	8	180	90	80
D1_8_180_90_80_355_80	166.59	39.42	39.42	355	8	180	90	80
D1_6.3_250_90_80_355_80	261.49	39.42	39.42	355	6.3	250	90	80
D2_6.3_180_90_80_355_80	168.66	39.42	39.42	355	6.3	180	90	80
D2_6.3_250_90_80_355_80	261.49	39.42	39.42	355	6.3	250	90	80
D2_8_180_90_80_355_80	166.59	39.42	39.42	355	8	180	90	80

The equivalent of the Table 4.1 has also been studied, but for an R joint detail instead of a D1 joint. To have a better perception of the parameters present in the models under study, their identification organises as follows:

- The first parameter identifies the joint detail in analysis;
- The second one refers to the thickness of the chord in compression, t_o ;
- The third relates to width of the chord in compression, b_o ;
- The fourth addresses the width of the brace in compression, b_1 ;
- The fifth parameter depicts the width of the brace in tension, b_2 ;
- The sixth refers to the yield strength of the chord, f_{y0} , that will be the same for the entire truss;
- The last parameter designates eccentricity between the brace's axis, e .

Overall, the parameters studied correspond to the catalogued dimensions bellow and above the ones from the initial model, D1_6.3_180_90_80_355_0. For the study of the effect of the yield strength, the values used are the ones present in EC3-1-1 for hot rolled structural steel.

A D2 joint detail was employed in three models, with an 80 mm gap, to ascertain the influence of the increased joint rigidity in the truss, along with attaining a comparison of the performance between the three joint details covered in the context of this thesis.

In contrast to Chapter 3, in the parametric study the dimensions of the profiles were obtained directly from the Celsius catalogue [43]. Figure 4.2 shows the profile dimensions of a generic truss used to model the cases studied and displayed in Table 4.1.

The initial out-of-plane displacements applied to all the models were an average of the values used in the three trusses calibrated in Chapter 3 and modelled in the same manner. Table 4.2 illustrates the values applied in the nodes A and B, outlined in Figure 4.2. Regarding the parametric study for the yield strength of the chord, the steel characteristics used can be viewed in Table 4.3.

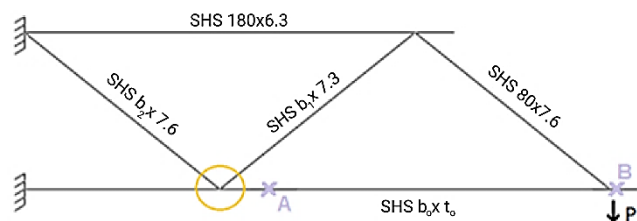


Figure 4.2: Warren truss studied.

Table 4.2: Initial out-of-plane displacement for the parametric studies.

Node	Horizontal [mm]	Vertical [mm]
A	167	167
B	167	0

Table 4.3: Steel properties for ABAQUS.

	S355	S235	S275	S420	S460
f_y [MPa]	355	235	275	420	460
f_u [MPa]	510	360	430	540	560
ϵ	0.07381	0.05952	0.07381	0.05714	0.04762
E [GPa]	210				
ρ [ton/mm ²]	7.85E-9				
ν	0.3				

4.2 Results from the analysis

The present subchapter displays the load-displacement curves of the parametric numerical studies and the deformation of the critical joint, except when the failure mode differs. The global truss deformation for the models and the Von Mises stress distribution values, in MPa, can be consulted in Annex I. A cut of the chord at the critical node is also presented in Appendix I, II and III in order to have a more accurate perception of the deformation of the braces inside the chord.

4.2.1 Parameter: t_0

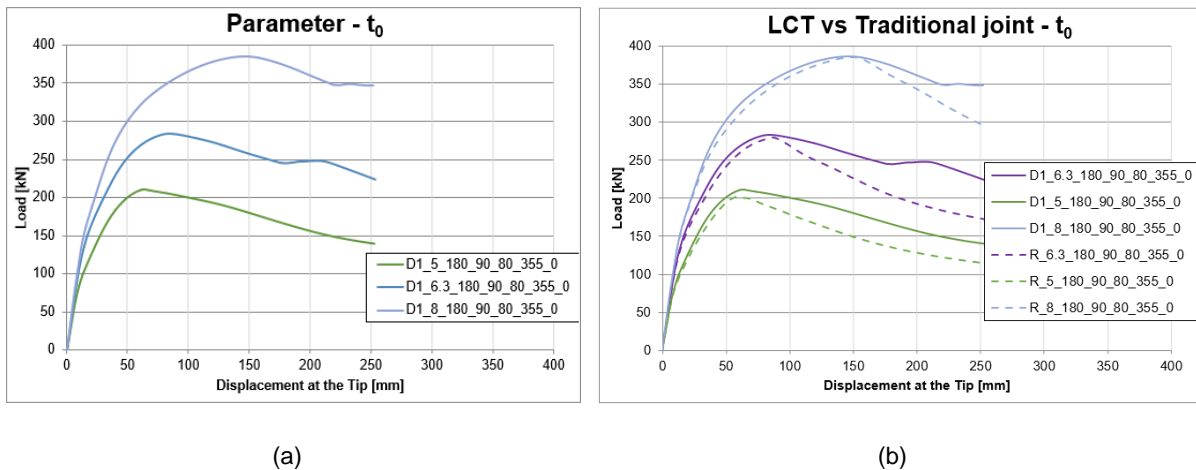


Figure 4.3: Load-displacement curve for: (a) t_0 parameter study; (b) comparison between D1 and R for the t_0 parameter study.

As perceptible in Figure 4.3 (a), the greater the area of the inferior chord, the higher the maximum load and the greater the stiffness of the structure. From Figure 4.3 (b), when compared to a regular detail, it is observed that a D1 detail has little impact on the global resistance of the truss. However, the decrease in chord thickness leads to an increase in the influence the type of detail has on the truss resistance,

going from a 0.22% to 4.36% difference for the peak load, with a chord with a thickness of 8 mm and 5 mm, respectively. For a thickness of 6.3 mm, the peak load increases 1.45%.

- *Model D1_6.3_180_90_80_355_0 vs R_6.3_180_90_80_355_0*



Figure 4.4: Critical joint deformation for $t_0 = 6.3$ mm.

- *Model D1_5_180_90_80_355_0 vs R_5_180_90_80_355_0*



Figure 4.5: Critical joint deformation for $t_0 = 5$ mm.

- *Model D1_8_180_90_80_355_0 vs R_8_180_90_80_355_0*



Figure 4.6: Critical joint deformation for $t_0 = 8$ mm.

Observing the deformations present in Figures 4.4, 4.5 and 4.6, it is noticeable the improvement of the joint behaviour for the trusses with a D1 detail. With decreasing thickness, there is an increase in the deformation susceptibility of the chord.

4.2.2 Parameter: b_0

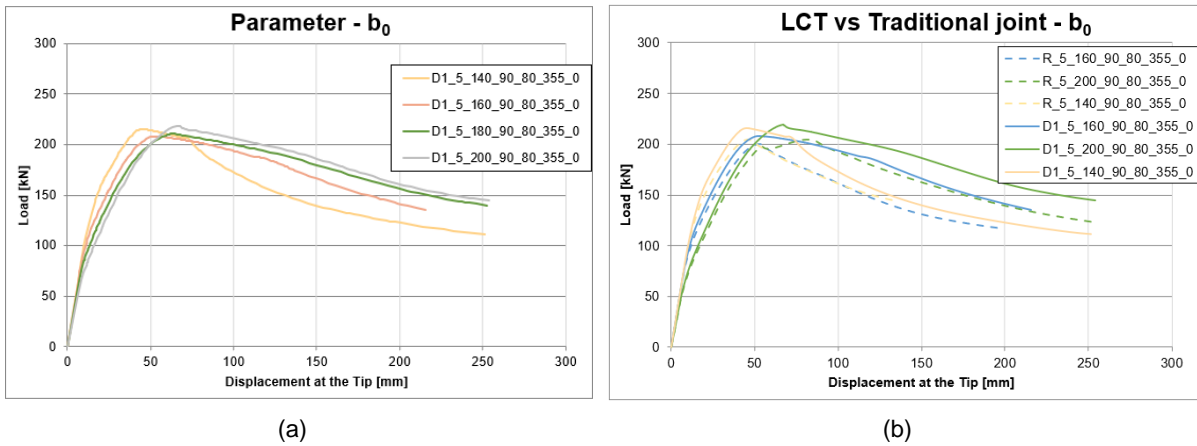


Figure 4.7: Load-displacement curve for $t_0 = 5$ mm: (a) b_0 parameter study; (b) comparison between D1 and R for the b_0 parameter study.

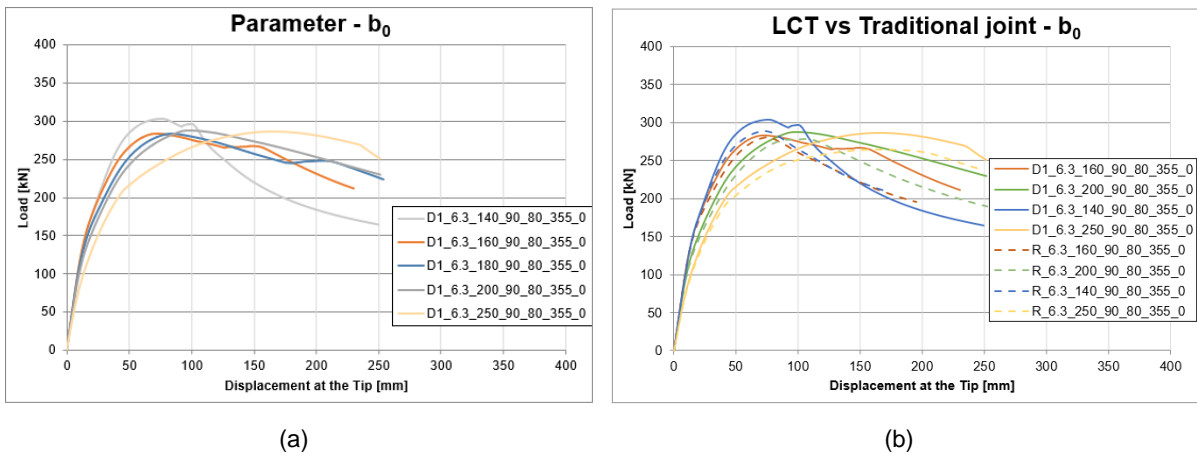


Figure 4.8: Load-displacement curve for $t_0 = 6.3$ mm: (a) b_0 parameter study; (b) comparison between D1 and R for the b_0 parameter study.

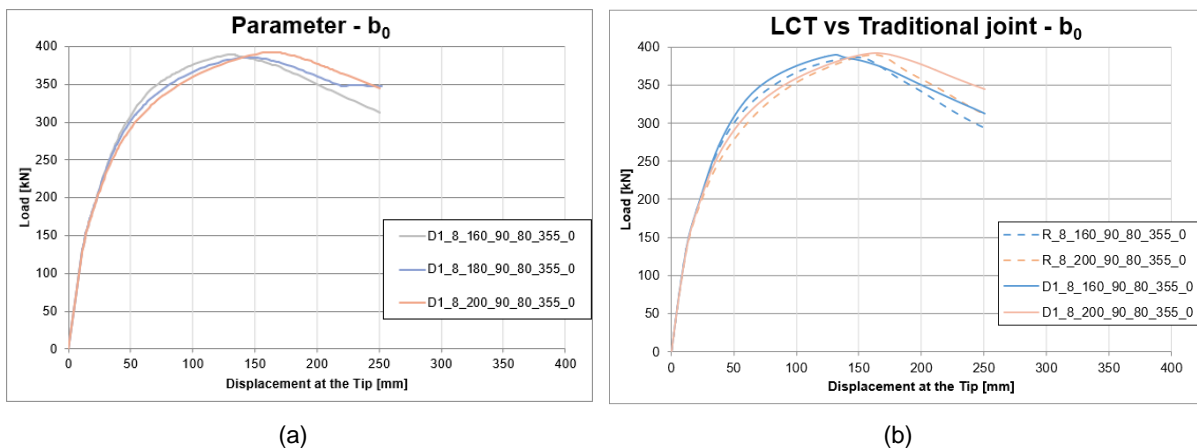


Figure 4.9: Load-displacement curve for $t_0 = 8$ mm: (a) b_0 parameter study; (b) comparison between D1 and R for the b_0 parameter study.

Figures 4.7 (a), 4.8 (a) and 4.9 (a) indicate that varying the chord's width does not have a significant influence on the peak load of the truss. However, as the width decreases, there is an increase in the stiffness of the truss, less notable for a chord thickness of 8 mm. As mentioned previously, Figures 4.7 (b), 4.8 (b) and 4.9 (b) show that a D1 detail has little influence on the global resistance of the truss. Still, the decrease in chord's thickness increases the difference between the details D1 and R performance. Table 4.4 displays the increase in peak load from a regular connection to a connection with a D1 detail.

Table 4.4: Parameter b_0 - peak load increase, in percentage, from a regular detail to a D1 detail.

	b_0 [mm]					
	140	160	180	200	250	
Chord's thickness [mm]	5	5.17	3.98	4.36	7.18	-
	6.3	5.00	1.12	1.45	3.22	8.14
	8	-	0.86	-1.03	0.77	-

- Model *D1_6.3_140_90_80_355_0* vs *R_6.3_140_90_80_355_0*



Figure 4.10: Critical joint deformation for $b_0 = 140$ mm and $t_0 = 6.3$ mm.

- Model *D1_6.3_160_90_80_355_0* vs *R_6.3_160_90_80_355_0*



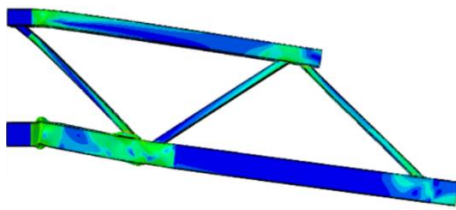
Figure 4.11: Critical joint deformation for $b_0 = 160$ mm and $t_0 = 6.3$ mm.

- Model *D1_6.3_200_90_80_355_0* vs *R_6.3_200_90_80_355_0*

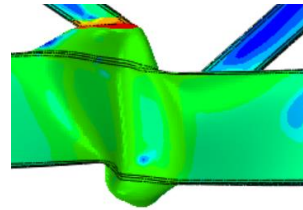


Figure 4.12: Critical joint deformation for $b_0 = 200$ mm and $t_0 = 6.3$ mm.

- *Model D1_6.3_250_90_80_355_0 vs R_6.3_250_90_80_355_0*



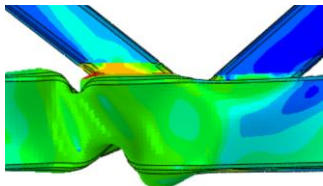
D1_6.3_250_90_80_355_0



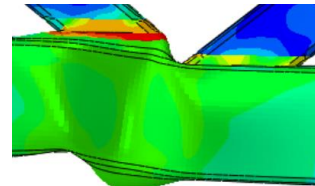
R_6.3_250_90_80_355_0

Figure 4.13: Truss deformation and critical joint deformation for $b_0 = 250$ mm and $t_0 = 6.3$ mm.

- *Model D1_5_140_90_80_355_0 vs R_5_140_90_80_355_0*



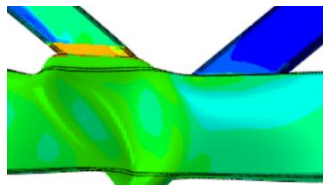
D1_5_140_90_80_355_0



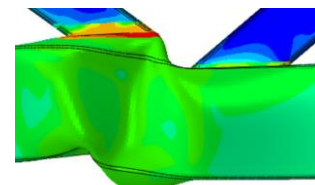
R_5_140_90_80_355_0

Figure 4.14: Critical joint deformation for $b_0 = 140$ mm and $t_0 = 5$ mm.

- *Model D1_5_160_90_80_355_0 vs R_5_160_90_80_355_0*



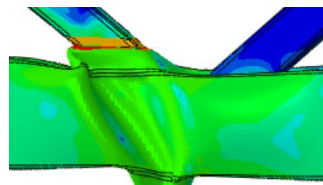
D1_5_160_90_80_355_0



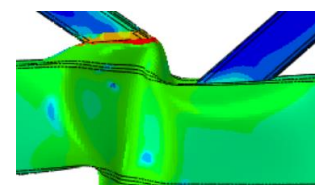
R_5_160_90_80_355_0

Figure 4.15: Critical joint deformation for $b_0 = 160$ mm and $t_0 = 5$ mm.

- *Model D1_5_200_90_80_355_0 vs R_5_200_90_80_355_0*



D1_5_200_90_80_355_0



R_5_200_90_80_355_0

Figure 4.16: Critical joint deformation for $b_0 = 200$ mm and $t_0 = 5$ mm.

- Model *D1_8_160_90_80_355_0* vs *R_8_160_90_80_355_0*

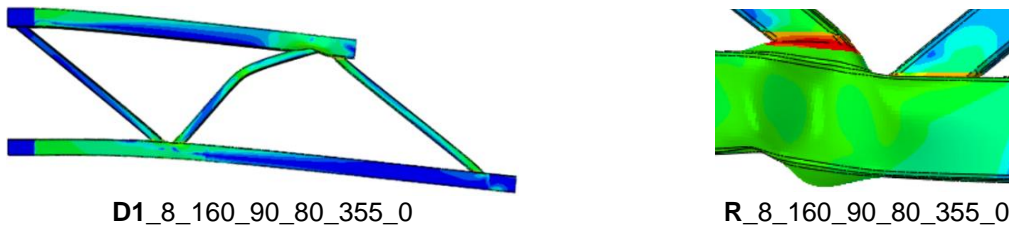


Figure 4.17: Truss deformation and critical joint deformation for $b_0 = 160$ mm and $t_0 = 8$ mm.

- Model *D1_8_200_90_80_355_0* vs *R_8_200_90_80_355_0*



Figure 4.18: Critical joint deformation for $b_0 = 200$ mm and $t_0 = 8$ mm.

The deformations present in Figures 4.10 to Figure 4.18 depict the improvement of the joint behaviour for the trusses with a D1 detail. In the majority of the models, the failure mode occurs in the critical node. The few exceptions include the models *D1_5_140_90_80_355_0* and *D1_6.3_140_90_80_355_0*, where the failure mode consisted of the local buckling of the chord in the proximity of the critical node. Meanwhile, in the model *D1_6.3_250_90_80_355_0*, the failure mode occurred near the fixed support and for *D1_8_160_90_80_355_0* in the compressed brace.

4.2.3 Parameter: b_1

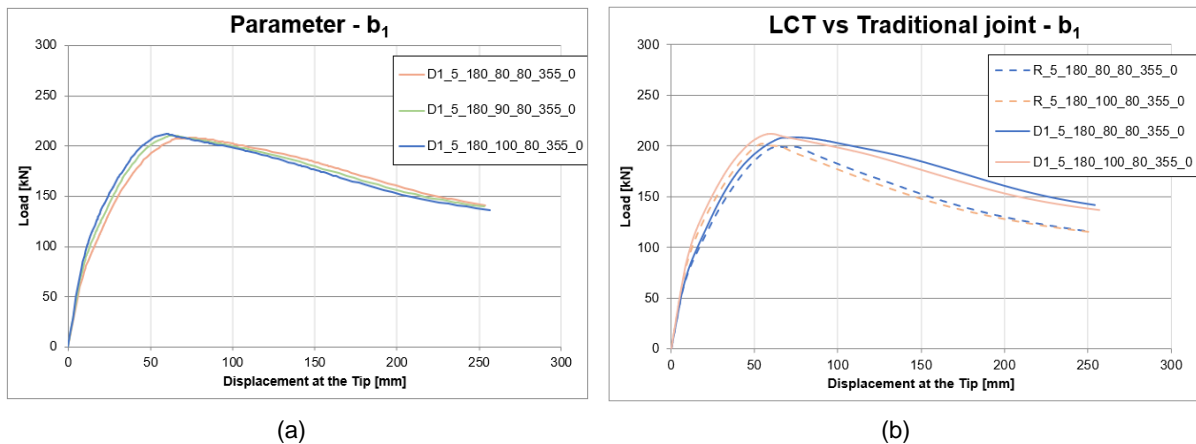


Figure 4.19: Load-displacement curve for $t_0 = 5$ mm: (a) b_1 parameter study; (b) comparison between D1 and R for the b_1 parameter study.

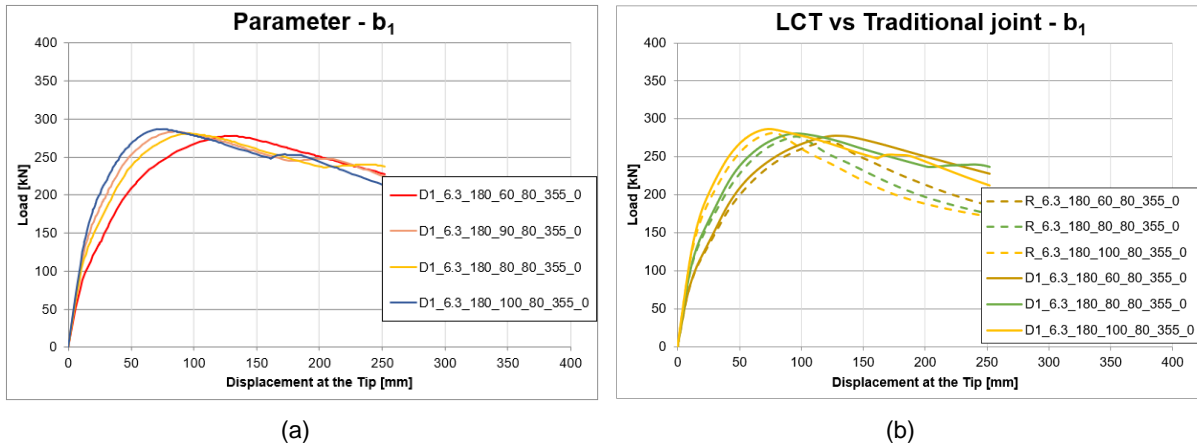


Figure 4.20: Load-displacement curve for $t_0 = 6.3$ mm: (a) b_1 parameter study; (b) comparison between D1 and R for b_1 parameter study.

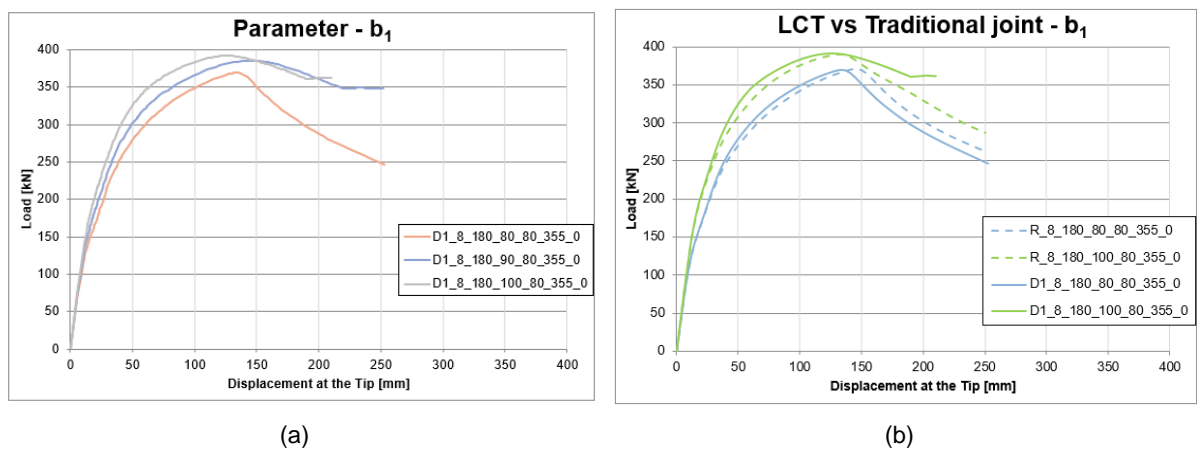


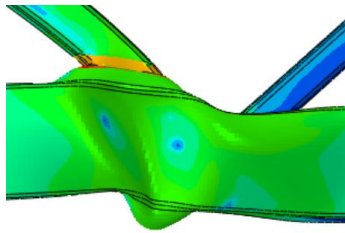
Figure 4.21: Load-displacement curve for $t_0 = 8$ mm: (a) b_1 parameter study; (b) comparison between D1 and R for b_1 parameter study.

With the increase in the width of the compressed brace, for a chord thickness of 5 mm and 6.3 mm, Figures 4.19 (a), 4.20 (a) and 4.21 (a) show that this parameter does not significantly affect the global resistance of the truss. Figure 4.21 (a) indicates a decrease in peak load for the smaller value of the brace width although, it must be considered that the failure mode was the buckling of the brace. Consistently with the analysis of the previous parameters, Figures 4.19 (b), 4.20 (b) and 4.21 (b) show that changing the detail does not have a lot of influence on the global resistance of the truss. Table 4.5 displays the increase in peak load from a regular connection to a connection with a D1 detail. Regarding the global rigidity of the models, decreasing the width of the compressed brace causes a decrease of rigidity.

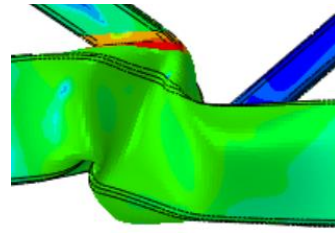
Table 4.5: Parameter b_1 - peak load increase, in percentage, from a regular detail to a D1 detail.

	b_1 [mm]		
	60	80	100
Chord's thickness [mm]	5	-	4.30
	6.3	2.65	1.56
	8	-	-0.33

- *Model D1_6.3_180_60_80_355_0 vs R_6.3_180_60_80_355_0*



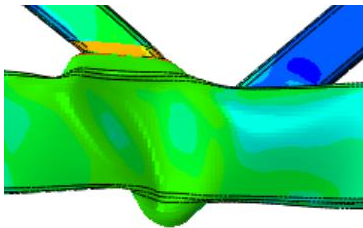
D1_8_180_60_80_355_0



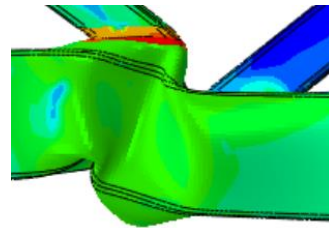
R_8_180_60_80_355_0

Figure 4.22: Critical joint deformation for $b_1 = 60$ mm and $t_0 = 6.3$ mm.

- *Model D1_6.3_180_80_80_355_0 vs R_6.3_180_80_80_355_0*



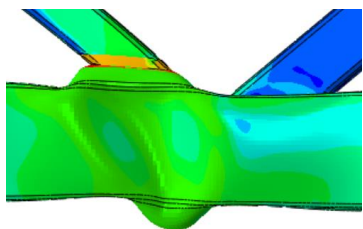
D1_6.3_180_80_80_355_0



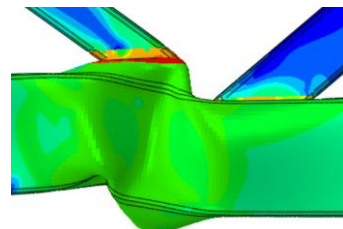
R_6.3_180_80_80_355_0

Figure 4.23: Critical joint deformation for $b_1 = 80$ mm and $t_0 = 6.3$ mm.

- *Model D1_6.3_180_100_80_355_0 vs R_6.3_180_100_80_355_0*



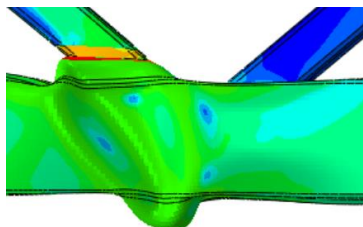
D1_6.3_180_100_80_355_0



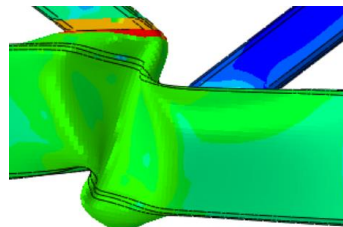
R_6.3_180_100_80_355_0

Figure 4.24: Critical joint deformation for $b_1 = 100$ mm and $t_0 = 6.3$ mm.

- *Model D1_5_180_80_80_355_0 vs R_5_180_80_80_355_0*



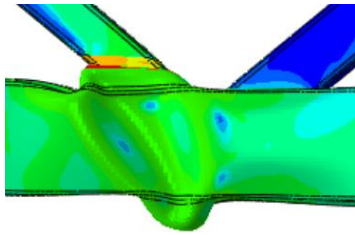
D1_5_180_80_80_355_0



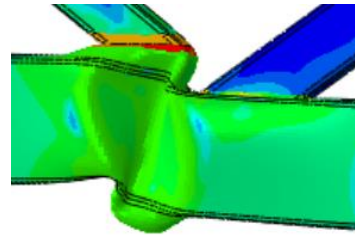
R_5_180_80_80_355_0

Figure 4.25: Critical joint deformation for $b_1 = 80$ mm and $t_0 = 5$ mm.

- *Model D1_5_180_100_80_355_0 vs R_5_180_100_80_355_0*



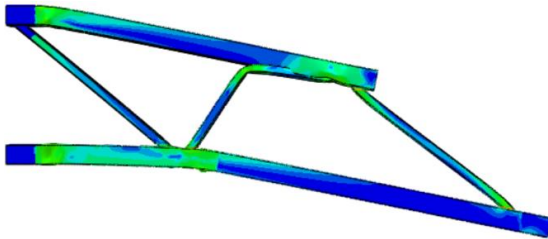
D1_5_180_100_80_355_0



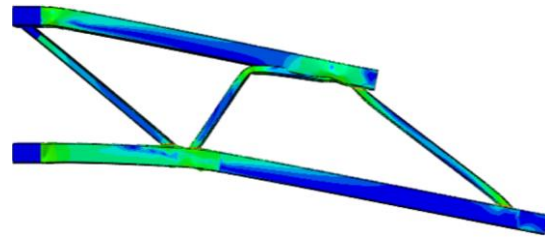
R_5_180_100_80_355_0

Figure 4.26: Critical joint deformation for $b_1 = 100$ mm and $t_0 = 5$ mm.

- *Model D1_8_180_80_80_355_0 vs R_8_180_80_80_355_0*



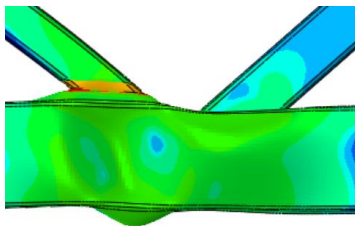
D1_8_180_80_80_355_0



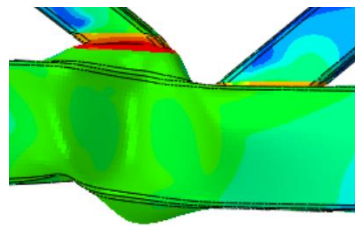
R_8_180_80_80_355_0

Figure 4.27: Truss deformation for $b_1 = 80$ mm and $t_0 = 8$ mm.

- *Model D1_8_180_100_80_355_0 vs R_8_180_100_80_355_0*



D1_8_180_100_80_355_0



R_8_180_100_80_355_0

Figure 4.28: Critical joint deformation for $b_1 = 100$ mm and $t_0 = 8$ mm.

Like the previous analysis, the trusses with a D1 detail have better performance and where, for most of the models, the failure mode is in the critical node. Figure 4.27 demonstrates that the decrease of the width of the compressed brace led to its buckling indicating that, a chord with 8 mm of thickness increases the rigidity of the critical joint resulting in a different failure mode.

4.2.4 Parameter: b_2

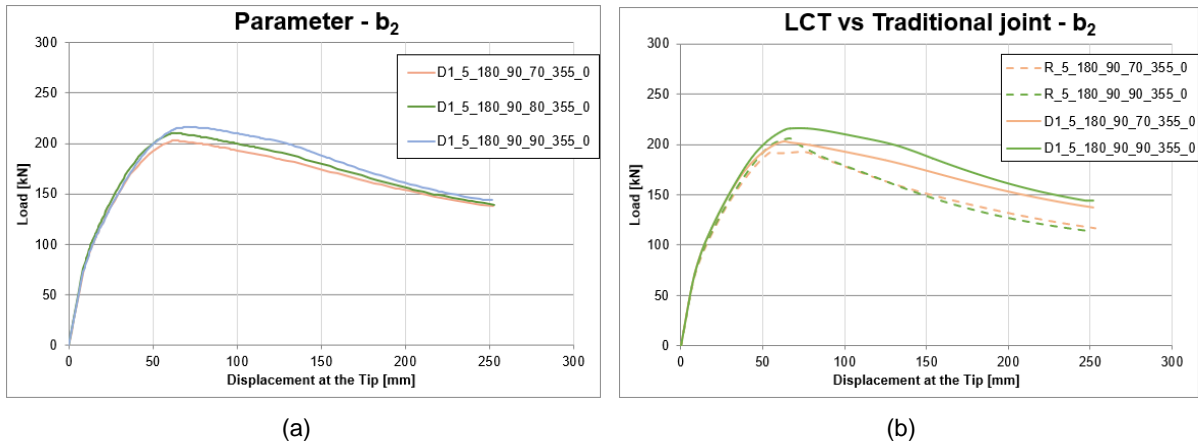


Figure 4.29: Load-displacement curve for $t_0 = 5$ mm: (a) b_2 parameter study; (b) comparison between D1 and R for the b_2 parameter study.

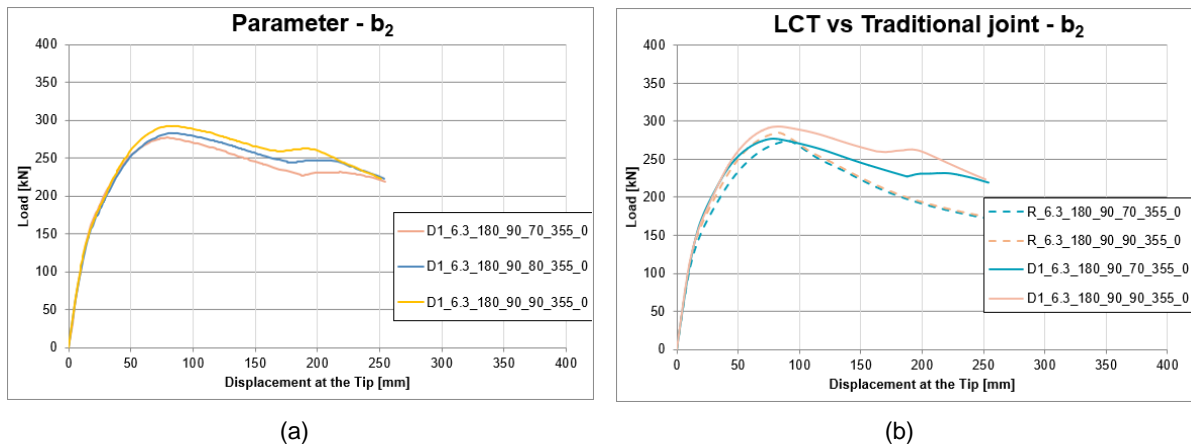


Figure 4.30: Load-displacement curve for $t_0 = 6.3$ mm: (a) b_2 parameter study; (b) comparison between D1 and R for the b_2 parameter study.

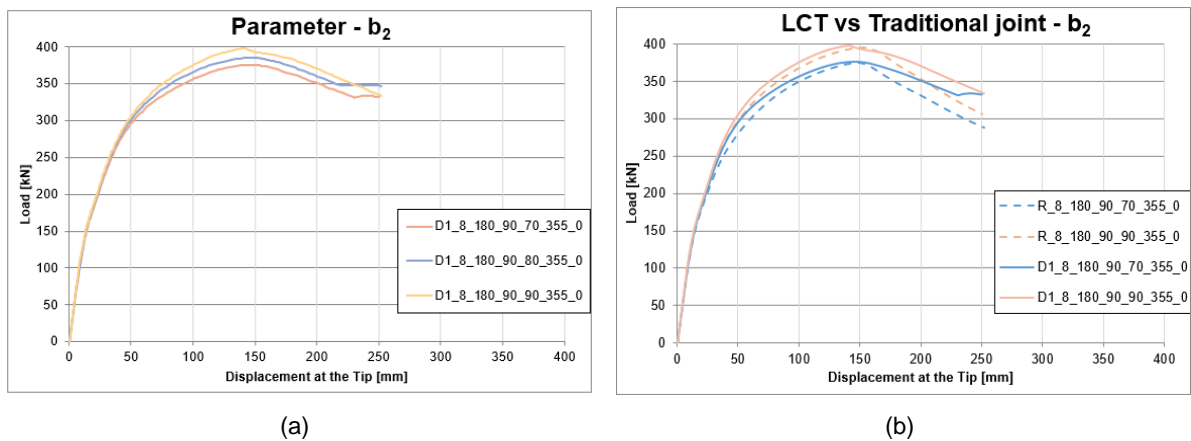


Figure 4.31: Load-displacement curve for $t_0 = 8$ mm: (a) b_2 parameter study; (b) comparison between D1 and R for the b_2 parameter study.

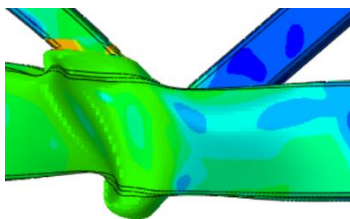
Figures 4.29 (a), 4.30 (a) and 4.31 (a) show a slight increase in the global resistance of the truss when increasing the width of the tensioned chord, while maintaining a similar rigidity. As for the Figures 4.29

(b), 4.30 (b) and 4.31 (b), it's displayed that changing the detail does not have a lot of influence on the global resistance of the truss. Table 4.6 displays the increased percentage in the maximum load from a regular connection to a connection with a D1 detail.

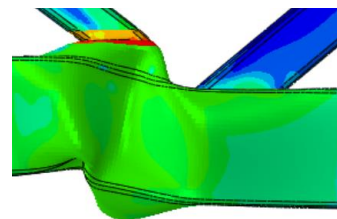
Table 4.6: Parameter b_2 – peak load increase, in percentage, from a regular detail to a D1 detail.

	b_2 [mm]	
	70	90
	5	5.23
Chord's thickness [mm]	6.3	1.20
	8	0.34

- *Model D1_6.3_180_90_70_355_0 vs R_6.3_180_90_70_355_0*



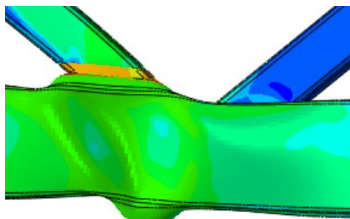
D1_6.3_180_90_70_355_0



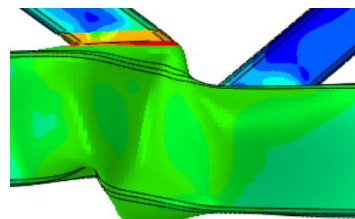
R_6.3_180_90_70_355_0

Figure 4.32: Critical joint deformation for $b_2 = 70$ mm and $t_0 = 6.3$ mm.

- *Model D1_6.3_180_90_90_355_0 vs R_6.3_180_90_90_355_0*



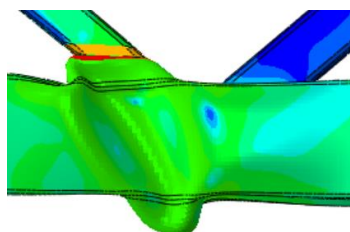
D1_6.3_180_90_90_355_0



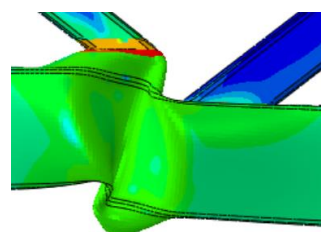
R_6.3_180_90_90_355_0

Figure 4.33: Critical joint deformation for $b_2 = 90$ mm and $t_0 = 6.3$ mm.

- *Model D1_5_180_90_70_355_0 vs R_5_180_90_70_355_0*



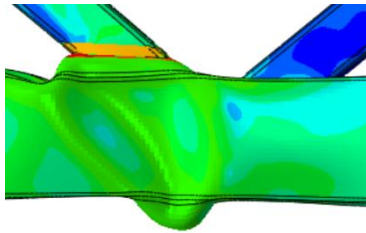
D1_5_180_90_70_355_0



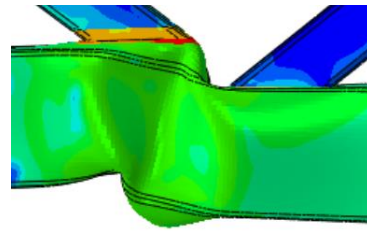
R_5_180_90_70_355_0

Figure 4.34: Critical joint deformation for $b_2 = 70$ mm and $t_0 = 5$ mm.

- Model *D1_5_180_90_90_355_0* vs *R_5_180_90_90_355_0*



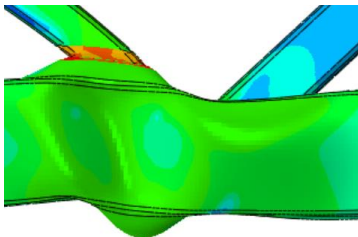
D1_5_180_90_90_355_0



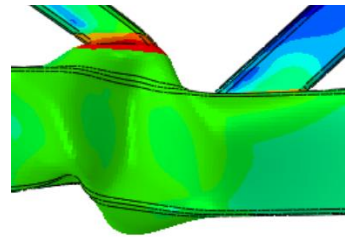
R_5_180_90_90_355_0

Figure 4.35: Critical joint deformation for $b_2 = 90$ mm and $t_0 = 5$ mm.

- Model *D1_8_180_90_70_355_0* vs *R_8_180_90_70_355_0*



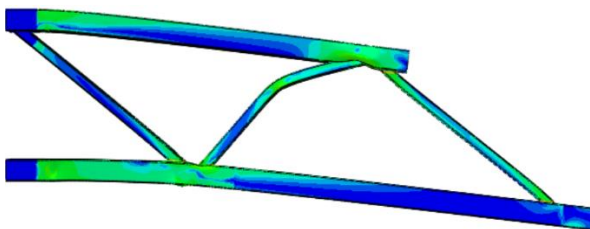
D1_8_180_90_70_355_0



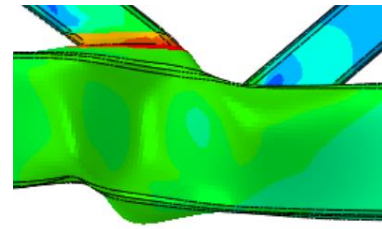
R_8_180_90_70_355_0

Figure 4.36: Critical joint deformation for $b_2 = 70$ mm and $t_0 = 8$ mm.

- Model *D1_8_180_90_90_355_0* vs *R_8_180_90_90_355_0*



D1_8_180_90_90_355_0



R_8_180_90_90_355_0

Figure 4.37: Truss deformation and critical joint deformation for $b_2 = 90$ mm and $t_0 = 8$ mm.

Generally, the failure mode occurs in the critical joint although, for model *D1_8_180_90_90_355_0* displayed in Figure 4.37, the increase of the width of the tensioned brace causes the compressed brace to buckle. When a traditional detail is applied, the rigidity of the joint reduces, causing the failure mode to happen in the critical node.

4.2.5 Parameter: f_{y0}

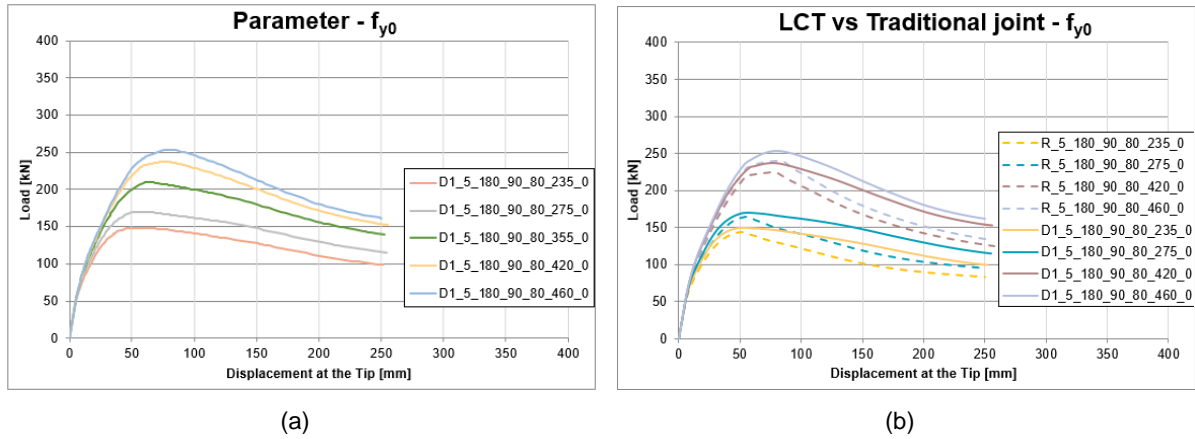


Figure 4.38: Load-displacement curve for $t_0 = 5$ mm: (a) f_{y0} parameter study; (b) comparison between D1 and R for the f_{y0} parameter study.

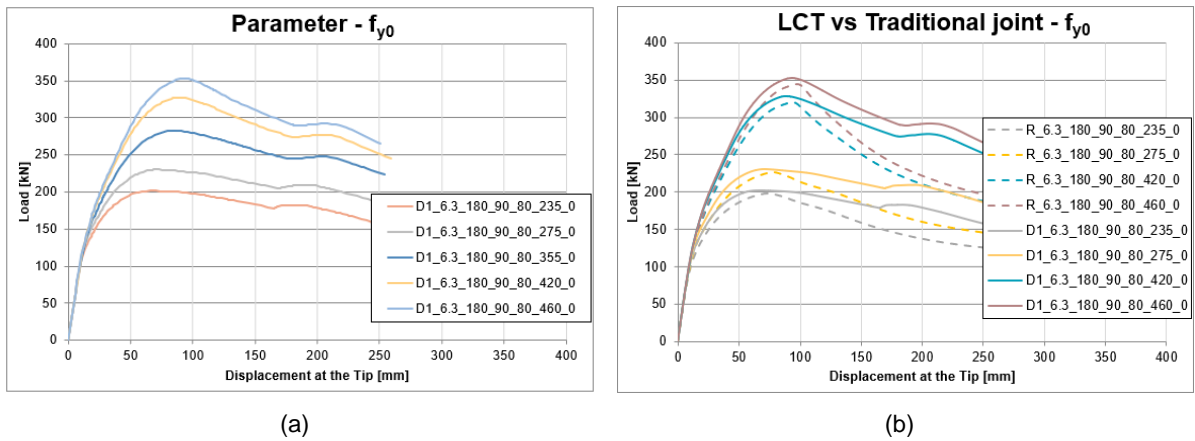


Figure 4.39: Load-displacement curve for $t_0 = 6.3$ mm: (a) f_{y0} parameter study; (b) comparison between D1 and R for the f_{y0} parameter study.

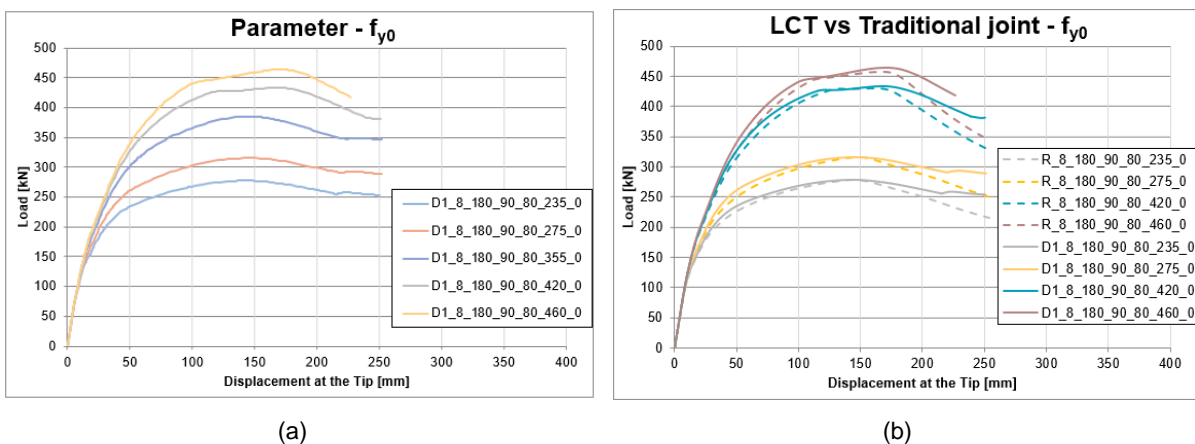


Figure 4.40: Load-displacement curve for $t_0 = 8$ mm: (a) f_{y0} parameter study; (b) comparison between D1 and R for the f_{y0} parameter study.

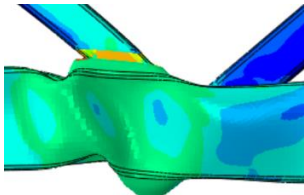
Figures 4.38 (a), 3.39 (a) and 3.40 (a) indicate that upon increasing the steel grade, as expected, the resistance of the trusses increases, along with their rigidity. Table 4.7 shows the peak load difference

between applying a D1 detail and a regular detail. Once again, for higher values of chord thickness, the influence of the type of detail decreases.

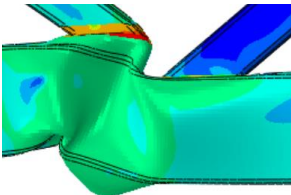
Table 4.7: Parameter f_{y0} - peak load increase, in percentage, from a regular detail to a D1 detail.

	f_{y0} [MPa]				
	235	275	420	460	
Chord's thickness [mm]	5	3.22	3.29	5.41	5.81
6.3	1.59	1.61	2.36	2.48	
8	-0.07	-0.38	0.93	1.37	

- Model *D1_6.3_180_90_80_235_0* vs *R_6.3_180_90_80_235_0*



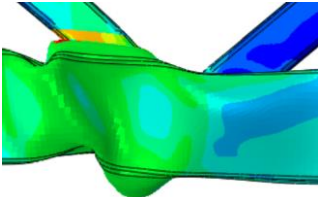
D1_6.3_180_90_80_235_0



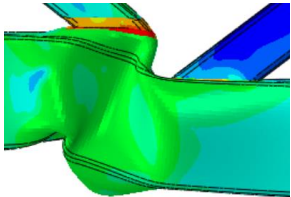
R_6.3_180_90_80_235_0

Figure 4.41: Critical joint deformation for $f_{y0} = 235$ mm and $t_0 = 6.3$ mm.

- Model *D1_6.3_180_90_80_275_0* vs *R_6.3_180_90_80_275_0*



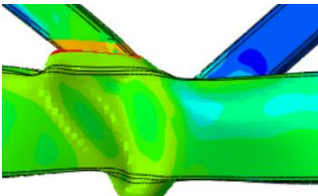
D1_6.3_180_90_80_275_0



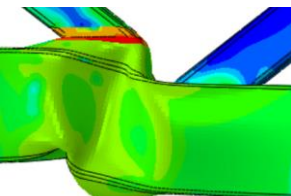
R_6.3_180_90_80_275_0

Figure 4.42: Critical joint deformation for $f_{y0} = 275$ mm and $t_0 = 6.3$ mm.

- Model *D1_6.3_180_90_80_420_0* vs *R_6.3_180_90_80_420_0*



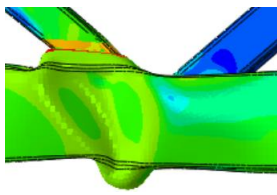
D1_6.3_180_90_80_420_0



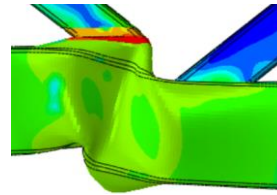
R_6.3_180_90_80_420_0

Figure 4.43: Critical joint deformation for $f_{y0} = 420$ mm and $t_0 = 6.3$ mm.

- *Model D1_6.3_180_90_80_460_0 vs R_6.3_180_90_80_460_0*



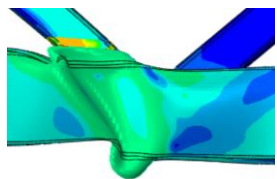
D1_6.3_180_90_80_460_0



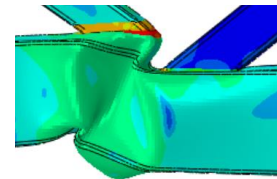
R_6.3_180_90_80_460_0

Figure 4.44: Critical joint deformation for $f_{y0} = 460$ mm and $t_0 = 6.3$ mm.

- *Model D1_5_180_90_80_235_0 vs R_5_180_90_80_235_0*



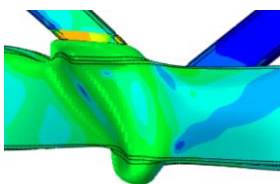
D1_5_180_90_80_235_0



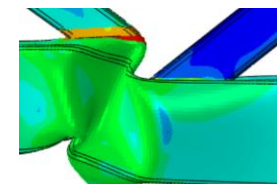
R_5_180_90_80_235_0

Figure 4.45: Critical joint deformation for $f_{y0} = 235$ mm and $t_0 = 5$ mm.

- *Model D1_5_180_90_80_275_0 vs R_5_180_90_80_275_0*



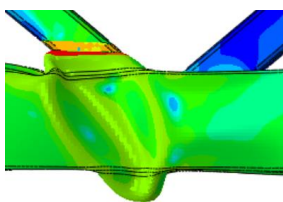
D1_5_180_90_80_275_0



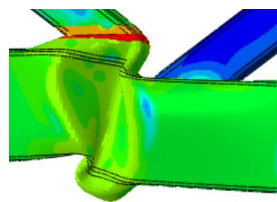
R_5_180_90_80_275_0

Figure 4.46: Critical joint deformation for $f_{y0} = 275$ mm and $t_0 = 5$ mm.

- *Model D1_5_180_90_80_420_0 vs R_5_180_90_80_420_0*



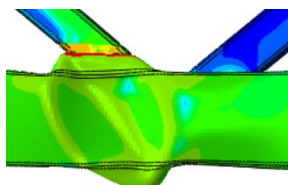
D1_5_180_90_80_420_0



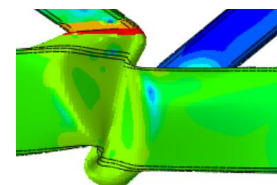
R_5_180_90_80_420_0

Figure 4.47: Critical joint deformation for $f_{y0} = 420$ mm and $t_0 = 5$ mm.

- *Model D1_5_180_90_80_460_0 vs R_5_180_90_80_460_0*



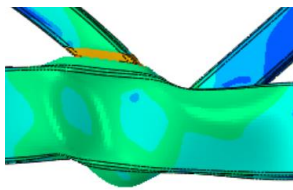
D1_5_180_90_80_460_0



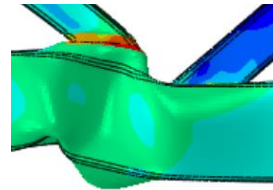
R_5_180_90_80_460_0

Figure 4.48: Critical joint deformation for $f_{y0} = 460$ mm and $t_0 = 5$ mm.

- *Model D1_8_180_90_80_235_0 vs R_8_180_90_80_235_0*



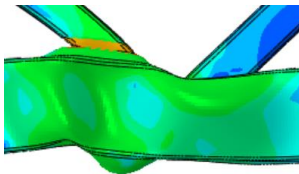
D1_8_180_90_80_235_0



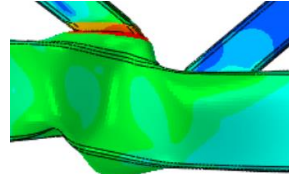
R_8_180_90_80_235_0

Figure 4.49: Critical joint deformation for $f_{y0} = 235$ mm and $t_0 = 8$ mm.

- *Model D1_8_180_90_80_275_0 vs R_8_180_90_80_275_0*



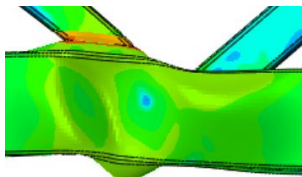
D1_8_180_90_80_275_0



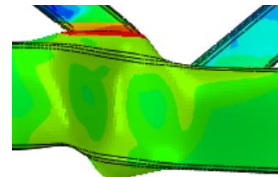
R_8_180_90_80_275_0

Figure 4.50: Critical joint deformation for $f_{y0} = 275$ mm and $t_0 = 8$ mm.

- *Model D1_8_180_90_80_420_0 vs R_8_180_90_80_420_0*



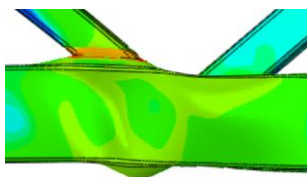
D1_8_180_90_80_420_0



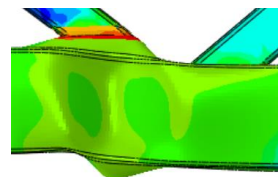
R_8_180_90_80_420_0

Figure 4.51: Critical joint deformation for $f_{y0} = 420$ mm and $t_0 = 8$ mm.

- *Model D1_8_180_90_80_460_0 vs R_8_180_90_80_460_0*



D1_8_180_90_80_460_0



R_8_180_90_80_460_0

Figure 4.52: Critical joint deformation for $f_{y0} = 460$ mm and $t_0 = 8$ mm.

The joints deformations present in Figure 4.41 to Figure 4.52 display the decrease in deformation when a D1 detail is employed over a regular joint. The failure mode occurred in the critical node for all the models studied.

4.2.6 Parameter: g

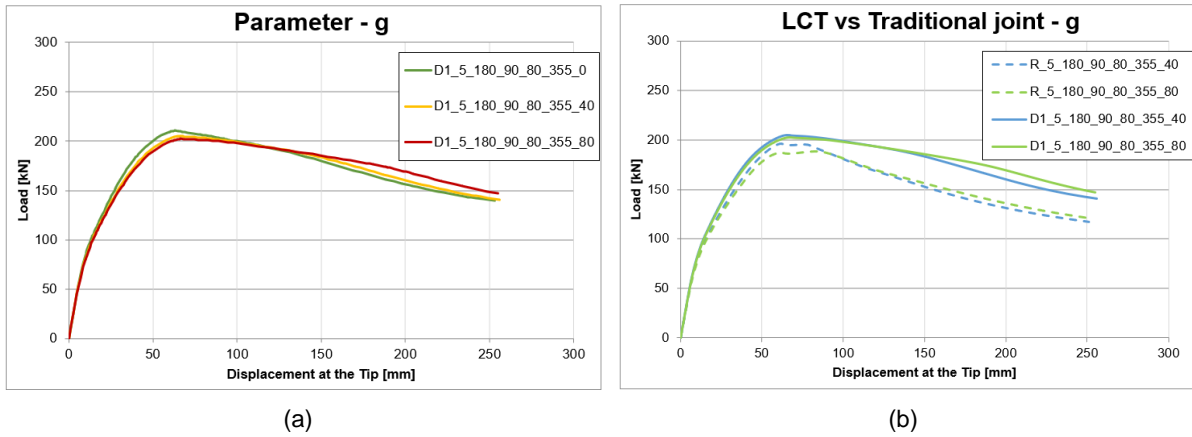


Figure 4.53: Load-displacement curve for $t_0 = 5$ mm: (a) g parameter study; (b) comparison between D1 and R for the g parameter study.

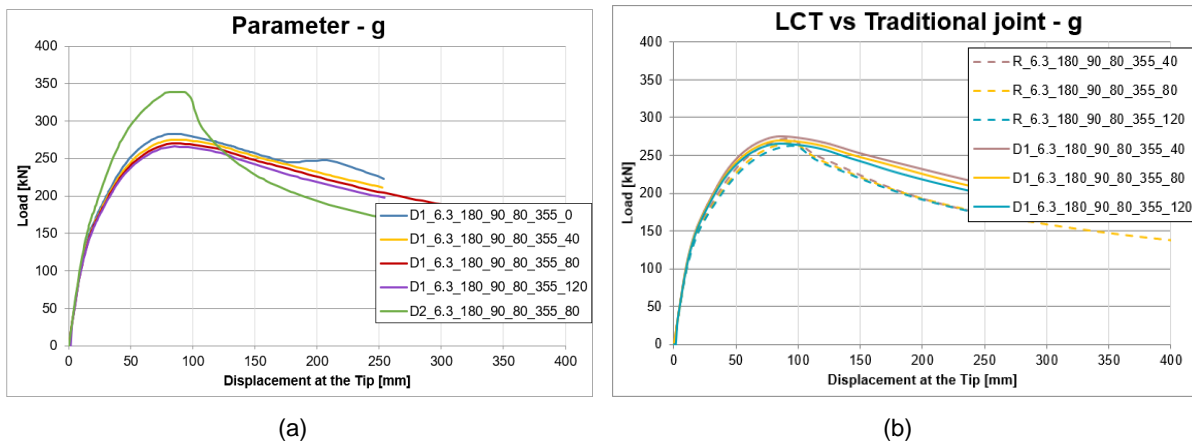


Figure 4.54: Load-displacement curve for $t_0 = 6.3$ mm: (a) g parameter study; (b) comparison between D1 and R for the g parameter study.

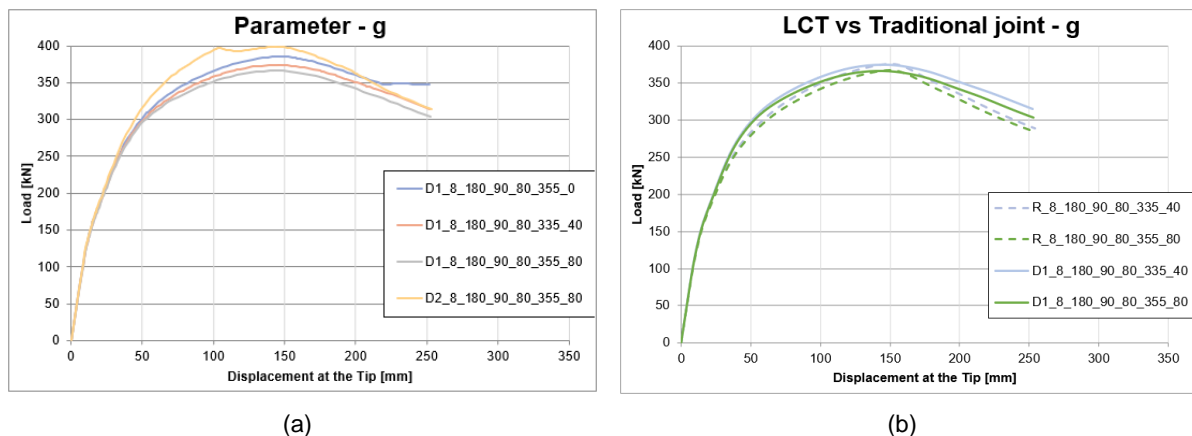


Figure 4.55: Load-displacement curve for $t_0 = 8$ mm: (a) g parameter study; (b) comparison between D1 and R for g parameter study.

Figures 4.53 (a), 4.54 (a) and 4.55 (a) indicate that, for smaller chord thickness, both the rigidity and the peak load of the models are not significantly influenced by the variation of the gap between the braces.

It is noticeable in Figure 4.54 (a) and 4.55 (a) that a D2 joint detail provides a relevant influence on the truss's global resistance. Figures 4.54 (b), 4.55 (b) and 4.56 (b), once again, indicate that a D1 joint detail provides a more significant improvement of global truss behaviour for smaller values of chord's thickness. The percentage of peak load increase, due to a D1 and D2 detail, is shown in Table 4.8.

Table 4.8: Parameter g - peak load increase, in percentage, from a regular detail to a LCT detail.

		g [mm]				
		40	80	120		
Chord width [mm]		180	180	250	180	
Chord's thickness [mm]	5	D1	4.50	7.29	-	-
	6.3	D1	1.27	1.10	10.85	29.36
		D2	-	-0.46	23.66	-
	8	D1	-0.38	-0.36	-	-
		D2	-	-	-	8.39

- Model D1_6.3_180_90_80_355_40 vs R_6.3_180_90_80_355_40



D1_6.3_180_90_80_355_40 R_6.3_180_90_80_355_40

Figure 4.56: Critical joint deformation for g = 40 mm and t₀ = 6.3 mm.

- Model D1_6.3_180_90_80_355_80 vs R_6.3_180_90_80_355_80



D1_6.3_180_90_80_355_80 R_6.3_180_90_80_355_80

Figure 4.57: Critical joint deformation for g = 80 mm and t₀ = 6.3 mm.

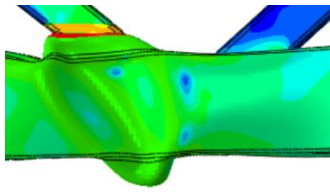
- Model D1_6.3_180_90_80_355_120 vs R_6.3_180_90_80_355_120



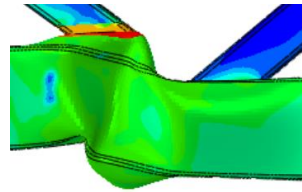
D1_6.3_180_90_80_355_120 R_6.3_180_90_80_355_120

Figure 4.58: Critical joint deformation for g = 120 mm and t₀ = 6.3 mm.

- *Model D1_5_180_90_80_355_40 vs R_5_180_90_80_355_40*



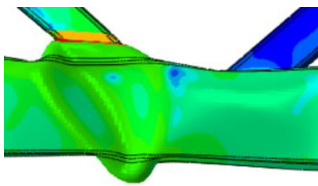
D1_5_180_90_80_355_40



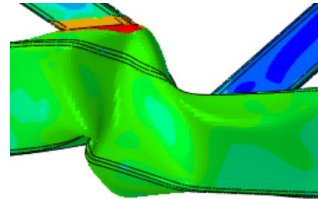
R_5_180_90_80_355_40

Figure 4.59: Critical joint deformation for $g = 40$ mm and $t_0 = 5$ mm.

- *Model D1_5_180_90_80_355_80 vs R_5_180_90_80_355_80*



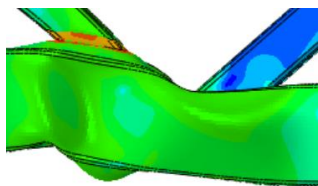
D1_5_180_90_80_355_80



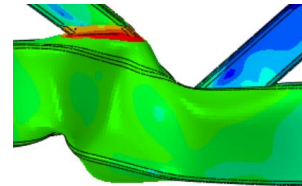
R_5_180_90_80_355_80

Figure 4.60: Critical joint deformation for $g = 80$ mm and $t_0 = 5$ mm.

- *Model D1_8_180_90_80_355_40 vs R_8_180_90_80_355_40*



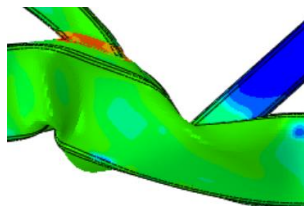
D1_8_180_90_80_355_40



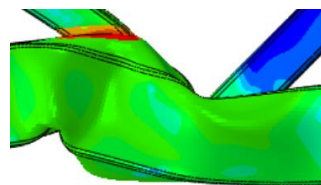
R_8_180_90_80_355_40

Figure 4.61: Critical joint deformation for $g = 40$ mm and $t_0 = 8$ mm.

- *Model D1_8_180_90_80_355_80 vs R_8_180_90_80_355_80*



D1_8_180_90_80_355_80



R_8_180_90_80_355_80

Figure 4.62: Critical joint deformation for $g = 80$ mm and $t_0 = 8$ mm.

- *Model D1_6.3_250_90_80_355_80 vs R_6.3_250_90_80_355_80*

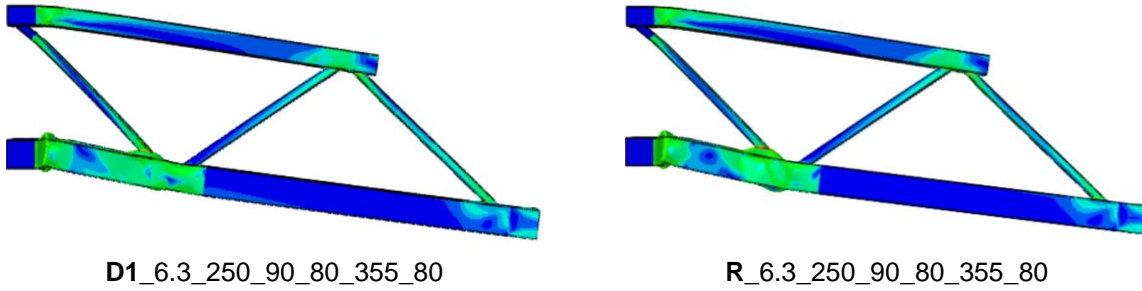


Figure 4.63: Truss deformation for $g = 80$ mm, $t_0 = 6.3$ mm and $b_0 = 250$ mm.

- *Model D2_6.3_180_90_80_355_80*

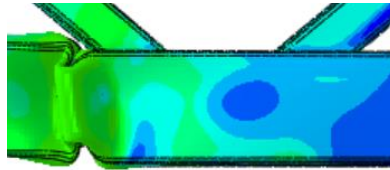


Figure 4.64: Critical joint deformation for $g = 80$ mm, $t_0 = 6.3$ mm and detail D2.

- *Model D2_6.3_250_90_80_355_80*

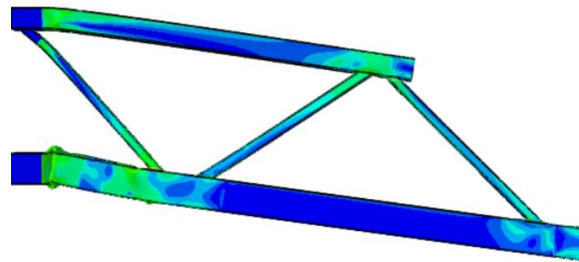


Figure 4.65: Truss deformation for $g = 80$ mm, $t_0 = 6.3$ mm, $b_0 = 250$ mm and detail D2.

- *Model D2_8_250_90_80_355_80*

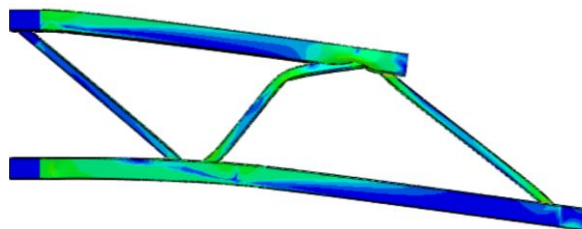


Figure 4.66: Truss deformation for $g = 80$ mm, $t_0 = 8$ mm, $b_0 = 250$ mm and detail D2.

With the increase in the gap between braces, the failure mode remains in the critical joint. However, increasing the chord's width to 250 mm leads to a failure mode situated in the compressed chord near the support. Figure 4.65 confirms that the prolongation of the two braces, into the chord, increases the node rigidity, leading to a failure mode outside the critical node. As for the model D2_8_250_90_80_355_80, displayed in Figure 4.66, the failure mode takes place in the compressed brace.

4.3 Analysis of the results

Parameter: b_o

For a chord with $b_o = 160$ mm and a D1 joint detail, only with a chord thickness of $t_o = 8$ mm does the compressed brace buckles. To better understand what led to a deformation outside the critical joint, the ratios between the slenderness, λ , of the chord and the braces were calculated and displayed in Table 4.9.

Table 4.9: Slenderness ratio for parameter b_o .

t_o	5	6.3	8
$\frac{\lambda_{brace\ 2}}{\lambda_{chord}}$	0.35	0.44	0.56
$\frac{\lambda_{brace\ 1}}{\lambda_{chord}}$	0.40	0.5	0.63

Parameter: b_1

For a D1 and R joint, when studying the variation of width of the compressed braced, for $b_1 = 80$ mm and a chord thickness of $t_o = 8$ mm, the buckling occurred in the chord in compression. The ratios between the slenderness of the compressed brace and the chord can be seen in Table 4.10.

Table 4.10: Slenderness ratio for parameter b_1

t_o	5	6.3	8
$\frac{\lambda_{brace\ 1}}{\lambda_{chord}}$	0.31	0.39	0.5

Parameter: b_2

As for the variation of the tensioned brace, when $b_2 = 90$ mm and the critical node has a D1 detail, again, only for a chord thickness of 8 mm does the deformation happen in the compressed brace. Table 4.11 depicts the ratios between the slenderness of the tensioned brace and the chord.

Table 4.11: Slenderness ratio for parameter b_2

t_o	5	6.3	8
$\frac{\lambda_{brace\ 2}}{\lambda_{chord}}$	0.35	0.44	0.56

It is perceptible, from Tables 4.9, 4.10 and 4.11, that the ratios, for a chord thickness of 8 mm, are higher or equal to 0.5. This proves that for a brace to chord slenderness ratio of 0.5, or superior, the truss is likely to buckle in the compressed brace.

Parameter: g

When increasing the gap between the braces, for a D1 joint detail, large deformations of the bottom chord were observed. Therefore, a D2 detail was studied leading to different failure modes. For a thickness of the chord of 6.3 mm the deformation occurred in the inferior chord and, for 8 mm, took place in the brace in compression. This can be explained by a significant increase of rigidity in the node, which caused the deformation to occur outside the connection.

Comparing D1 with R and D2

Overall, analysing the results presented in the previous subchapter, that compare between a truss with a D1 and a R joint detail, it can be concluded that detail D1 has a better behaviour after buckling, not presenting such an accentuated slope, as well as a higher node resistance. However, in some cases the difference between the peak loads is not very substantial. For a chord thickness of 6.3 mm, an increase of its width to 250 mm, was studied to inquire if it will increase the difference between joint details. As can be observed in Figure 4.67, the joint D1 has more impact in the truss resistance for chords with more width.

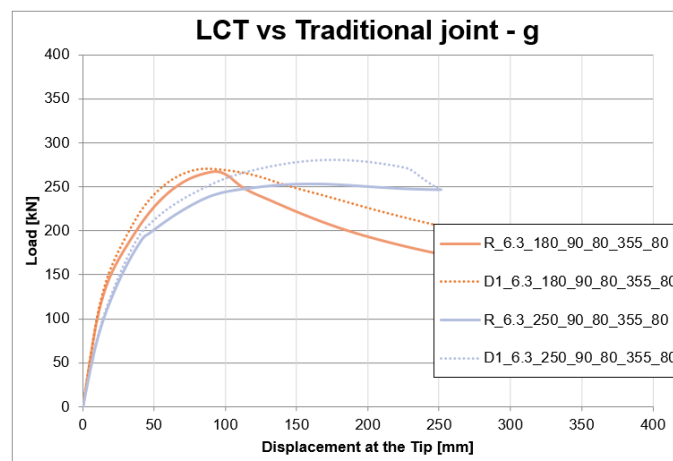


Figure 4.67: Load-displacement curve reflecting the chord's width influence.

In the previous subchapter, when observing the figures comparing the load-displacement curves of traditional and innovative LCT joints it is perceptible that the influence of the type of detail depends on the thickness, and hence on the slenderness, of the truss elements. As an example, a truss with a 5 mm chord thickness has 4.14 % more influence in the truss resistance than one with a thickness of 8 mm. Thus, this can also explain why the difference in peak load is not as perceptible in the model with a chord thickness of 180 mm.

In order to have a better perception of the way the detail applied to the critical node influences its deformation and resistance, Figure 4.68 was elaborated. Depicting a comparison between a D1, a D2 and a R joint detail, it is clear the major improvement in resistance capacity and rigidity that the D2 detail gives to the truss. Prolonging the two braces into the chord also led to a different failure mode, establishing the influence of the type of detail in the behaviour of the truss.

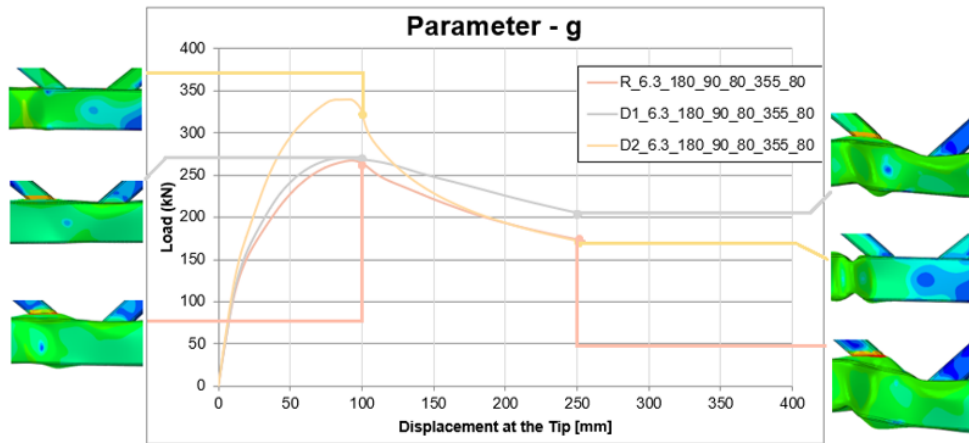


Figure 4.68: Influence of the joint detail in its deformation and resistance.

The influence of the innovative connections is also perceptible in Figure 4.10 and Figure 4.14, two examples where a detail D1 leads to a change in the failure mode. The increase in the node rigidity leads to the deformation of the chord outside the connection. Figures 4.17 and Figure 4.37 establish that prolonging brace members impacts the failure mode of the truss, inducing buckling on the compressed brace instead of the critical node.

Another relevant indicator of the influence of the type of joint detail applied is the resistance of the critical node itself. Focusing, for example, on model 6.3_180_90_80_355_80, as suggested in a previous research [44], to apply the deformation limit criteria it is necessary to measure the vertical displacement in the nodes marked in Figure 4.69 and employ the following equations:

$$\Delta B1 = |B11 - B21| \tag{4.2}$$

$$\Delta B2 = |B12 - B22| \tag{4.3}$$

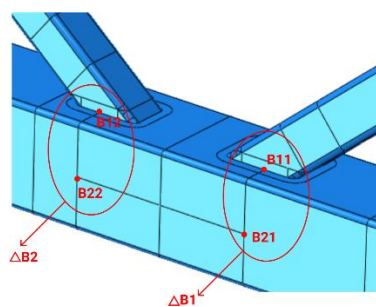


Figure 4.69: Nodes used for the deformation limit criteria.

Considering that the vertical displacement limit corresponding to node failure is $0.03 d_0$, and thus 5.4 mm for a chord diameter of 180 mm, Figure 4.70 represents the vertical displacements of the critical node for the models under consideration. Analysing Figure 4.70 (a), (b) and (c), it can be concluded that node failure occurred in all the trusses in the compressed brace. When dealing with a D1 joint detail, the compressed brace corresponds to the one that was not extended to the chord, explaining why it was responsible for the node failure. As for a D2 detail, apart from the node failure of the compressed brace,

the failure of the truss was reached due to a localized buckling of the chord, in the proximity of the critical node.

Table 4.12 displays the node failure values for a D1 and D2 joint detail, as well as the percentage increase when compared to a traditional joint. Despite the results present in Table 4.12 indicating that the LCT type of detail did not have an impact on the node resistance, as referred before, they do increase the global resistance of the structure, as well as rigidity, more significantly for smaller values of chord thickness, bigger gaps between braces, chord widths and higher steel grades. LCT details also influence the failure mode of the truss, being the model 6.3_180_90_80_355_80 an example of that. For a D1 and a regular joint detail, the failure mode of the truss is in the critical node, while the use of a D2 detail led to the failure mode of the compressed chord outside the critical node.

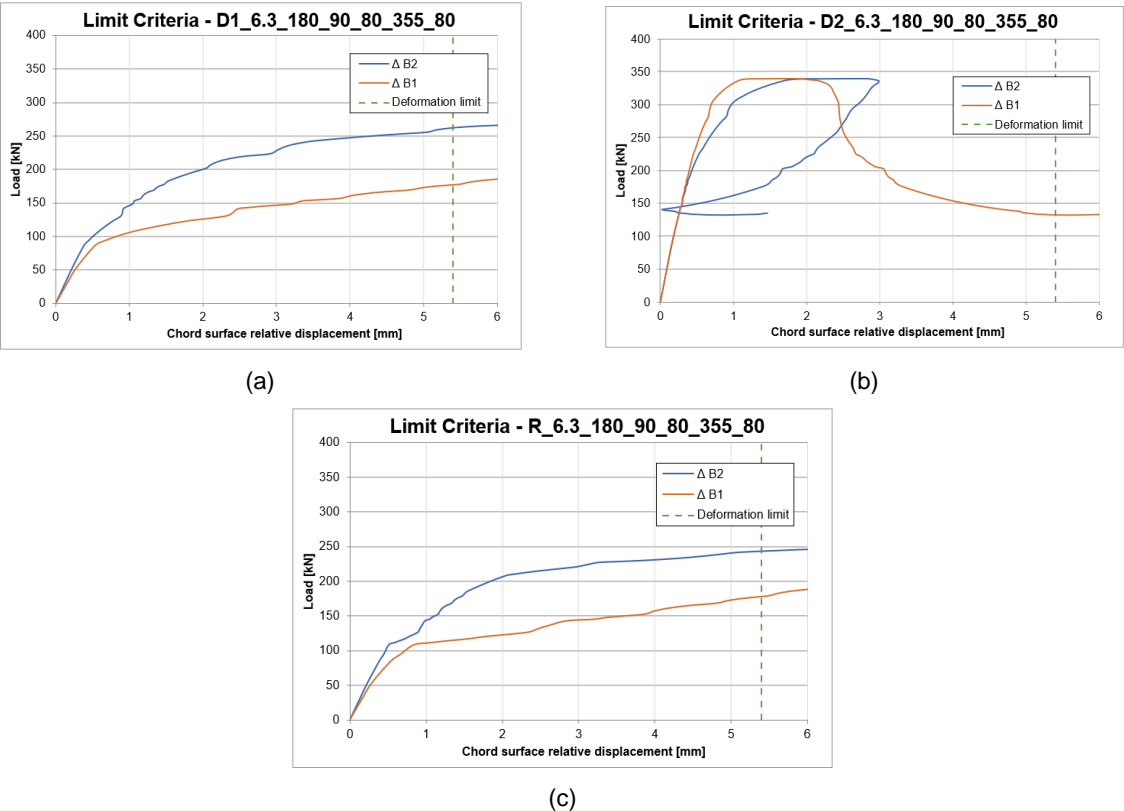


Figure 4.70: Load-displacement curve for the critical node with a: (a) D1 joint detail; (b) D2 joint detail; (c) R joint detail.

Table 4.12: Critical node resistance for model 6.3_180_90_80_355_80, and increased resistance, in percentage, from a regular detail to a LCT detail.

Joint detail	Node resistance [kN]	[%]
D1	178.36	- 0.34
D2	132.10	- 26.19
R	178.98	-

5 Case study

5.1 Design of the truss

To design a simply supported Warren truss, that allows the study of the advantages in the use of an LCT detail, some general recommendations were considered.

The decision to use a SHS cross-section was due to their structural efficiency and the connection between members is welded due to their design simplicity [45]. To get an efficient layout of the truss members, the angle between the brace members in relation to the chords was kept between at least 30° [22] and 55° [46], leading to an inclination of the diagonal members of 38.7°. As for the height of the truss, it is suggested a range of 0.5 to 5 m [47], and taking into consideration the 18m span, the structure was designed with 1.2 m. Since the economic value is also very important when designing a truss girder, the weight of the truss parts was taken into account to produce a more economically sensible solution.

Figure 5.1 schematizes the designed truss to be studied. Since the upper chord is compressed, the nodes 1, 2, 5, 7, 9, 11, 13, 15 were constrained to prevent lateral displacements and maintain the out-of-plane chord buckling between the joints.

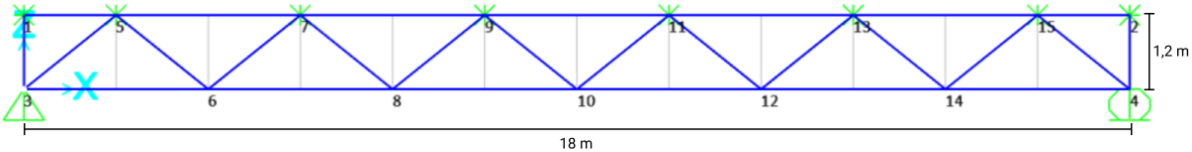


Figure 5.1: Designed truss to be studied.

For S355 steel, Table 5.1 presents the resulting cross-section dimensions obtained. A displacement of 84 mm was applied at the compressed joints along the top chord. When designing the truss, the mid-span limit deformation and the maximum tension in the braces and chords was taken into account.

Table 5.1: Cross-section dimensions for the truss elements.

	Width [mm]	Thickness [mm]
Chords	140	5
Braces	90	8

In a preliminary analysis, the truss designed in SAP 2000 with the dimensions present in Table 5.1, obtained a reasonable deformation at mid-span of 0.104 m, corresponding to approximately L/180.

Figure 5.2 displays the Von Mises stress distributions, in MPa, for the designed truss from SAP 2000.

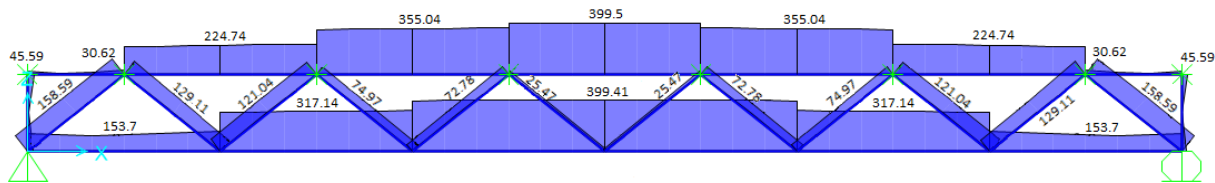


Figure 5.2: Von Mises stress distributions, in MPa, for the designed truss from SAP 2000.

5.2 Numerical studies

It is in the manufacture of the structures that most cost and time are spent. Due to the modification of the form of the truss, the use of a gap simplifies the construction process in addition to facilitating the passage of equipment. Considering the relevance of joint gaps in a truss, it was concluded that, apart from evaluating the performance of D1 joints, it was relevant to study the effects of the gap on the behaviour of the truss. As displayed in Figure 5.3 (e), an eccentricity of 20 mm was applied to the truss with a D1 joint in the top nodes and a regular joint in the bottom ones. This eccentricity value took into consideration the recommended length of at least $(t_1 + t_2)$ [22] and no more than 50 mm [47].

To facilitate the identification of the models under study, the following terminology was adopted:

- The first letter refers to the joint detail on the upper nodes of the truss;
- The second letter identifies the joint detail applied in the bottom truss nodes;
- The last letter specifies the eccentricity, between the braces axis, on the upper joints.

The models studied in ABAQUS are schematised in Figure 5.3.

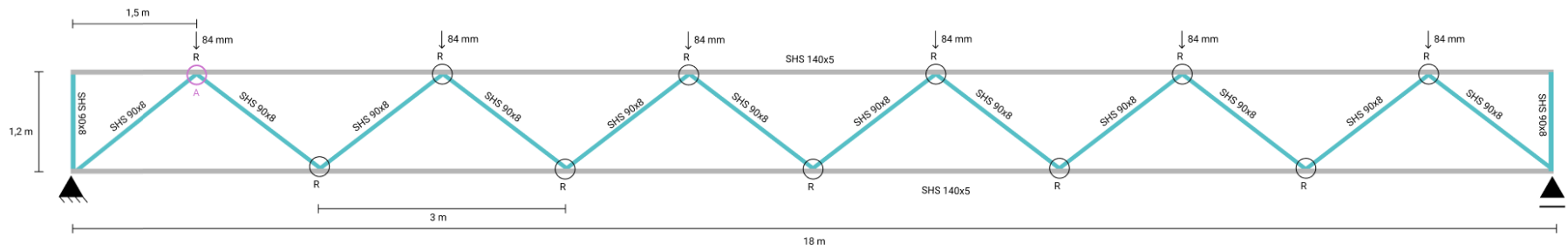
Material

The steel characteristics used in the models are represented in Table 5.2.

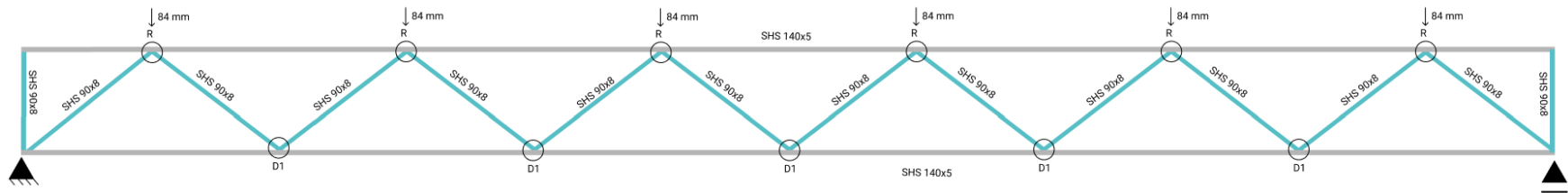
Table 5.2: Steel properties

S355	
f_y [MPa]	355
f_u [MPa]	510
ϵ	0.07381
E [GPa]	210
ρ [ton/mm ³]	7.85E-9
ν	0.3

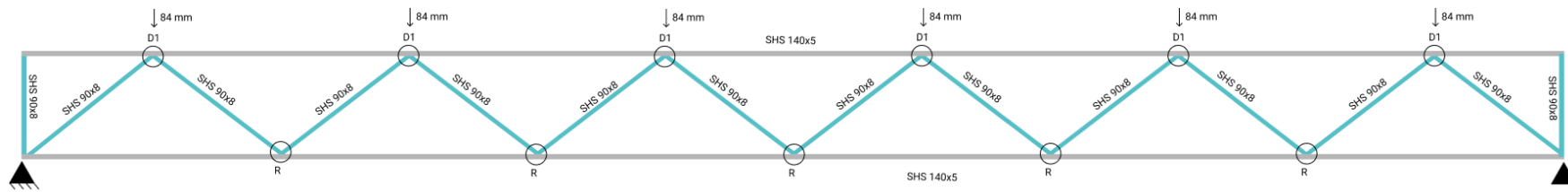
The modelling procedure, as well as the welds geometry and mechanical characteristics, employed in chapter 3 were also used to numerically model the present structure. No imperfections were introduced to the models and, to prevent out-of-plane displacements, the constraints applied to the upper connections of the structure followed the same modelling technique used in chapter 3.



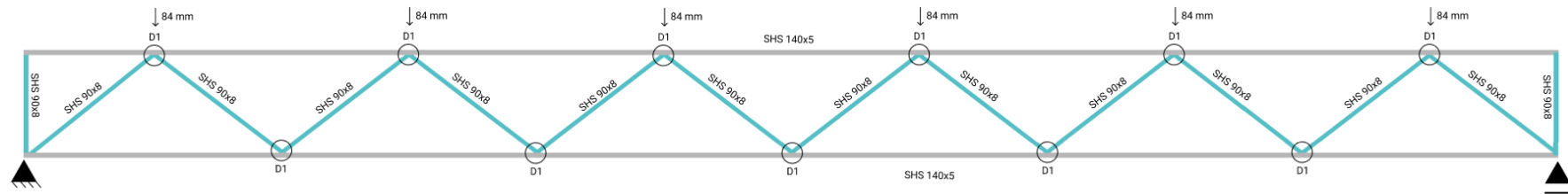
(a)



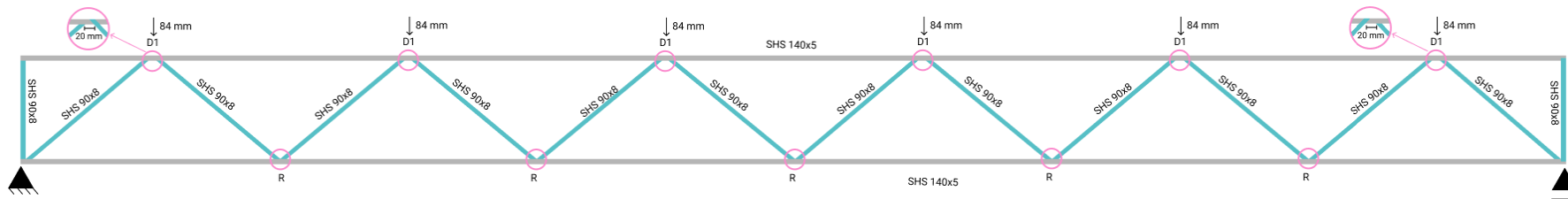
(b)



(c)



(d)



(e)

Figure 5.3: Layout of the models studied: (a) R_R_0; (b) R_D1_0; (c) D1_R_0; (d) D1_D1_0; (e) D1_R_20.

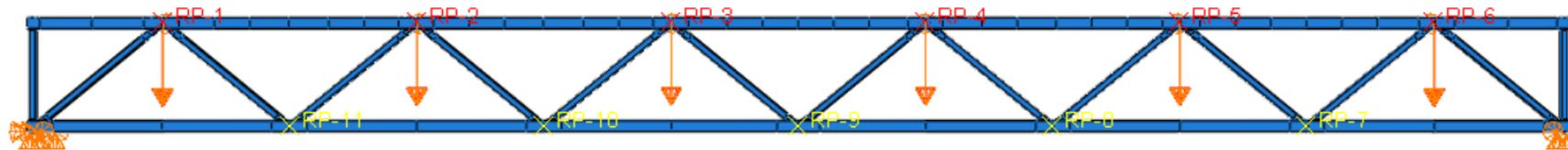


Figure 5.4: Boundary conditions and applied displacements.

Mesh

Figure 5.5 represents the number of elements and the sizing control applied to structure under consideration, as well as the direction of its reduction in size and consequent increase in the number of elements. A balance between the geometry of the structure and processing time was taken into consideration when deciding the values in question, leading to a processing time of approximately 9 hours.

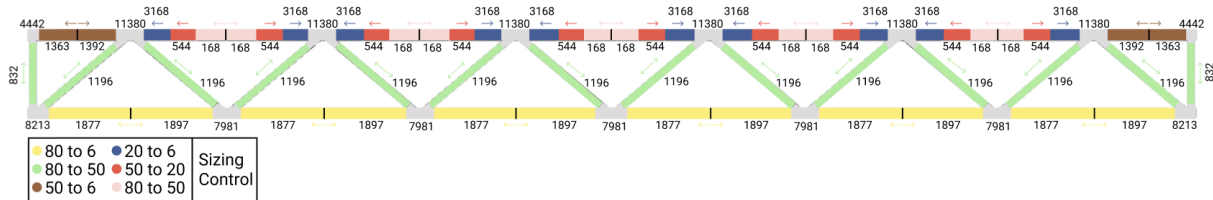


Figure 5.5: Local element sizing control and number of elements for the structure.

5.3 Results from the analysis

The given subchapter presents the results of the numerical analyses performed in ABAQUS, including the Von Mises stress distribution, in MPa. The joint deformations depicted in the present subchapter are regarding node A, marked in Figure 5.3 (a).

Model D1_D1_0



Figure 5.6: Deformed configuration and Von Mises stress distribution for D1_D1_0.

The maximum mid-span vertical displacement obtained from the numerical modelling is 77.7 mm.

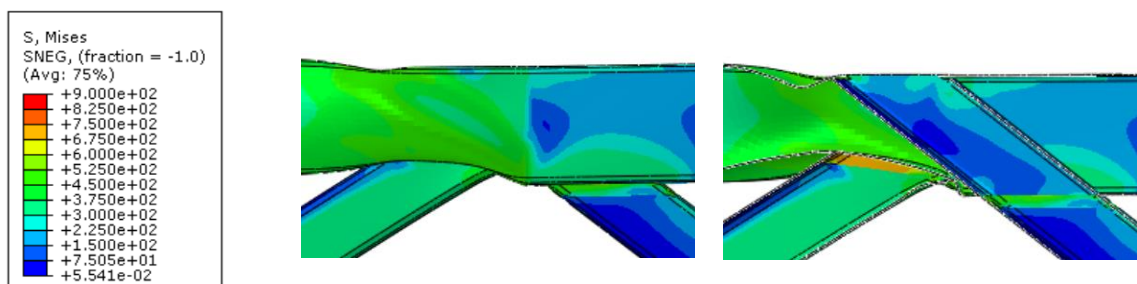


Figure 5.7: Joint deformation and Von Mises stress distribution for D1_D1_0

Model R_R_0



Figure 5.8: Deformed configuration and Von Mises stress distribution for R_R_0.

The maximum mid-span vertical displacement obtained from the numerical modelling is 68.6 mm.

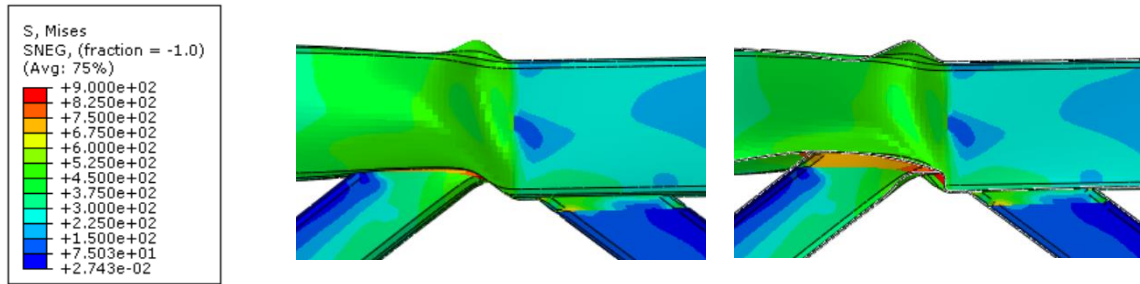


Figure 5.9: Joint deformation and Von Mises stress distribution for R_R_0.

Model D1_R_0



Figure 5.10: Deformed configuration and Von Mises stress distribution for D1_R_0.

The maximum mid-span vertical displacement obtained from the numerical modelling is 84 mm.

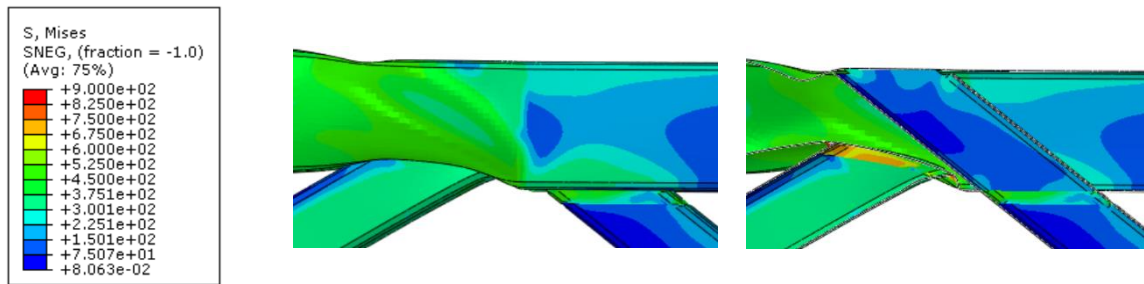


Figure 5.11: Joint deformation and Von Mises stress distribution for D1_R_0.

Model R_D1_0



Figure 5.12: Deformed configuration and Von Mises stress distribution for R_D1_0.

The maximum mid-span vertical displacement obtained from the numerical modelling is 84 mm.

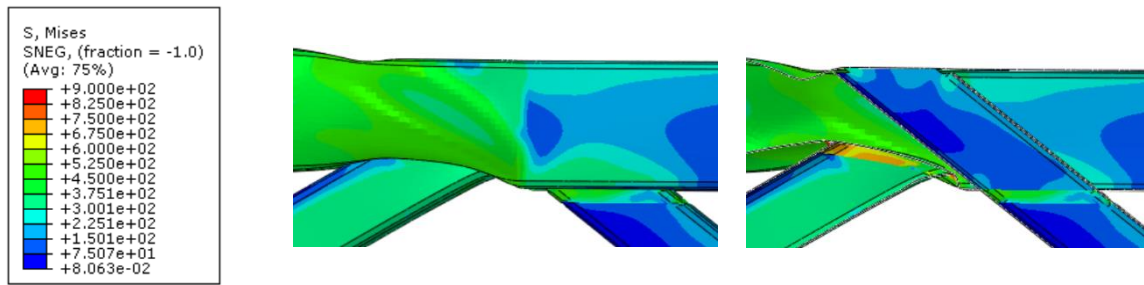


Figure 5.13: Joint deformation and Von Mises stress distribution for R_D1_0.

Model D1_R_20

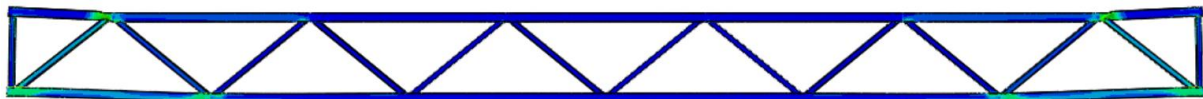


Figure 5.14: Deformed configuration and Von Mises stress distribution for D1_R_20.

The maximum mid-span vertical displacement obtained from the numerical modelling is 77.7 mm.

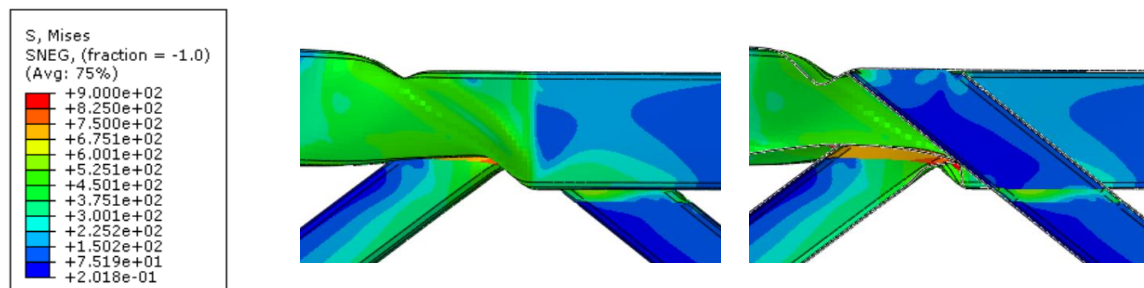


Figure 5.15: Joint deformation and Von Mises stress distribution for D1_R_20.

All the model represented in ABAQUS displayed a smaller mid-span vertical displacement when compared to the values obtained from SAP 2000. Since the modelling in ABAQUS is more complex and detailed, it is reasonable to assume the truss girder rigidity is better portrayed in the numerical models.

5.4 Analysis of the results

The results introduced in the following subchapter allude to node A referred in the previous subchapter.

Comparing R_R_0 with R_D1_0, D1_R_0 and D1_D1_0

Analysing the results for the models present in Figure 5.16 it is concluded that only the nodes in compression condition the behaviour of the structure since the models R_D1_0 and R_R_0 present a very similar behaviour. Therefore, there is no advantage in using the same geometry as model R_D1_0, where there is a detail D1 in tension. A D1 joint detail only significantly influences the peak load if it is in compression, as observed in the increase of the yield strength of the D1_R_0 model. Another conclusion

that can be taken when comparing models D1_D1_0 and D1_R_0 is the advantage of the latter, which is assumed preferable for taking less time, labour and material in the fabrication process, reducing the overall truss construction costs, while still achieving a similar performance and strength.

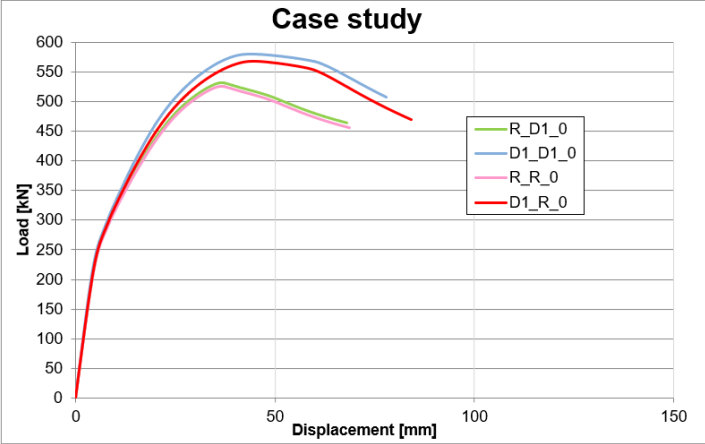


Figure 5.16: Comparison between model R_R_0 and the models R_D1_0, D1_R_0 and D1_D1_0.

Comparing R_R_0 with D1_R_0

From Figure 5.17, model D1_R_0 improves the behaviour of the structure, increasing 7.88% its maximum load when comparing to the R_R_0 model, proving the benefits in the use of an LCT joint detail over a traditional joint.

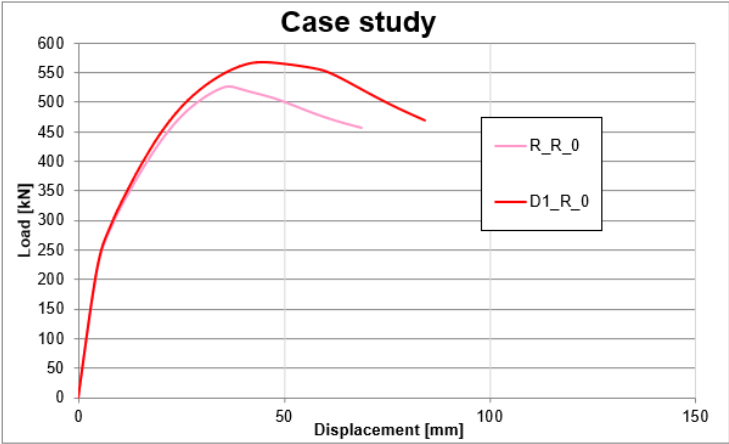


Figure 5.17: Comparison between models R_R_0 and D1_R_0.

Comparing R_R_0 with D1_R_20

Following the conclusion derived from the comparison between models R_D1_0 and D1_R_0, a gap was applied only to the nodes in compression.

Given that, it is visible in Figure 5.18 that, when comparing the models D1_R_20 and R_R_0, with a detail D1 it is possible to have a gap of 20 mm and obtain a similar ultimate load capacity as a structure with only regular joints. Thus, detail D1 allows one to increase the ultimate load or to have larger

eccentricities but with the same yielding strength capacity as a structure with regular welded connections.

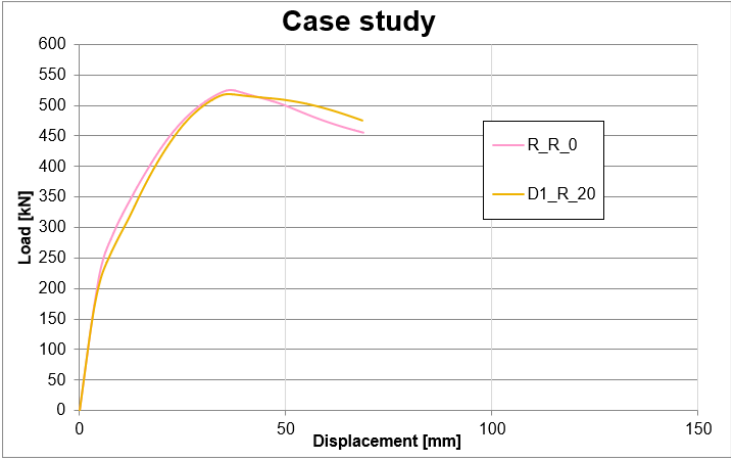


Figure 5.18: Comparison between models R_R_0 and D1_R_20.

6 Conclusions and Future Developments

6.1 Conclusions

The work presented allowed the fulfilment of the main objective of this dissertation, which is to attest that the LASTEICON details, fabricated using laser cutting technology, substantially improve the global behaviour of the structure. In terms of resistance and stiffness, they present a more advantageous option when compared to conventional manufacturing techniques.

After validating the numerical models, the parametric studies showed that a higher resistance and rigidity with LCT details, when compared to the regular ones, is achievable. Moreover, the decrease in chord thickness increases the influence the type of detail has on the truss resistance. For example, in the parametric study of the chord thickness, the difference between the peak load of a truss with a D1 detail and a regular detail, for a thickness of 8 mm is 0.22% and for a 5 mm thickness is 4.36%.

Overall, the deformations in the critical joints with a D1 detail depict the improvement of the behaviour of the connection. For the models with a chord thickness of 8 mm, in which the failure mode did not occur in the joint but in the compressed brace, the calculation of the brace to chord slenderness ratio led to the conclusion that such a phenomenon only happens for a ratio of 0.5 or superior.

Although few models were run in the parametric study with a D2 detail, it proves to be the most effective in increasing the global resistance of the truss, as expected, given that both braces penetrate the chord increasing the node rigidity. This significant increase of rigidity also leads to a failure mode outside the critical node.

A more detailed assessment was carried for the gap parameter to understand the influence of the type of joint detail in the resistance of the critical node. The results of the analysis indicate that the LCT type of detail did not have an impact on the node resistance although they do increase the global resistance of the structure, as well as rigidity. Their impact is particularly significant for smaller values of chord thickness, bigger chord widths and gaps between braces and higher steel grades. LCT details also influence the failure mode of the truss since, for a D1 and a traditional joint detail, the failure mode of the truss is in the critical node, while the use of a D2 detail led to the failure mode of the compressed chord outside the critical node.

As for the applicability of a D1 type of joint to a larger structure, the results confirmed the benefits of its use. Compared to the use of a traditional detail throughout the truss, the application of the LCT detail in the compressed nodes increases 7.88% the ultimate load. Regarding the implementation of an eccentricity, an increase of the gap between the braces in the compressed joints, with a D1 detail, allows the same resistance as a structure with only regular joints and no gap. This allows for an easier construction process, lowering the fabrications costs and environmental impact while still achieving similar performance and strength. It is also worth highlighting that it is preferable to apply the LCT

detailing only in the compressed joints rather than in the whole truss since, for similar structural behaviour, the overall truss construction costs decrease.

6.2 Future Developments

Following the calibration of the numerical models and having established its ability to represent the realistic behaviour of the structure, a more extensive study should be undertaken covering CHS profiles and Pratt trusses, to assure the global applicability of the LASTEICON joints.

To deepen the knowledge of this innovative joint performance and improve market acceptance, it is important to further the study regarding:

- Low cycle fatigue;
- Fire performance;
- More challenging architectural geometries designed to automate the fabrication procedure and minimize welding;
- LCT joints behaviour in frame corners;
- Vertical splicing of columns.

Following the same procedure carried out in the framework of the LASTEICON project and the present thesis, experimental tests should be performed in order to calibrate the numerical models to be used to investigate the topics listed above. A parametric study at local and global levels to identify the influence of component dimensions, material properties and welding configurations, along with fabrication tolerances, should be undertaken.

To introduce LCT joints in the construction sector, the final step is to propose design guidelines and worked examples as well as evaluate the environmental and economic impact.

Bibliography

- [1] World Steel Association, "World Steel in Figures," 2020. [Online]. Available: <http://www.worldsteel.org/wsif.php>.
- [2] European Commission, "The European Green Deal," 2019. [Online]. Available: <https://eur-lex.europa.eu/legal-content/EN/TXT/PDF/?uri=CELEX:52019DC0640&from=EN>.
- [3] "Research Fund for Coal and Steel (RFCS) | European Commission." https://ec.europa.eu/info/research-and-innovation/funding/funding-opportunities/funding-programmes-and-open-calls/research-fund-coal-and-steel-rfcs_en (accessed Feb. 10, 2021).
- [4] C. Castiglioni, "LASTEICON Project Proposal," 2015.
- [5] B. S. C. P. Dias, "Numerical Models on Innovative Steel Hollow Section Joints for Truss Girders using Laser Cut Technology," MSc Thesis, Instituto Superior Técnico, Lisbon, 2017.
- [6] G. D'Amato, "Numerical and Experimental Analysis of Innovative Joints for HSS Truss Girders," MSc Thesis, Politecnico Di Milano, Italy, 2018.
- [7] J. P. M. Serralha, "Numerical studies on prototype CHS and open sections welded joints for steel truss girders with the use of laser cutting technology," MSc Thesis, Instituto Superior Técnico, Lisbon, 2017.
- [8] M. Harničárová, J. Zajac, and A. Stoić, "Comparison of different material cutting technologies in terms of their impact on the cutting quality of structural steel," *Tech. Gaz.*, vol. 17, no. 3, pp. 371–376, 2010.
- [9] R. Alope, V. Girish, R. F. Scrutton, and P. A. Molian, "A model for prediction of dimensional tolerances of laser cut holes in mild steel thin plates," *Int. J. Mach. Tools Manuf.*, vol. 37, no. 8, pp. 1069–1078, 1997.
- [10] A. Kanyilmaz, "The problematic nature of steel hollow section joint fabrication, and a remedy using laser cutting technology: A review of research, applications, opportunities," *Eng. Struct.*, vol. 183, no. February 2018, pp. 1027–1048, 2019, doi: 10.1016/j.engstruct.2018.12.080.
- [11] D. Andrés *et al.*, "Characterization of heat affected zones produced by thermal cutting processes by means of Small Punch tests," *Mater. Charact.*, vol. 119, pp. 55–64, 2016, doi: 10.1016/j.matchar.2016.07.017.
- [12] J. A. Packer, J. Wardenier, Y. Kurobane, D. Dutta, and N. Yeomans, "Design guide for rectangular hollow section (RHS) joints under predominantly static loading." CIDECT, 1992.
- [13] J. A. Packer, J. Wardenier, Y. Kurobane, D. Dutta, and N. Yeomans, "Design guide for circular hollow section (CHS) joints under predominantly static loading.pdf." CIDECT, 1991.
- [14] T. E. of E. Britannica, "Truss," *Encyclopedia Britannica*, 2014. <https://www.britannica.com/technology/truss-building> (accessed Mar. 04, 2021).

- [15] R. Golden, "The Advantages of Trusses," *Hunker*. <https://www.hunker.com/12296537/the-advantages-of-trusses> (accessed Mar. 04, 2021).
- [16] W. Yang, J. Lin, N. N. Gao, and R. Yan, "Experimental study on the static behavior of reinforced warren circular hollow section (CHS) tubular trusses," *Appl. Sci.*, vol. 8, no. 11, 2018, doi: 10.3390/app8112237.
- [17] U. Kirsch, "Optimal topologies of structures," *Appl. Mech. Rev.*, vol. 42, no. 8, pp. 223–239, Aug. 1989, doi: 10.1115/1.3152429.
- [18] J. Smith, J. Hodgins, I. Oppenheim, and A. Witkin, "Creating models of truss structures with optimization," *ACM Trans. Graph.*, vol. 21, no. 3, pp. 295–301, 2002, doi: 10.1145/566570.566580.
- [19] J. Wardenier, *HOLLOW SECTIONS Hollow Sections in Structural Applications*. CIDECT, 2001.
- [20] B. Goreng, R. Tinyou, and A. Syam, *Steel Designers' Handbook*, 7th ed. Sydney: UNSW Press, 2005.
- [21] A. El-Sheikh, "New space truss system - From concept to implementation," *Eng. Struct.*, vol. 22, no. 9, pp. 1070–1085, 2000, doi: 10.1016/S0141-0296(99)00051-6.
- [22] Comité Européen de Normalisation (CEN), "EN 1992-1-8. Eurocode 3: Design of steel structures - Part 1-8: Design of joints." Brussels, 2005.
- [23] I. Radić, D. Markulak, and M. Mikolin, "Design and FEM modelling of steel truss girder joints," *Strojarstvo*, vol. 52, no. 2, pp. 125–135, 2010.
- [24] X. L. Zhao, "Deformation limit and ultimate strength of welded T-joints in cold-formed RHS sections," *J. Constr. Steel Res.*, vol. 53, no. 2, pp. 149–165, 2000, doi: 10.1016/S0143-974X(99)00063-2.
- [25] J. A. Yura, N. A. Zettlemoyer, and I. F. Edwards, "Ultimate Capacity Equations for Tubular Joints ." May 05, 1980, doi: 10.4043/3690-MS.
- [26] Y. S. Choo, X. D. Qian, J. Y. R. Liew, and J. Wardenier, "Static strength of thick-walled CHS X-joints - Part I. New approach in strength definition," *J. Constr. Steel Res.*, vol. 59, no. 10, pp. 1201–1228, 2003, doi: 10.1016/S0143-974X(03)00054-3.
- [27] X. L. Zhao, J. Wardenier, J. A. Packer, and G. J. van der Vegte, "New IIW (2008) static design recommendations for hollow section joints," in *Tubular Structures XII*. CRC press, 2008.
- [28] I. S. Mayor, G. V. Nunes, A. M. S. Freitas, J. A. V. Requena, and A. H. Araújo, "Theoretical and experimental analysis of RHS/CHS K gsp joints," vol. 66, no. 3, pp. 295–300, 2013.
- [29] S. S. Bhavikatti, *Finite Element Analysis*. 2005.
- [30] A. D. Christitsas, D. T. Pachoumis, C. N. Kalfas, and E. G. Galoussis, "FEM analysis of conventional and square bird-beak SHS joint subject to in-plane bending moment - experimental study," *J. Constr. Steel Res.*, vol. 63, no. 10, pp. 1361–1372, 2007, doi: 10.1016/j.jcsr.2006.12.006.

- [31] S. T. Lie, Z. M. Yang, S. P. Chiew, and C. K. Lee, "The ultimate behaviour of cracked square hollow section T-joints," *Adv. Steel Constr.*, vol. 3, no. 1, pp. 443–458, 2007, doi: 10.1016/b978-008044637-0/50162-1.
- [32] K. Mitsui, A. Sato, M. Latour, V. Piluso, and G. Rizzano, "Experimental analysis and FE modeling of square hollow sections under combined axial and bending loads," *Ce/Papers*, vol. 1, no. 2–3, pp. 4732–4739, 2017, doi: 10.1002/cepa.535.
- [33] Dassault Systèmes, *Abaqus/CAE User's Guide*. 2014.
- [34] M. Abambres and M. R. Arruda, "Finite element analysis of steel structures - A review of useful guidelines," *Int. J. Struct. Integr.*, vol. 7, no. 4, pp. 490–515, 2016, doi: 10.1108/IJSI-07-2015-0020.
- [35] M. C. Bittencourt, L. R. O. De Lima, P. C. G. S. Vellasco, J. G. S. Silva, and L. F. C. Neves, "A Numerical Analysis of Tubular Joints under Static Loading," 2007.
- [36] J. J. Del Coz Díaz, M. A. Serrano López, C. López-Colina Pérez, and F. P. Álvarez Rabanal, "Effect of the vent hole geometry and welding on the static strength of galvanized RHS K-joints by FEM and DOE," *Eng. Struct.*, vol. 41, pp. 218–233, 2012, doi: 10.1016/j.engstruct.2012.03.050.
- [37] A. Jurčíková and M. Rosmanit, "The Evaluation of Load-Bearing Capacity of the Planar CHS Joint Using Finite Modeling," vol. 7, no. 10, pp. 729–732, 2013.
- [38] Comité Européen de Normalisation (CEN), "EN 1993-1-5. Eurocode 3: Design of steel structures- Part 1-5: Plated structural elements." Brussels, 2006.
- [39] M. Johansson and T. Löfberg, "Modelling of pitched truss beam with Finite Element method," p. 142, 2011.
- [40] L. Calado, J. Proença, R. da Silva, and G. D'Amato, "Deliverable 2.4 - Report on tests of truss girders," 2019.
- [41] L. Calado, J. Proença, R. da Silva, and G. D'Amato, "Task 4.2 - Guidelines for the design of truss girders." 2019.
- [42] L. Calado, J. Proença, R. da Silva, and G. D'Amato, "Task 3.2 - Calibration of numerical models truss girders." 2019.
- [43] Tata Steel Europe Limited, "Celsius 355 NH technical guide," 2018, [Online]. Available: www.tatasteel.com.
- [44] L. Calado, J. M. Proença, P. M. Mendes, and J. F. A. Sio, "Preliminary numerical analysis on substructure trusses." Instituto Superior Técnico, Lisbon, 2018.
- [45] T. B. C. S. Association and T. S. C. Institute, "Handbook of Structural Steelwork - Eurocode Edition," no. 55, 2013, [Online]. Available: www.steelconstruction.info.

[46] CTICM and SCI, *STEEL BUILDINGS IN EUROPE: Single-Storey Steel Buildings - Part 5: Detailed Design of Trusses*.

[47] T. Tiainen, K. Mela, T. Jokinen, and M. Heinisuo, "High Strength Steel in Tubular Trusses," no. 8, pp. 6–11, 2014.

APPENDIX

APPENDIX I: Truss models deformations and Von Mises stress distribution with a D1 joint detail

Parameter: t_0

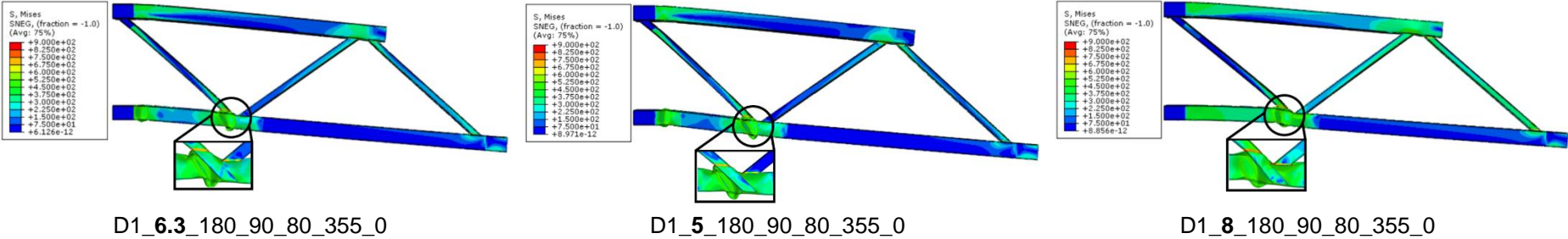
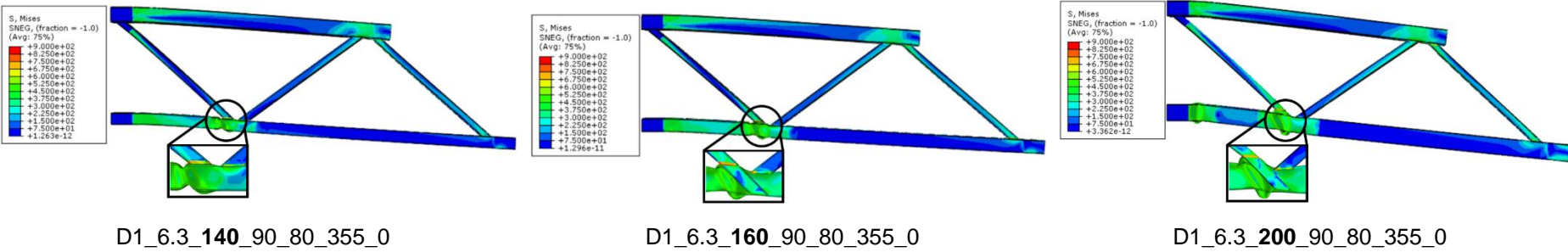
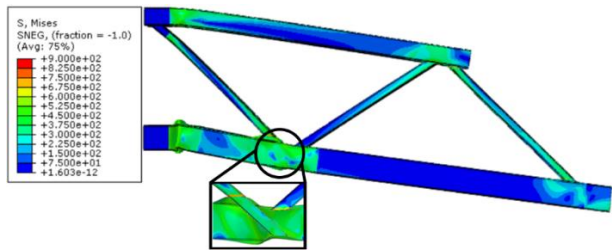


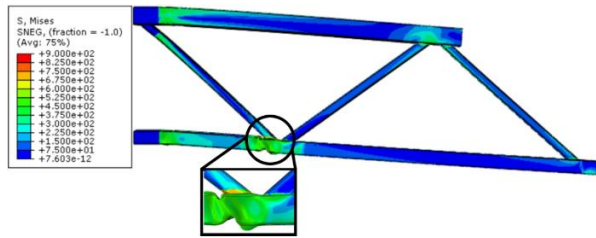
Figure I.1: Deformations and Von Mises stress distributions for the t_0 parameter and D1 joint detail

Parameter: b_0

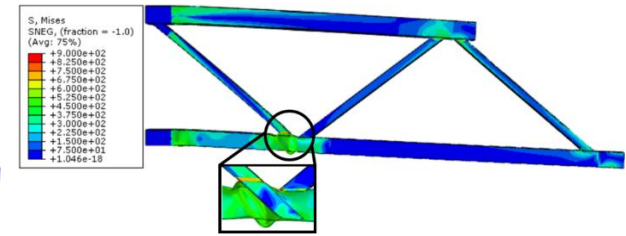




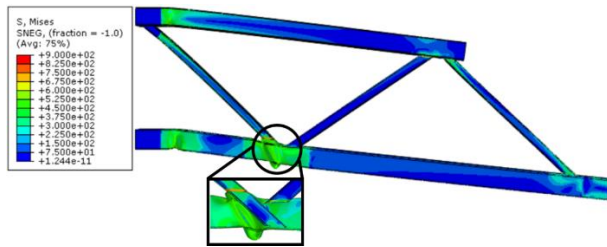
D1_6.3_180_90_80_355_0



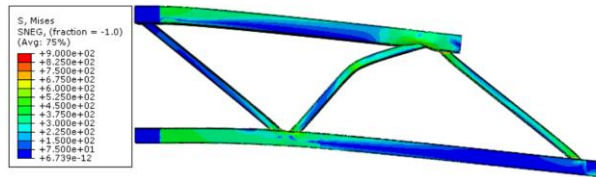
D1_5_180_90_80_355_0



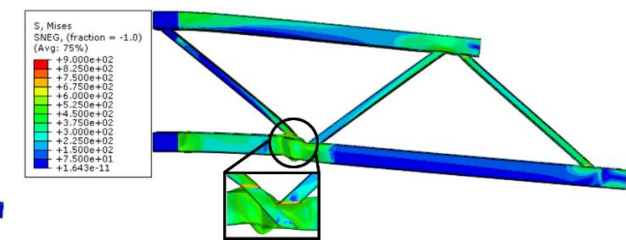
D1_8_180_90_80_355_0



D1_6.3_250_90_80_355_0



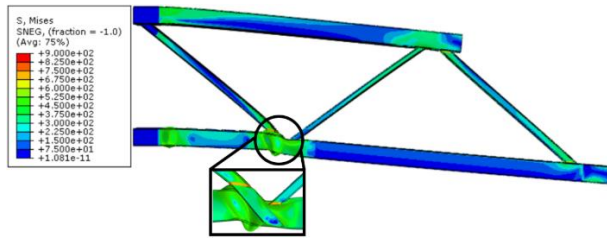
D1_5_140_90_80_355_0



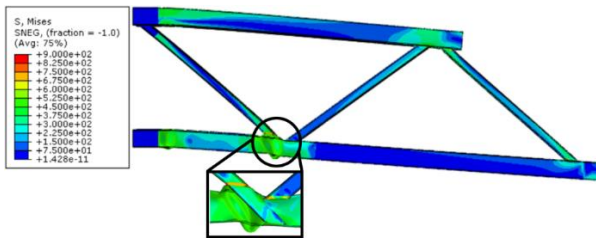
D1_5_160_90_80_355_0

Figure I.2: Deformations and Von Mises stress distributions for the b_0 parameter and D1 joint detail

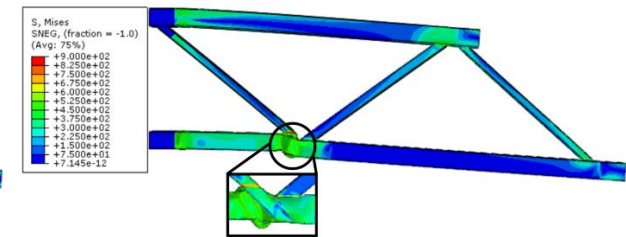
Parameter: b_1



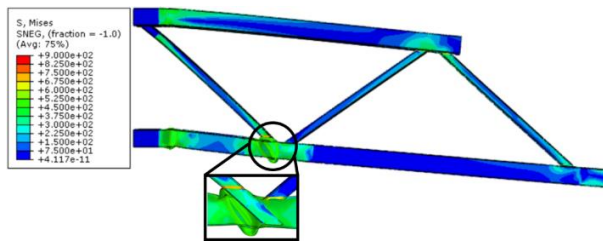
D1_6.3_180_60_80_355_0



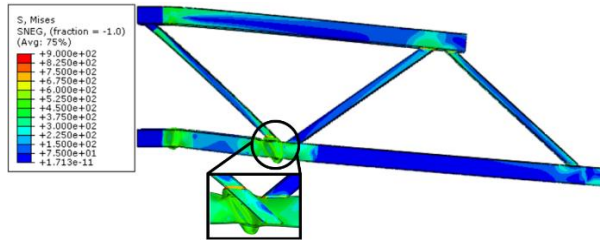
D1_6.3_180_80_80_355_0



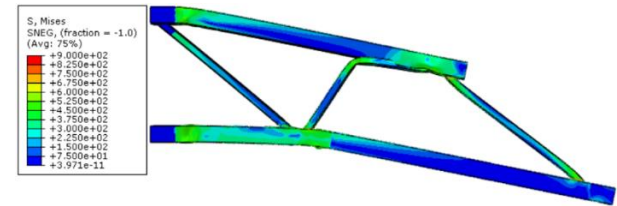
D1_6.3_180_100_80_355_0



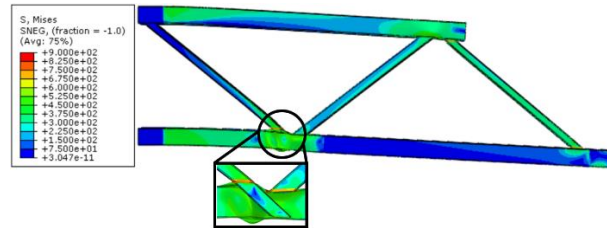
D1_5_180_80_80_355_0



D1_5_180_100_80_355_0



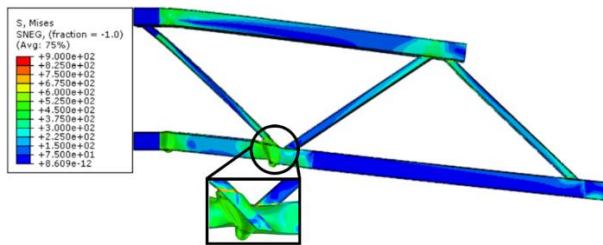
D1_8_180_80_80_355_0



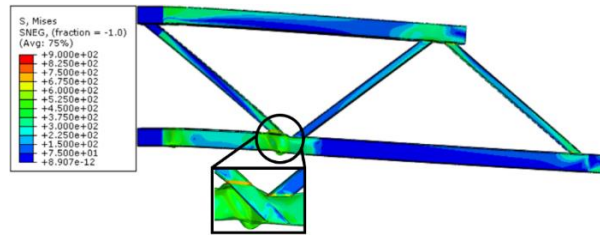
D1_8_180_100_80_355_0

Figure I.3: Deformations and Von Mises stress distributions for the b_1 parameter and D1 joint detail

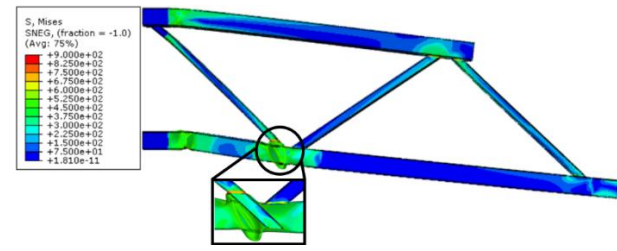
Parameter: b_2



D1_6.3_180_90_70_355_0



D1_6.3_180_90_90_355_0



D1_5_180_90_70_355_0

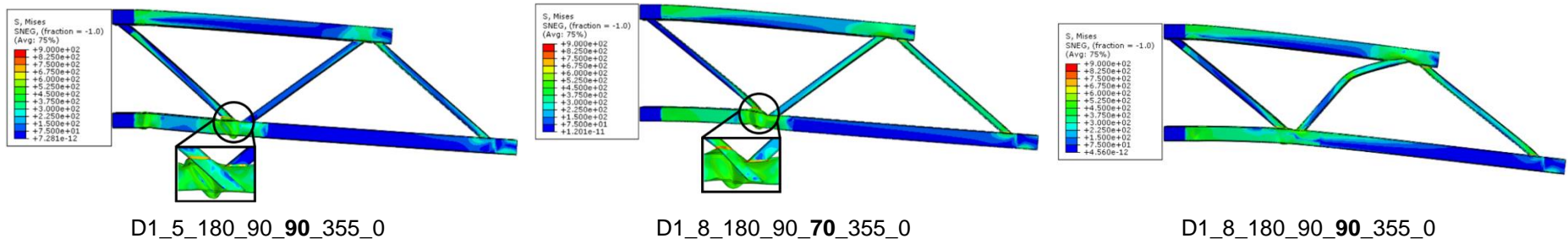
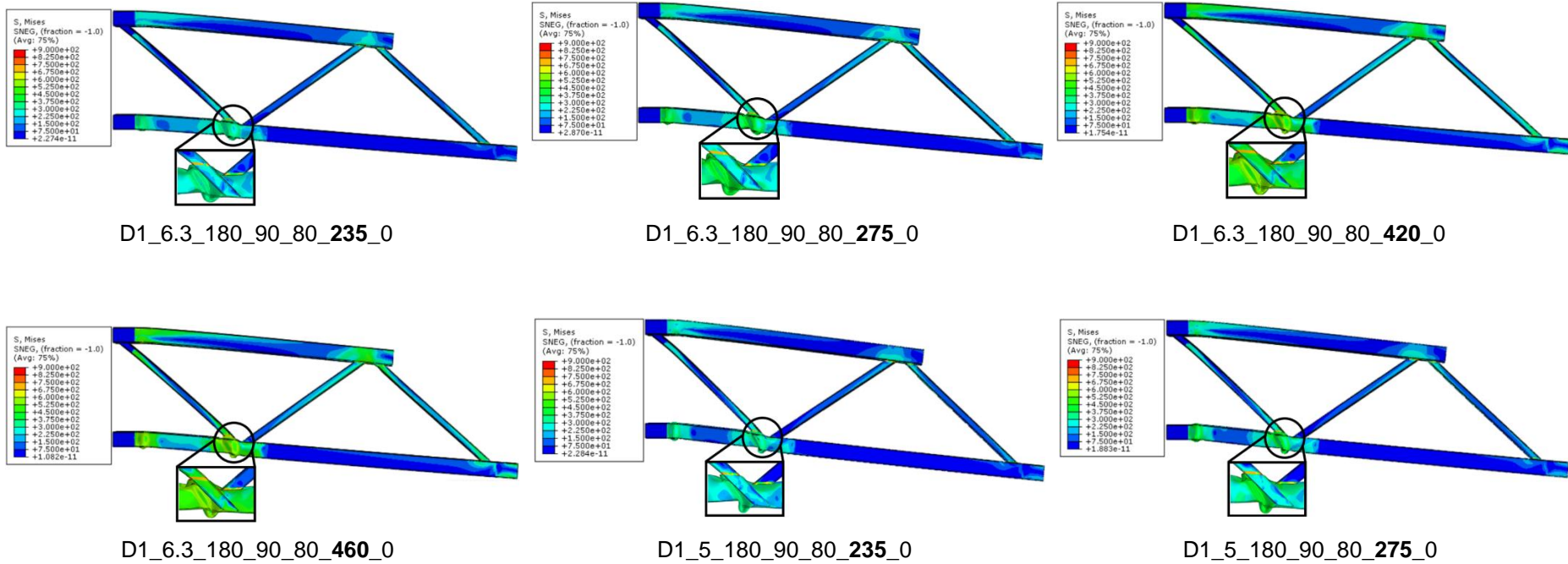
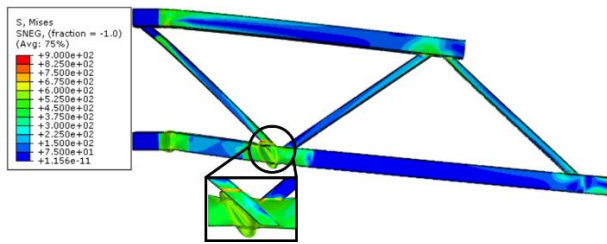


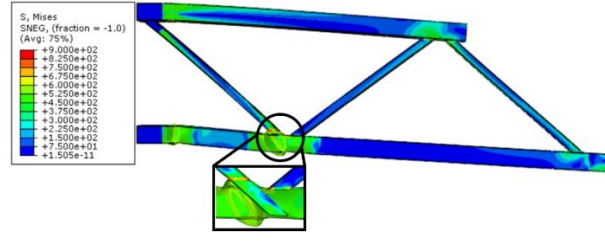
Figure I.4: Deformations and Von Mises stress distributions for the b_2 parameter and D1 joint detail

Parameter: f_{y0}

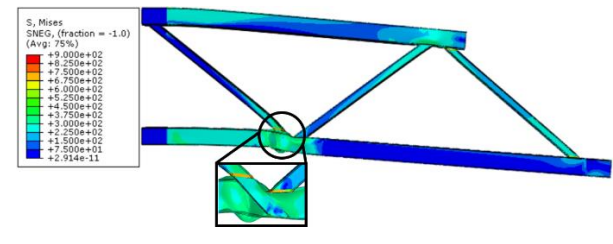




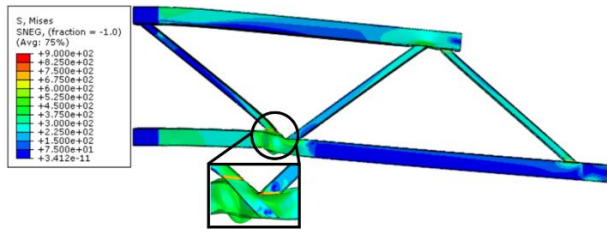
D1_5_180_90_80_420_0



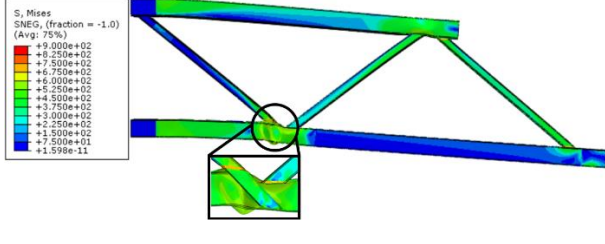
D1_5_180_90_80_460_0



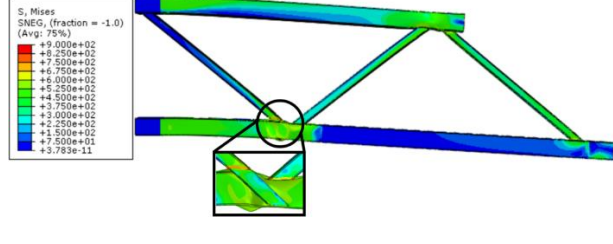
D1_8_180_90_80_235_0



D1_8_180_90_80_275_0



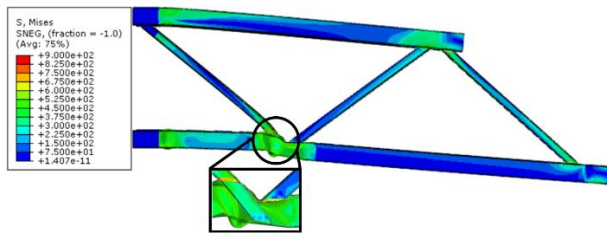
D1_8_180_90_80_420_0



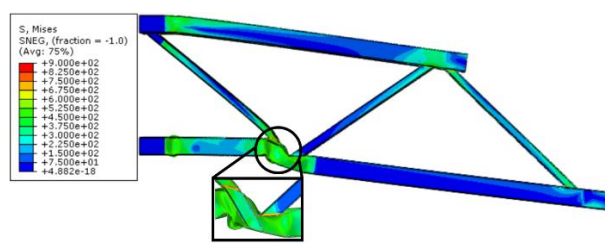
D1_8_180_90_80_460_0

Figure I.5: Deformations and Von Mises stress distributions for the f_{y0} parameter and D1 joint detail

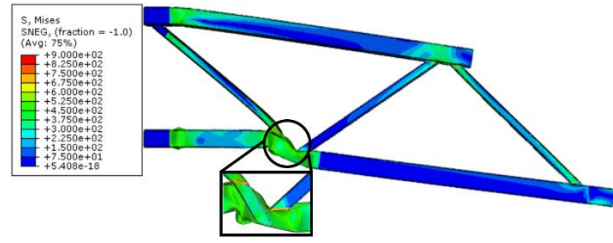
Parameter: g



D1_6.3_180_90_80_355_40



D1_6.3_180_90_80_355_80



D1_6.3_180_90_80_355_120

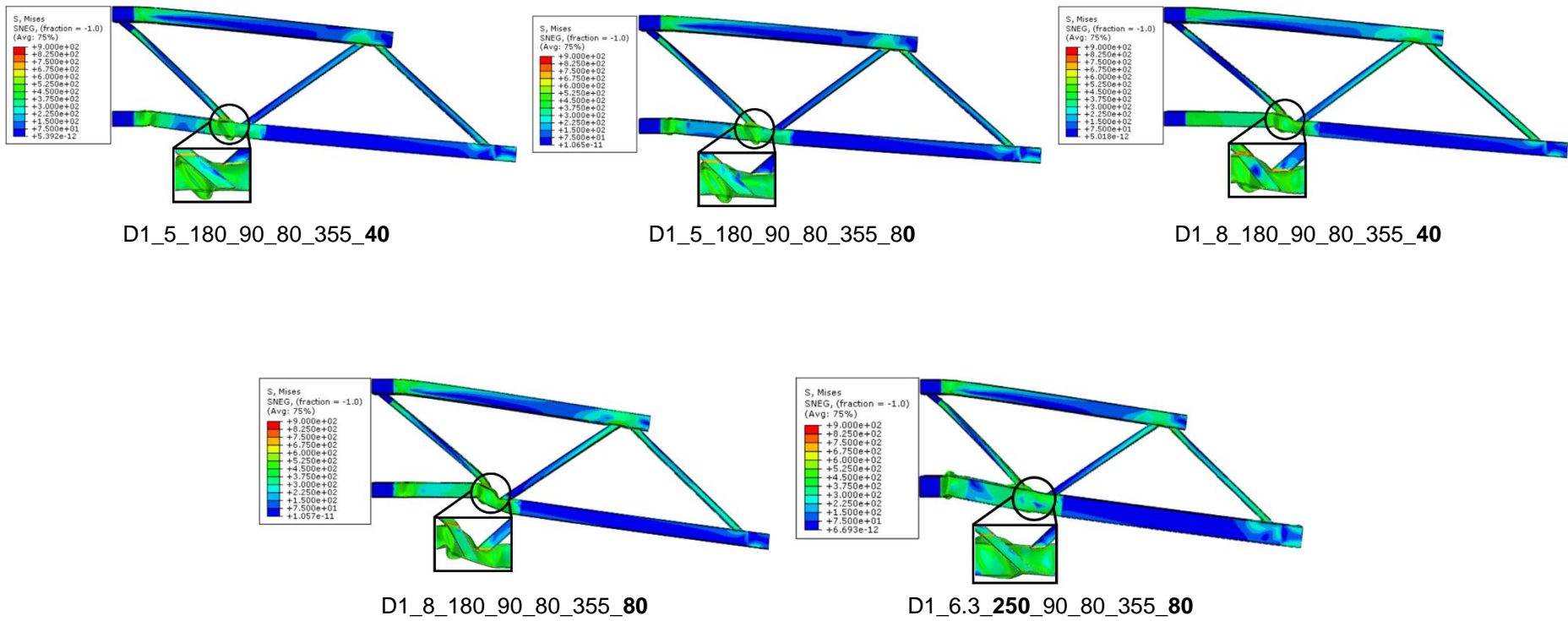


Figure I.6: Deformations and Von Mises stress distributions for the g parameter and D1 joint detail

APPENDIX II: Truss models deformations and Von Mises stress distribution with a R joint detail

Parameter: t_0

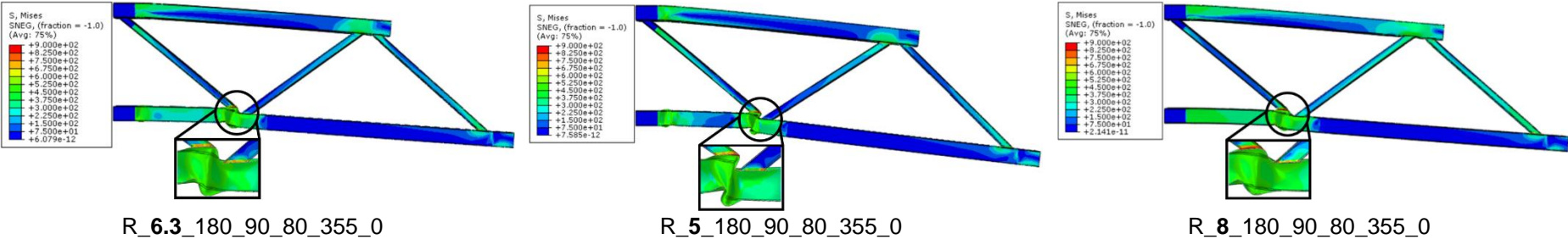
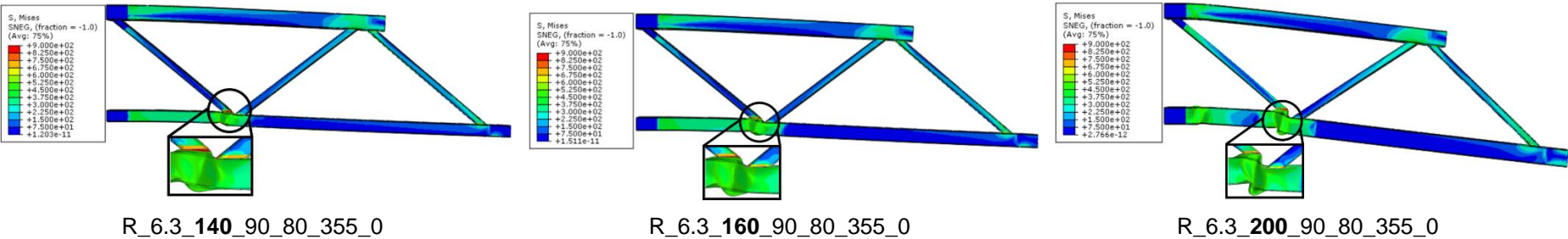
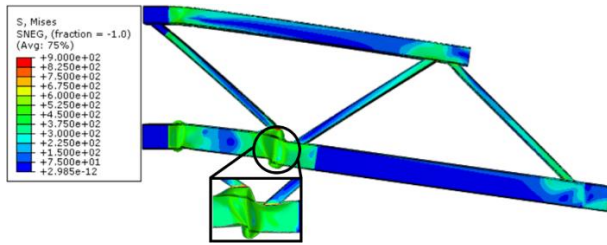


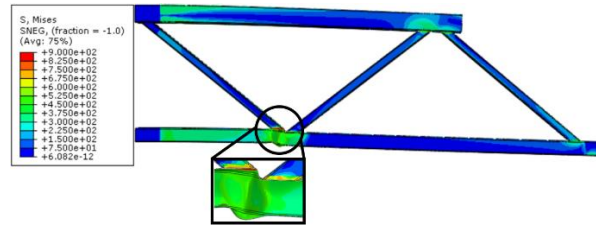
Figure II.1: Deformations and Von Mises stress distributions for the t_0 parameter and R joint detail

Parameter: b_0

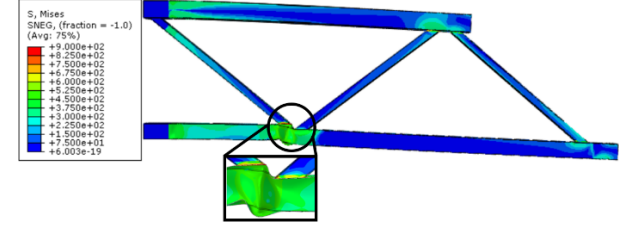




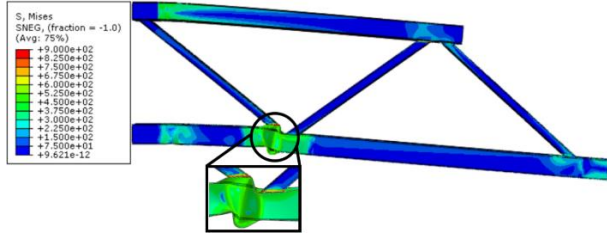
R_6.3_250_90_80_355_0



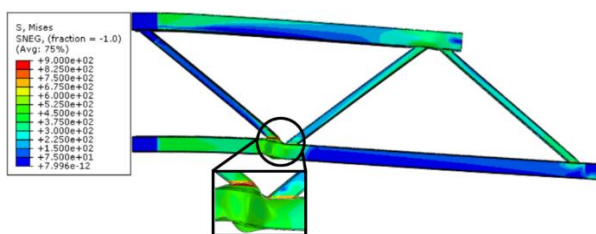
R_5_140_90_80_355_0



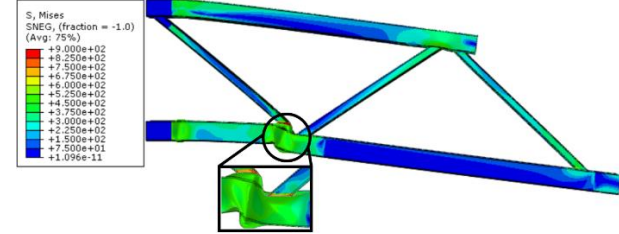
R_5_160_90_80_355_0



R_5_200_90_80_355_0



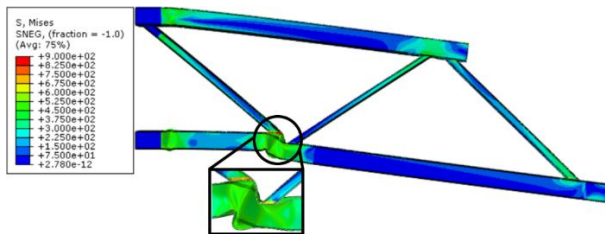
R_8_160_90_80_355_0



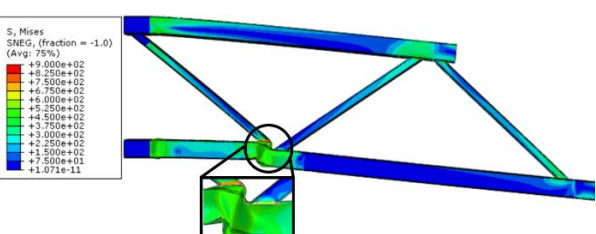
R_8_200_90_80_355_0

Figure II.2: Deformations and Von Mises stress distributions for the b_0 parameter and R joint detail

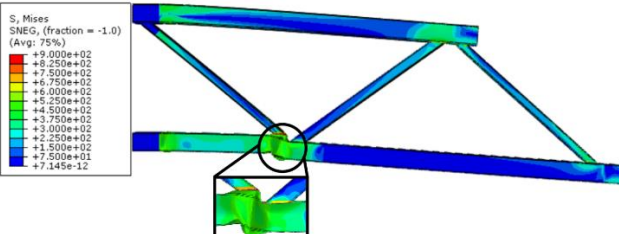
Parameter: b_1



R_6.3_180_60_80_355_0



R_6.3_180_80_80_355_0



R_6.3_180_100_80_355_0

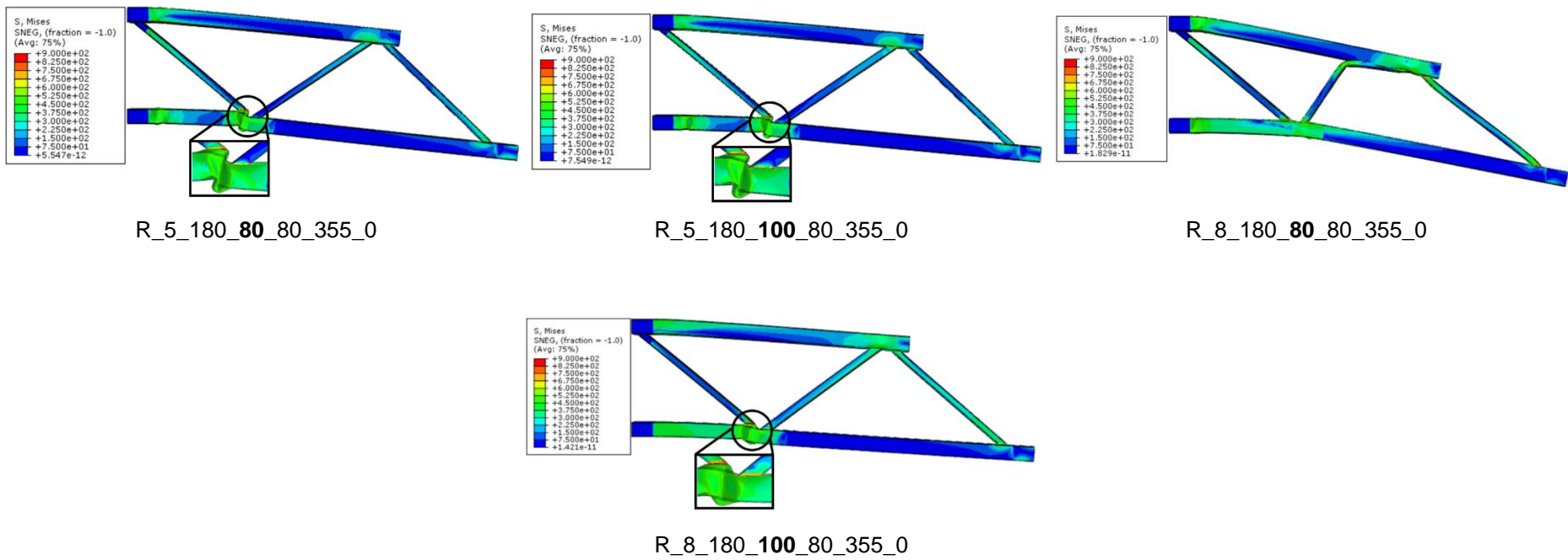
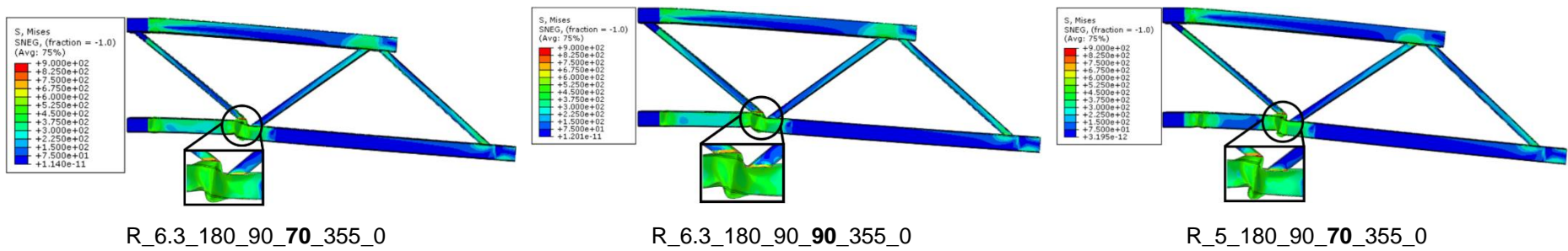


Figure II.3: Deformations and Von Mises stress distributions for the b_1 parameter and R joint detail

Parameter: b_2



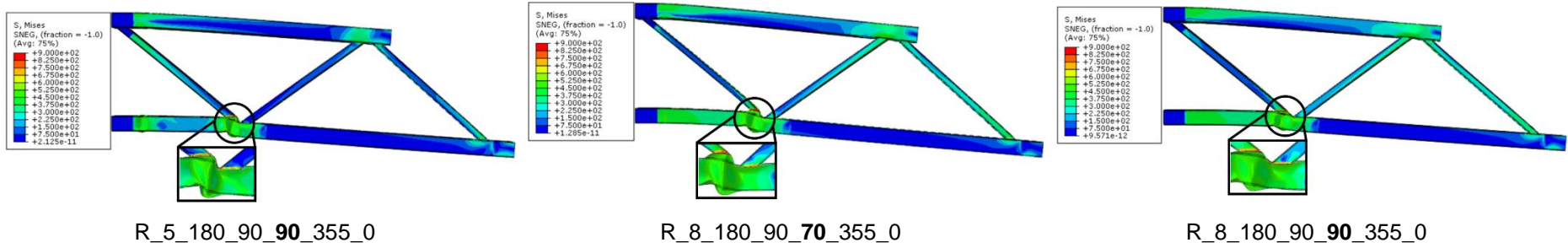
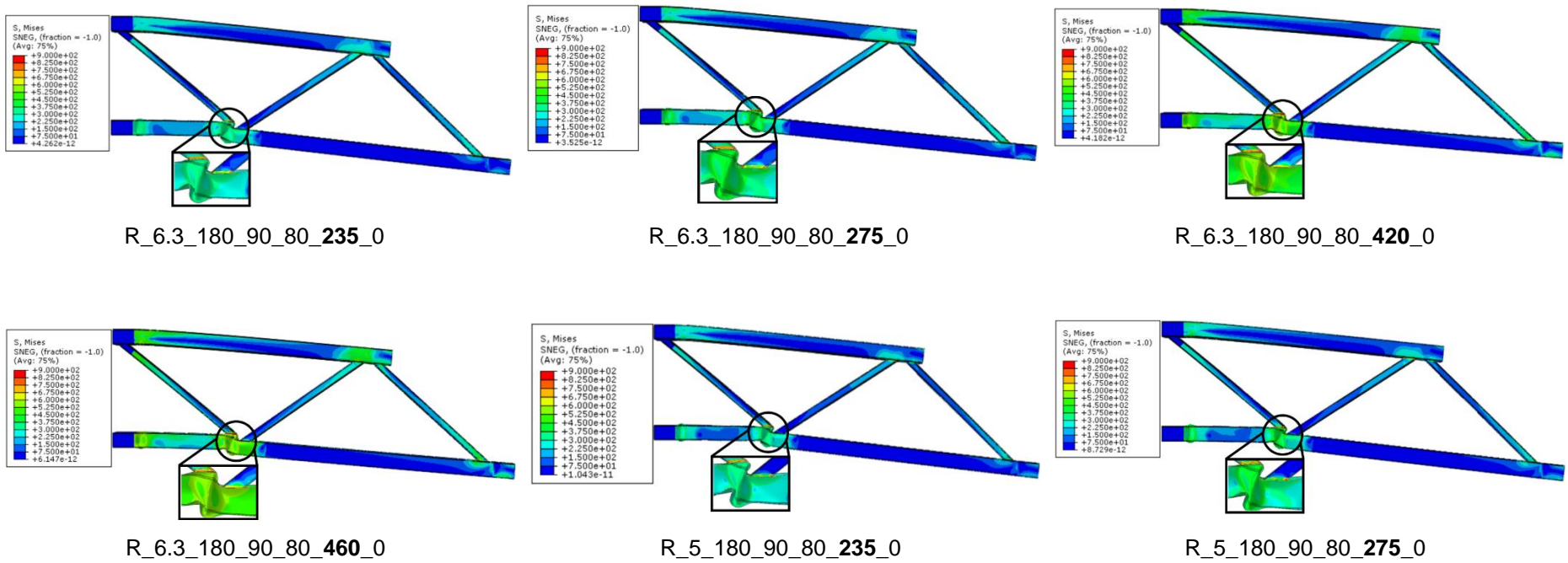


Figure II.4: Deformations and Von Mises stress distributions for the b_2 parameter and R joint detail

Parameter: f_{y0}



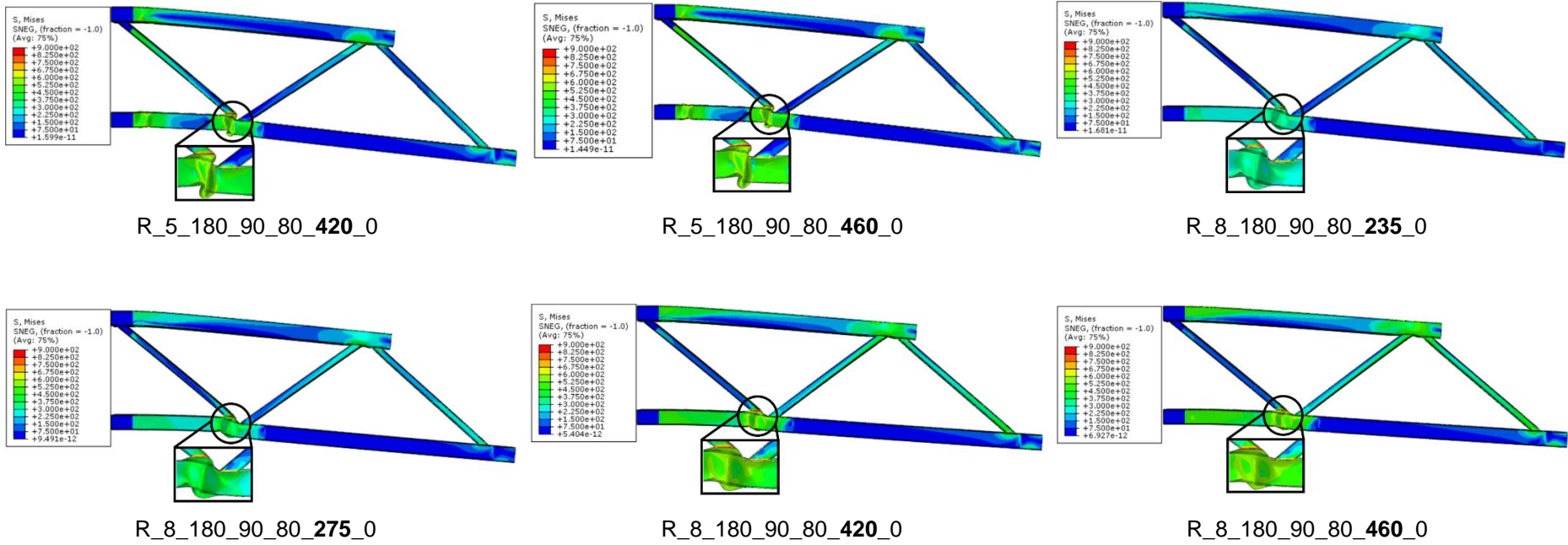
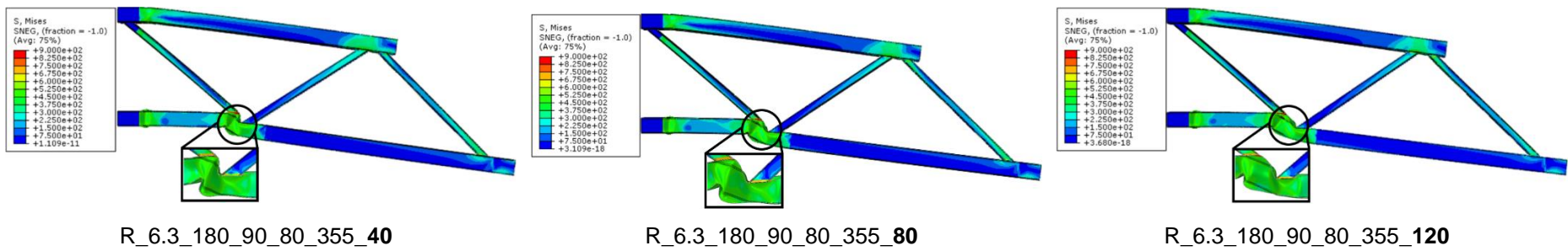
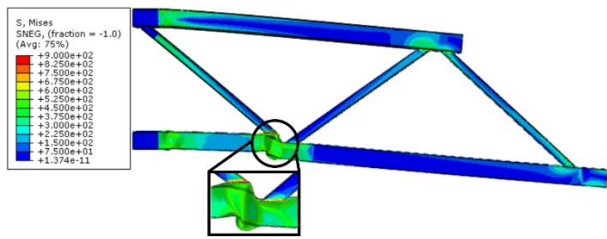


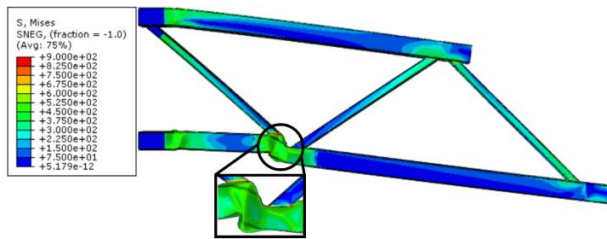
Figure II.5: Deformations and Von Mises stress distributions for the f_{y0} parameter and R joint detail

Parameter: g

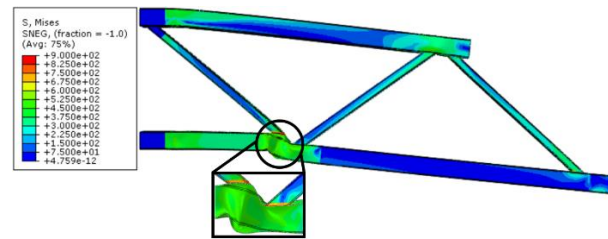




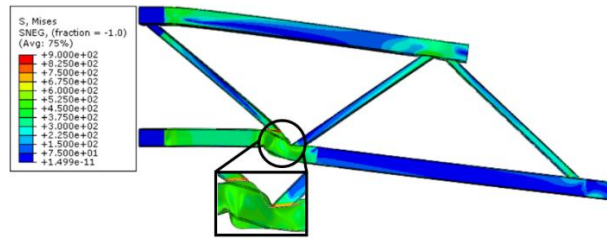
R_5_180_90_80_355_40



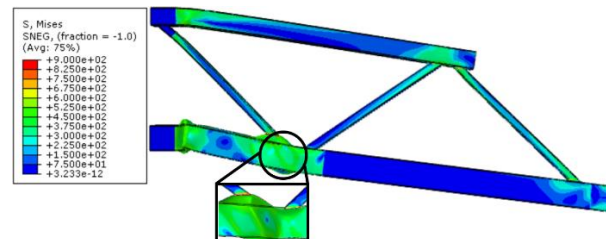
R_5_180_90_80_355_80



R_8_180_90_80_355_40



R_8_180_90_80_355_80



R_6.3_250_90_80_355_80

Figure II.6: Deformations and Von Mises stress distributions for the g parameter and R joint detail

APPENDIX III: Truss models deformations and Von Mises stress distribution with a D2 joint detail

Parameter: g

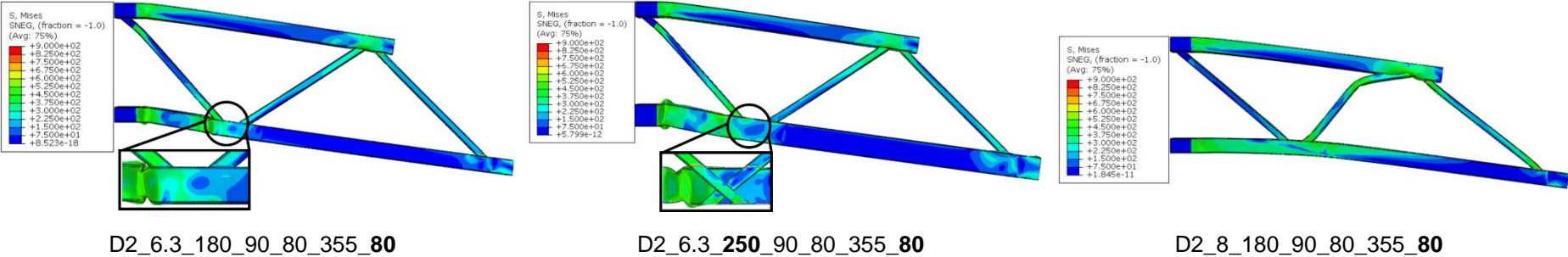


Figure III.1: Deformations and Von Mises stress distributions for the g parameter and D2 joint detail